

UC Riverside

UC Riverside Electronic Theses and Dissertations

Title

Models of Chemical Structure and Dynamics via Nuclear Magnetic Resonance and Ab Initio Computational Chemistry

Permalink

<https://escholarship.org/uc/item/96s2r136>

Author

Lai, Jinfeng

Publication Date

2009

Peer reviewed|Thesis/dissertation

UNIVERSITY OF CALIFORNIA
RIVERSIDE

Models of Chemical Structure and Dynamics via Nuclear Magnetic Resonance and
Ab Initio Computational Chemistry

A Dissertation submitted in partial satisfaction
of the requirements for the degree of

Doctor of Philosophy

in

Chemistry

by

Jinfeng Lai

August 2009

Dissertation Committee:

Dr. Leonard J. Mueller, Chairperson
Dr. David F. Bocian
Dr. Jingsong Zhang

Copyright by
Jinfeng Lai
2009

The Dissertation of Jinfeng Lai is approved:

Committee Chairperson

University of California, Riverside

ACKNOWLEDGMENTS

The text of this thesis in part is a reprint of the material as it appears in:

Journal of Physical Chemistry B **2009**, *113*, 11696

I would like to acknowledge the following individuals for their contributions:

L.J. Mueller directed and supervised the research which forms the basis for this thesis.

M. F. Dunn and D. Niks prepared the sample of tryptophan synthase and provided valuable discussions on experiments for Chapter II.

F. Zaera conceived the surface science experiment of cinchona alkaloids for Chapter III.

Y. Tian assisted in part of the liquid-state and solid-state NMR experiments.

L. Chen designed the pulse of CTUC for part of NMR experiment in Chapter II.

Z. Ma and L. Mink carried out the solubility measurements for Chapter III.

G. Leskowitz designed the theoretical analysis and data fitting of Chapter IV.

J.M. Kaiser designed and built the probe for doing NMR experiment.

Reproduced in part with permission from:

Journal of Physical Chemistry B **2009**, *113*, 11696

Copyright 2009 American Chemical Society

From a more global perspective, I would like to thank my research adviser Professor Leonard Mueller, a famous NMR scientist, and more important for me, an outstanding educator and a warm-hearted friend. He is always there to give me a hand whenever I encountered problem. Without his guidance and support, this research would have been impossible and I would have never made it through to the hardest parts of the climb. Also, I would like to thank Professor Michael Dunn and Professor Francisco Zaera. Collaboration with these two outstanding scientists is one of the most rewarded and memorial experiences of mine. In addition, I would like to thank Professor David Bocian and Professor Jingsong Zhang for their advices on my thesis. Last but not least, I would also like to thank all of my lab mates and friends who made the journey of my Ph. D. study more enjoyable and my life in UCR so colorful.

ABSTRACT OF THE DISSERTATION

Models of Chemical Structure and Dynamics via Nuclear Magnetic Resonance and
Ab Initio Computational Chemistry

by

Jinfeng Lai

Doctor of Philosophy, Graduate Program in Chemistry
University of California, Riverside, August 2009
Dr. Leonard J. Mueller, Chairperson

The combination of nuclear magnetic resonance (NMR) and *ab initio* calculations has become one of the most powerful tools to solve important structural and energetic problems in the field of chemistry. Chemical shifts observed in NMR present detailed information about local electronic structure while dynamic NMR allows us to extract kinetic and thermodynamic properties without perturbing equilibrium. *Ab initio* calculations are able to interpret the chemical shifts in terms of the chemical structure and provide detailed analysis of the energetic components that make up the process probed by dynamic NMR. This work involves three important applications of this powerful combination tool.

First, we present a combined X-ray, solid-state NMR, and *ab initio* study of the 140 kDa enzyme tryptophan synthase that allows for the determination of chemical structure for the key enzymatic intermediates in the enzyme cycle. The results support the ketoenamine and dipolar forms that are in fast exchange with each other in the quionoid intermediate, a result that we believe has mechanistic implications. The structural characterization of this enzymatic intermediate provides insight into the energetic and chemical transformations responsible for biological function.

Second, the combination of NMR and *ab initio* calculations has been applied to the field of catalysis. We find that specific position of the peripheral substitutions outside the central chiral pocket accounts for most of the discrepancies in fundamental physicochemical properties among related cinchona alkaloids via a combination of energetic and entropic effects. These differences in physicochemical properties are ultimately responsible for the differences in chemical reactivity that make each molecule so unique.

Finally, we make use of dynamic NMR and *ab initio* calculations to investigate the rotational barriers of a series of pyridine thiocarboxamides, and identify different electronic and structural factors that contribute to changes in the energetic processes. Comparison between thiocarboxamides and their corresponding amide analogues highlights the important role of the resonance interaction proposed by the canonical amide resonance model.

TABLE OF CONTENTS

	Page
ACKNOWLEDGMENTS	IV
ABSTRACT	VI
TABLE OF CONTENTS	VIII
LIST OF FIGURES	XII
LIST OF TABLES	XV
CHAPTER I	
INTRODUCTION	1
1.1 OVERVIEW OF COMPUTATIONAL CHEMISTRY.....	2
1.1.1 SCHRÖDINGER EQUATION.....	3
1.1.1.1. MOLECULAR HAMILTONIAN.....	4
1.1.1.2 BORN-OPPENHEIMER APPROXIMATION.....	5
1.1.2 HARTREE-FOCK THEORY.....	6
1.1.2.1 MOLECULAR ORBITALS.....	6
1.1.2.2 BASIS SETS.....	8
1.1.2.3 VARIATIONAL PRINCIPLE.....	8
1.1.2.4 ROOTHANN-HALL EQUATIONS.....	9
1.1.3. ELECTRON CORRELATION METHODS.....	10
1.1.3.1 CONFIGURATION INTERACTION.....	10
1.1.3.2 MØLLER-PLESSET PERTURBATION THEORY.....	11
1.1.3.3 DENSITY FUNCTION THEORY.....	12
1.1.4 MOLECULAR MECHANICS.....	14

1.1.5 SEMI-EMPIRICAL METHODS.....	16
1.1.6 PRACTICAL CONSIDERATION.....	17
1.1.6.1 CHOICE OF THEORY AND BASIS SET FOR MODEL SYSTEM...	17
1.1.6.2 HYBRID CALCUALITON WITH ONIOM MODEL.....	18
1.2 CALCULATION OF CHEMICAL SHIFT.....	19
1.2.1 BASIC ASPECTS OF CHEMICAL SHIFT.....	19
1.2.2 CALCULATION METHODS FOR CHEMICAL SHIFT.....	21
1.2.3 PRACTICAL CONSIDERATION.....	22
REFERENCE.....	23

CHAPTER II

CHARACTERIZATION OF ENZYMATIC INTERMEDIATES IN TRYPTOPHAN SYNTHASE VIA SOLID-STATE NMR, X-RAY CRYSTALLOGRAPHY AND AB INITIO CALCULATIONS.....	25
ABSTRACT.....	25
2.1 INTRODUCTION.....	26
2.2 MATERIALS AND METHODS.....	31
2.2.1 MATERIALS.....	31
2.2.2 SOLID-STATE NMR.....	31
2.2.3 AB INITIO CALCULATIONS.....	32
2.3 RESULTS AND DISCUSSION.....	33
2.3.1 BACKGROUND.....	33
2.3.2 THE PYRUVATE SIDE REACTION AND STRATEGY FOR ASSIGNING THE MAS ¹³ C NMR SPECTRA.....	36

2.3.3 ASSIGNMENTS OF QUINONOID INTERMEDIATE VIA SOLID- STATE NMR SPECTROSCOPY.....	38
2.3.4 AB INITIO CALCULATIONS.....	44
2.5 CONCLUSION.....	57
REFERENCE.....	59
CHAPTER III	
INFLUENCE OF PERIPHERAL GROUPS ON THE PHYSICAL AND CHEMICAL BEHAVIOR OF CINCHONA ALKALOIDS.....	62
ABSTRACT.....	62
3.1 INTRODUCTION.....	63
3.2 EXPERIMENTAL SECTION.....	64
3.3 RESULTS.....	65
3.4 DISCUSSION.....	83
3.5 CONCLUSION.....	86
REFERENCE.....	87
CHAPTER IV	
THE ROTATIONAL BARRIERS IN PYRIDINE THIOCARBOXAMIDES: DYNAMIC NUCLEAR MAGNETIC RESONANCE AND AB INITIO STUDIES.....	90
ABSTRACT.....	90
4.1 INTRODUCTION.....	91
4.2 MATERIALS AND METHODS.....	94
4.3 RESULTS AND DISCUSSION.....	96

4.3.1 COMPARISON AMONG REGIOISOMERS AND AB INITIO CALULATIONS.....	102
4.3.2 COMPARISON TO AMIDE ANALOGUES AND NBO ANALYSIS....	108
4.4 CONCLUSION.....	112
REFERENCE.....	114
 CHAPTER V	
CONCLUSTION AND OUTLOOK.....	118
REFERENCE.....	124
 APPENDIX.....	
THE ONIOM OPTIMIZED COORDINATES OF INDOLINE QUINONOID INTERMEDIATE (MODEL 0-1010)	125

LIST OF FIGURES

Page

CHAPTER I

Figure 1.1. Diagram of two-layer ONIOM model.....	19
---	----

CHAPTER II

Figure 2.1. α - and β -subunits of an $\alpha\beta$ -dimeric unit of the tryptophan synthase tetramer.....	27
Figure 2.2. Organic structures of reactants, products, and intermediates identified in the tryptophan synthase α - and β -reaction.....	28
Figure 2.3. Quinonoid intermediates.....	30
Figure 2.4. UV/Vis spectra of intermediates.....	35
Figure 2.5. The solid-state NMR spectra of E(Q) _{indoline}	40
Figure 2.6. The solid-state NMR spectra of E(Q) _{2-AP}	41
Figure 2.7. ONIOM structure model of indoline quinonoid cut out from X-ray crystal structure.....	46
Figure 2.8. Models of indoline quinonoid.....	48
Figure 2.9. Comparison of the calculated ¹³ C chemical shifts of indoline quinonoid with experimental results.....	52
Figure 2.10. The root mean square deviation (RMSD) of the calculated ¹³ C chemical shifts from the experimental results.....	53
Figure 2.11. <i>Ab initio</i> minimized structures and chemical shifts of the 2-AP quinonoid intermediate.....	56

CHAPTER III

Figure 3.1. Structure of the eight cinchona alkaloids.....	63
Figure 3.2. Comparative quantum-mechanics calculations of the energy of crystallization of cinchonine versus cinchonidine.....	66
Figure 3.3. Quantum-mechanics calculations of the energetics of CD and CN in each other's crystalline structures.....	68
Figure 3.4. Comparative solubility studies with cinchona alkaloids.....	69
Figure 3.5. Detail of 2D NOESY ¹ H NMR data for cinchonine and cinchonidine dissolved in perdeuteromethanol.....	70
Figure 3.6. 2D potential energy surfaces (PES) as a function of rotations around the two central bonds within the alcohol linker.....	72
Figure 3.7. Quantum-mechanics calculations for the differences in energy between cinchonidine (CD) and cinchonine (CN)	73
Figure 3.8. Temperature dependence of the solubilities of cinchonidine and cinchonine in ethanol and of cinchonidine in carbon tetrachloride...	75
Figure 3.9. Calculations of entropy contributions from the different vibrational and rotational modes of CD vs. CN.....	76
Figure 3.10. Adsorption geometries of cinchona alkaloids on platinum surfaces...	81

CHAPTER IV

Figure 4.1. Resonance model proposed by Pauling.....	91
Figure 4.2. The pyridine thiocarboxamides.....	94
Figure 4.3. Dynamic NMR spectra of thionicotinamide.....	98
Figure 4.4. Dynamic NMR spectra of thioisonicotinamide.....	99

Figure 4.5. The temperature dependence of the apparent rate data fit to transition state theory shown as a nonlinear fit.....	101
Figure 4.8. Rotational pathways and rotational barriers pyridine thiocarboxamides.....	104
Figure 4.9. Resonance structures for thionicotinamide and thioisonicotinamide..	107
Figure 4.10. Diagram showing the interaction between n_N and $\pi^*_{C=X}$	112

CHAPTER V

Figure 5.1. Stereo diagram of tryptophan synthase.....	121
--	-----

LIST OF TABLES

	Page
 CHAPTER II	
Table 2.1. Summary of Solid-state NMR Chemical Shifts of E(Q) _{indoline} and E(Q) _{2-AP} Species.....	42
 CHAPTER III	
Table 3.1. Entropy Contributions from Each Vibrational Mode in the Most Stable Configurations of CD and CN.....	77
Table 3.2. Entropies for Each of the 27 Most Stable Configurations, Cinchonidine.....	78
Table 3.3. Entropies for Each of the 27 Most Stable Configurations, Cinchonine... ..	79
 CHAPTER IV	
Table 4.1. Experimental Data Points for Thionicotinamide and Thioisonicotinamide.....	100
Table 4.2. Rotational Barrier of Pyridine Thiocarboxamides and Pyridine Carboxamides.....	102
Table 4.3. Molecular Parameters Optimized at the B3LYP/6-311G(d,p) Level...	105
Table 4.4. Natural Resonance Weights for Ground States of Thionicotinamide, Thioisonicotinamide, Nicotinamide, and Isonicotinamide at the MP2/6-311G(d,p) Level.....	109
Table 4.5. NBO Analysis of Ground States of Thionicotinamide, Thioisonicotinamide, Nicotinamide, and Isonicotinamide at the MP2/6-311G(d,p) Level.....	110

CHAPTER I

INTROCUCTION

Computational chemistry is basically the application of chemical, mathematical and computing skills to assist in solving interesting chemical problems. In some cases, computational chemistry is used to complement experimental studies by providing information which is hard to explore experimentally (for instance, transition state structures and energies). In other cases, computational chemistry is used to make predictions for later actual experiments, and investigate new materials which are too difficult to find. As a consequence of its usefulness, computational chemistry has been widely used by an increasing number of people nowadays, assisted by the advances in theoretical techniques as well as in computer power.

On the other hand, since its first detection in 1938 and first studies in bulk materials in 1946, nuclear magnetic resonance (NMR) has developed from an interesting and important study of a physical phenomenon to an indispensable technique in a very wide variety of fields. As a structural method, NMR spans three states of matter, which sets it apart from other structural techniques. In structural biology, NMR competes and complements with x-ray crystallography in providing precise three-dimensional structures for protein and other macromolecules. Furthermore, NMR exceeds x-ray crystallography in furnishing information on internal mobility and overall molecular motion of both large and small molecules. Among all the NMR parameters, chemical shift is the most important one in the determination of the biological structure.

This chapter attempts to provide a brief summary of the basic theory of computational chemistry, together with calculation methods for chemical shift, the most important parameter of NMR.

1.1 OVERVIEW OF COMPUTATIONAL CHEMISTRY

“The underlying physical laws necessary for the mathematical theory of a large part of physics and the whole of chemistry are thus completely known, and the difficulty is only that the exact application of these laws leads to equations much too complicated to be soluble.”

- P. A. M. Dirac, 1929

All molecular systems can be entirely described by the laws of quantum mechanics, and it is fairly straightforward to write down a Hamiltonian and Schrödinger Equation for a chemical system. However, an exact solution to the Schrödinger Equation is possible only for a few trivial molecular systems, such as the Particle-In-A-Box, the Harmonic Oscillator, and the Hydrogen Atom. For the rest of chemical systems, we must rely on a number of simplifying assumptions and procedures which numerically solve the Schrödinger equation to different levels of exactness. The challenge for computational chemists is to develop and test methods for the numerical solution of the Schrödinger equation for interesting molecular systems. In this section, we will provide an introductory overview of the methods developed over the years¹⁻⁶ and the theory underlying those methods.

1.1.1 SCHRÖDINGER EQUATION

From quantum mechanics we know the entities like electrons have both the particle-like and wave-like characteristics. The wavefunction of a particle is described by the time-dependent Schrödinger equation⁷ as:

$$\left(-\frac{\hbar^2}{8\pi^2m} \nabla^2 + V \right) \Psi(\vec{r}, t) = \frac{i\hbar}{2\pi} \frac{\partial \Psi(\vec{r}, t)}{\partial t}$$

Here, Ψ is the wavefunction, m is the particle mass, \hbar is Planck's constant, V is the potential field, and ∇ is the Laplacian

$$\frac{\partial^2}{\partial x^2} + \frac{\partial^2}{\partial y^2} + \frac{\partial^2}{\partial z^2}.$$

The probability distribution of the particle can be represented by the product of Ψ and its complex conjugate ($\Psi^*\Psi$, or $|\Psi|^2$).

If the potential field is not a function of time, the wavefunction can be rewritten as the product of a spatial function and a time function:

$$\Psi(\vec{r}, t) = \psi(\vec{r})\tau(t)$$

Substituting these new functions into the time-dependent Schrödinger equation, we will obtain two new equations, one of which is function of time alone, another one of which depends on the position of particle only. The latter one is the time-independent Schrödinger equation:

$$H\psi(\vec{r}) = E\psi(\vec{r})$$

For the chemical system we are interested in, this separation is valid. Therefore, from now on, we will focus on the time-independent Schrödinger equation exclusively.

1.1.1.1. MOLECULAR HAMILTONIAN

For a molecular system, Ψ is a function of the positions of electrons and the nuclei within the molecule. Basically, the Hamiltonian of this molecular system is made up of kinetic energy and potential energy terms:

$$H = T + V$$

The kinetic energy is the summation of ∇^2 over all the electrons and nuclei in the molecule:

$$T = T_e + T_n$$

In this equation, T_e , the kinetic energy of the electrons, can be written as

$$T_e = -\frac{h^2}{8\pi^2 m} \sum_i \left(\frac{\partial^2}{\partial x_i^2} + \frac{\partial^2}{\partial y_i^2} + \frac{\partial^2}{\partial z_i^2} \right)$$

where m is the electron mass. Similarly, the kinetic energy term for nuclei is written as

$$T_n = -\frac{h^2}{8\pi^2} \sum_I \frac{1}{M_I} \left(\frac{\partial^2}{\partial x_I^2} + \frac{\partial^2}{\partial y_I^2} + \frac{\partial^2}{\partial z_I^2} \right)$$

In this equation, M_I is the mass of nucleus I .

The potential energy component is the Coulomb repulsion between each pair to charge entities:

$$V = \frac{1}{4\pi\epsilon_0} \sum_j \sum_{k < j} \frac{e_j e_k}{r_{jk}}$$

where e_j and e_k are the charges on particle j and k , and r_{jk} is the distance from particle j to particle k . For a nucleus, the charge is Ze , where Z is the atomic number of this atom.

Therefore, the potential energy operator can be rewritten as:

$$V = \frac{1}{4\pi\epsilon_0} \left(- \sum_i^{\text{electrons}} \sum_I^{\text{nuclei}} \frac{Z_I e^2}{r_{iI}} + \sum_i^{\text{electrons}} \sum_{j<i} \frac{e^2}{r_{ij}} + \sum_I^{\text{nuclei}} \sum_{J<I} \frac{Z_I Z_J e^2}{r_{IJ}} \right)$$

The first term represents electron-nuclear attraction, the second term corresponds to electron-electron repulsion, and the third term is nuclear-nuclear repulsion. In brief,

$$V = V_{en} + V_{ee} + V_{nn}$$

1.1.1.2 BORN-OPPENHEIMER APPROXIMATION

Now we know that the full Hamiltonian can be written as:

$$H = T_e(\vec{r}) + T_n(\vec{R}) + V_{en}(\vec{r}, \vec{R}) + V_{ee}(\vec{r}) + V_{nn}(\vec{R})$$

This Hamiltonian equation neglects spin interaction and can be solved exactly for a two particle system (i.e. one electron and one nucleus). For a higher order system, we have to depend on certain approximations to simplify the solution of the Schrödinger equation, and the Born Oppenheimer approximation⁸ is the first of those approximations. It simplifies the molecular problem by separating the motions of electrons from the motion of the nuclei attributable to large difference in the velocity of the electron relative to the nuclei. In this approximation, the nuclei look fixed to the electrons, and the electrons move in a field of fixed nuclei. By making this assumption, we can neglect the kinetic energy term from the nuclei and write the electronic Hamiltonian as:

$$H^{elec} = T_e(\vec{r}) + V_{en}(\vec{r}, \vec{R}) + V_{ee}(\vec{r}) + V_{nn}(\vec{R})$$

Now this Hamiltonian describing the motion of electrons in the field of fixed nuclei satisfies the Schrödinger equation

$$H^{elec} \psi^{elec}(\vec{r}, \vec{R}) = E^{eff}(\vec{R}) \psi^{elec}(\vec{r}, \vec{R})$$

Solving this equation for electronic wavefunction will produce the effective nuclear potential function E^{eff} , which describes the potential energy surface of the chemical system and depends on the nuclear coordinates. Of course, the produced electronic wavefunction must be normalized and antisymmetric.

1.1.2 HARTREE-FOCK THEORY

Unfortunately an exact solution to this reduced Schrödinger equation is still impossible for most chemical systems without further approximations.

1.1.2.1 MOLECULAR ORBITALS

The next approximation is based on molecular orbital theory by assuming that the electrons act independently of each other. In this way, the electronic wavefunction (made up of n electrons) can be written as a combination of these molecular orbitals by forming their Hartree product:

$$\psi(\vec{r}) = \phi_1(\vec{r}_1)\phi_2(\vec{r}_2)\phi_3(\vec{r}_3)\dots\phi_n(\vec{r}_n)$$

However, such a function is not antisymmetric. To ensure the antisymmetry, we need to represent the wavefunction as a Slater determinant built over the orbitals, and this is also the simplest antisymmetric function that is a combination of molecular orbitals. Before forming it, electron spin, a factor that has been neglected so far, must be taken into account. The spin term can have the value of α or β corresponding to the spin up or spin down. Therefore, two spin functions, α and β , are defined as follows:

$$\begin{aligned}\alpha(\uparrow) &= 1 & \alpha(\downarrow) &= 0 \\ \beta(\uparrow) &= 0 & \beta(\downarrow) &= 1\end{aligned}$$

In order to include electron spin as part of the electronic wavefunction ψ , we can multiply the molecular orbital function by spin function to form spin orbital. And this spin orbital is a function of both the electron's coordinates and its spin.

For a closed shell system where every orbital is made up of a pair of electrons with different spins, the wavefunction of the n electrons for this system can be built as:

$$\psi(\bar{r}) = \frac{1}{\sqrt{n!}} \begin{vmatrix} \phi_1(\bar{r}_1)\alpha(1) & \phi_1(\bar{r}_1)\beta(1) & \phi_2(\bar{r}_1)\alpha(1) & \phi_2(\bar{r}_1)\beta(1) & \cdots & \phi_n(\bar{r}_1)\alpha(1) & \phi_n(\bar{r}_1)\beta(1) \\ \phi_1(\bar{r}_2)\alpha(2) & \phi_1(\bar{r}_2)\beta(2) & \phi_2(\bar{r}_2)\alpha(2) & \phi_2(\bar{r}_2)\beta(2) & \cdots & \phi_n(\bar{r}_2)\alpha(2) & \phi_n(\bar{r}_2)\beta(2) \\ \vdots & & & & & & \vdots \\ \phi_1(\bar{r}_i)\alpha(i) & \phi_1(\bar{r}_i)\beta(i) & \phi_2(\bar{r}_i)\alpha(i) & \phi_2(\bar{r}_i)\beta(i) & \cdots & \phi_n(\bar{r}_i)\alpha(i) & \phi_n(\bar{r}_i)\beta(i) \\ \phi_1(\bar{r}_j)\alpha(j) & \phi_1(\bar{r}_j)\beta(j) & \phi_2(\bar{r}_j)\alpha(j) & \phi_2(\bar{r}_j)\beta(j) & \cdots & \phi_n(\bar{r}_j)\alpha(j) & \phi_n(\bar{r}_j)\beta(j) \\ \vdots & & & & & & \vdots \\ \phi_1(\bar{r}_n)\alpha(n) & \phi_1(\bar{r}_n)\beta(n) & \phi_2(\bar{r}_n)\alpha(n) & \phi_2(\bar{r}_n)\beta(n) & \cdots & \phi_n(\bar{r}_n)\alpha(n) & \phi_n(\bar{r}_n)\beta(n) \end{vmatrix}$$

where $\frac{1}{\sqrt{n!}}$ is the normalization factor guaranteeing that

$$\int \psi^*(\bar{r})\psi(\bar{r})d\tau_1d\tau_2\cdots d\tau_n = 1$$

This matrix is not just a mathematical trick to form an antisymmetric wavefunction. It mixes all of the possible orbitals of all the electrons in the molecular system, exactly in agreement with the quantum mechanics, which specifies that an electron's location is not deterministic but rather consists of a probability density.

1.1.2.2 BASIS SETS

The next approximation is to write the molecular orbitals as a linear combination of pre-defined one electron functions known as basis functions:

$$\phi_i = \sum_{\mu=1}^N c_{\mu i} \chi_{\mu}$$

where $\chi_1 \cdots \chi_N$ are the basis functions of interest and $c_{\mu i}$ are the coefficients known as the molecular orbital expansion coefficients. The popular basis functions used in Gaussian and other *ab initio* electronic structure programs are gaussian-type basis functions, which have the general form:

$$g(\alpha, \vec{r}) = cx^n y^m z^l e^{-\alpha r^2}$$

where \vec{r} is composed of x, y , and z . α is the constant which determines the size of the function. Based on the number and types of basis functions, basis sets can be classified as minimal basis sets, split valence basis sets, polarized basis sets, diffuse function, and high angular momentum basis sets, in the order of increasing basis functions applied^{9,10}. General speaking, the larger the basis function, the more accurate the calculation of the energy of the system.

1.1.2.3 VARIATIONAL PRINCIPLE

Now the problem has become how to solve $c_{\mu i}$, the molecular orbital expansion coefficients. Hartree-Fock theory takes advantage of the variational principle, which

states that the energy of a system given by an approximate wavefunction is higher than the actual energy. By minimizing the energy

$$E_{approx.} = \frac{\int \psi_{approx}^* H \psi_{approx}}{\int \psi_{approx}^* \psi_{approx}}$$

where ψ_{approx} is the approximate wavefunction made by some initial guess, we can in an iterative manner converge at the actual energy due to the fact that

$$E_{approx} \geq E$$

1.1.2.4 Roothann-Hall Equations

In practice, we need to find the sets of coefficients that minimize the energy of the resultant wavefunction. Roothann and Hall^{11,12} derived the following equations describing the molecular orbital expansion coefficient, c_{vi} , based on the variational principle:

$$\sum_{v=1}^m (F_{\mu v} - \varepsilon_i S_{\mu v}) c_{vi} = 0 \quad \mu = 1, 2, \dots, N$$

Those equations can be rewritten in matrix form:

$$FC = SC\varepsilon$$

where each element is a matrix. F is known as Fock matrix, representing the average effects of the field of all the electrons on each orbital, while S is the overlap matrix, demonstrating the overlap between orbitals. ε is a diagonal matrix of orbital energies, in which each element ε_i is the one-electron orbital energy of molecular orbital χ_i .

The matrix form of Roothaan-Hall equations is not linear and can be solved iteratively, and the procedure to do this is called Self-Consistent Field (SCF) method. At convergence, the energy corresponds with a minimum, and the solution gives rise to a set of doubly occupied molecular orbitals, and also a set of orbitals which contain no electrons which are denoted virtual orbitals. The total number of orbitals is the same as the number of the basis functions used.

1.1.3. ELECTRON CORRELATION METHODS

From the discussion above, we know that Hartree-Fock theory provides an insufficient treatment of the correlation between the motions of the electrons with a molecular system, particularly that arising between electrons of opposite spin. Here we will briefly talk about three different approaches to deal with the electron correlation problem.

1.1.3.1 CONFIGURATION INTERACTION

In Hartree-Fock theory, the wavefunction is expressed as a single determinant. Configuration Interaction (CI) proceeds by replacing one or more occupied orbitals within the Hartree-Fock determinant with a virtual orbital, so as to construct other determinants. In this way, the wavefunction by the full CI method is a linear combination of the Hartree-Fock determinant and all possible substituted determinants, and can be written as:

$$\psi = b_0\psi_0 + \sum_s b_s\psi_s$$

Full CI is the most complete non-relativistic treatment of the molecular system. However, it is very expensive, and consequently only practical for the very smallest system. Practical configuration interaction truncates the CI expansion at different levels of substitution¹³⁻¹⁵. For instance, CIS (configuration interaction with single excitations) augments the Hartree-Fock by adding single excitations only. Likewise, CISD adds both single and double excitations, and CISDT adds singles, doubles, and triples, and so on. Quadratic Configuration Interaction (QCI) method restores the size-consistency to those limited CI, providing even greater accuracy. Other types of calculations in this family consist of CCSD (coupled cluster single and double excitation) and BD (Brueckner double excitation), as well as others. As each excitation into a virtual state creates a separate wavefunction in the Hartree Fock equation, these types of procedure come with large computational overhead. As a consequence of this overhead, those calculations are typically limited to smaller amounts of basis functions, and unfortunately converge quite slowly.

1.1.3.2 MØLLER-PLESSET PERTURBATION THEORY

The second popular approach to electron correlation problem is by the use of Møller-Plesset perturbation theory¹⁶. In this method, excited states are added to the wavefunction as perturbation on the ground state wavefunction. Assuming we have a wavefunction that can be divided into two parts:

$$H = H_0 + \lambda V$$

where H_0 is an exactly solvable part and λV is a perturbation applied to H_0 . Since V is a small perturbation, the perturbed wavefunction and energy can be expressed as a power series of V in the terms of the parameter λ as:

$$\psi = \psi^{(0)} + \lambda \psi^{(1)} + \lambda^2 \psi^{(2)} + \dots$$

$$E = E^{(0)} + \lambda E^{(1)} + \lambda^2 E^{(2)} + \dots$$

By substituting those perturbed wavefunction and energy back into the Schrödinger equation, we find that the second order correction to the ground state energy is given by the following

$$E^{(2)} = - \sum_t \frac{|\langle \psi^{(0)} | V | \psi_t \rangle|^2}{E_t - E^{(0)}}$$

Since this equation has truncated the expansion at second order it is commonly abbreviated as the MP2 level. By the same process, we can derive the third and fourth order energy corrections. The accuracy of an MP4 calculation is roughly equivalent to the accuracy of a CISD calculation. These techniques are not as computationally expensive as to the configuration interaction (CI) types of electron correlation but are still fairly restrictive in their computational requirements.

1.1.3.3 DENSITY FUNCTION THEORY

The third way to cope with electron correlation problem is Density Functional Theory (DFT), which is based on a strategy of modeling electron correlation by the use of general functionals of the electron density. Following on the pioneering work of Kohn and Sham^{17,18}, the electronic energy of a molecule system is partitioned into several terms:

$$E = E^T + E^V + E^J + E^{XC}$$

where E^T is the kinetic energy term, E^V includes the potential energy of the nuclear-electron attraction and the nuclear repulsion, and E^J represents the electron-electron repulsion. The final term E^{XC} is the exchange-correlation terms. All the terms except the nuclear-nuclear repulsion are functions of the electron density.

$E^T + E^V + E^J$ represents the classical energy of the charge distribution, while E^{XC} takes account of the remaining part of electron-electron interaction, including the exchange energy arising from the antisymmetry of the wavefunction as well as dynamic correlation in the motion of the individual electrons.

Density Functional Theory can be broken down into several classes, based on different treatments of E^{XC} . The simplest approximation to this exchange-correlation term is local density approximation (LDA), which is based only on the electron density. LDA method has been extensively used for band structure calculations. A more complex set of functionals are called gradient-corrected methods, which utilize the electron density and its gradient to define the exchange-correlation functional. In addition, there is also hybrid density functional which employ a combination of both the Hartree-Fock exchange energy and the density functional exchange correlation energy, and this type of E^{XC} can be defined as:

$$E_{hybird}^{XC} = c_{HF} E_{HF}^X + c_{DFT} E_{DFT}^{XC}$$

Attention should be paid that these hybrid functionals are essentially a combination of energies from various different functionals. For example, the exchange correlation energy of the popular B3LYP is defined via the following expression:

$$E_{B3LYP}^{XC} = E_{LDA}^X + c_0(E_{HF}^X - E_{LDA}^X) + c_X \Delta E_{B88}^X + E_{VWN3}^C + c_C(E_{LYP}^C - E_{VWN3}^C)$$

where $E_{Functional}^X$ represents the exchange energy of that functional, and $E_{Functional}^C$ represents correlation energy of the functional. c_0 , c_X , and c_C are the coefficients used to include the Hartree-Fock and LDA local exchange, Becke's gradient correction to LDA exchange, and LYP correlation correction to VWN3 local correlation functional. Generally, those coefficients have been determined through a comparison of calculated energies to that of experimentally determined values.

Density Functional Theory is a very effective computational method and has been widely used. It includes electron correlation without the usual computational expense of the true correlation methods, like Configuration Interaction. The only shortcoming of DFT relies on the fact that most of the commonly used functionals are derived from comparison of calculated values to experimental ones, and therefore the derived coefficients may be incorrect for some cases.

1.1.4 MOLECULAR MECHANICS

Molecular Mechanics is a category of method which actually does not rely on quantum mechanics at all. Instead, it views the molecule as a collection of atoms held together by purely classical forces, i.e. springs. In Molecular Mechanics, the potential energy of a molecular system is calculated using force fields, which predict how a particular change in geometry affects the molecular energy. The total energy change V_{total} , which includes all the contribution from different types of geometrical distortions, can be written as:

$$V_{total} = V_{stretch} + V_{bend} + V_{torsion} + V_{van-der-Waals} + V_{electrostatics} + \dots$$

In general, each term in this expansion depends on certain geometrical parameters. For instance, assuming that the stretch energy follows the harmonic oscillator model, we can write the stretch energy term as:

$$V_{stretch} = \frac{1}{2}k(R - R_{eq})^2$$

where the k values are tabulated for each bond. Other terms can be handled in a similar way. Different force fields have been developed for different molecular types, and different Molecular Mechanics methods are distinguished by how accurate their force fields are, and how many different terms they use to calculate the total energy. The procedures of Molecular Mechanics then iteratively vary the molecular structure to find the structure that minimizes the total energy V_{total} .

The greatest advantage of Molecular Mechanics is its computational speed. Since molecular mechanics is very cheap in terms of computer time, it is often the most popular method available to deal with large molecules containing thousands of atoms, especially those of biochemical interest such as proteins. Nevertheless, Molecular Mechanics has a few disadvantages. The main disadvantage is the lack of available parameters for many compound types, which limits the areas of applicability of the method. Also, as the electronic wavefunctions are not used in Molecular Mechanics, the information on quantities like dipole moments, orbital energies, and charge distributions will not be provided.

1.1.5 SEMI-EMPIRICAL METHODS

Semi-empirical methods are based on quantum mechanics, and set up with the same general structure as a Hartree-Fock calculation in that they have a Hamiltonian and a wave function. They do not solve the full Schrödinger Equation, but rather a truncated one that involves a simplified version of the full Hamiltonian. Parameters, derived from experimental and computed data, are applied to correct for the errors introduced by omitting part of the calculation. Since some of the calculations come from empirical data, this method is called semi-empirical. Different semi-empirical methods use different numbers and types of parameters, which affect the quality of the calculation.

Semi-empirical can be distinguished by two main categories, one of which is restricted to π electrons only, another of which is restricted to all valence electrons. An example of the former category is the Hückel method, which replaces the problem of organic π -conjugated system with one-electron Hamiltonian whose terms are empirically determined. The approximation applied in the latter category is considering only the valence electrons from the s and p atomic orbitals. This category is by far the larger group of methods, which include MNDO, AM1, PM3, etc.

Although more sophisticated than Molecular Mechanics methods, the ability to avoid solving the entire problem still makes Semi-empirical methods comparatively cheap. They can be applied to systems with hundreds of atoms and provide the information about molecular orbitals. The main disadvantage, as in the case of Molecular Mechanics, is that the answers it provides are only as good as the empirical parameters

used. In addition, it is not possible to compute all molecules using this method based on the fact that there are not suitable parameters for some atoms in those molecules.

1.1.6 PRACTICAL CONSIDERATION

From discussion above, we know that there are a number of approximations and other mathematical representations including a concept known as basis sets that are used in the computation. Just like the following table shows, with higher the level of theory and larger of basis sets, we can better approximates the "true" solution to Schrödinger's equation, but it is computationally more difficult and more "expensive".

<i>Basis Set Type</i>	<i>Electron Correlation</i> →					...	Full CI
	HF	MP2	MP3	MP4	QCISD(T)		
Minimal						...	
Split-Valence						...	
Polarized						...	
Diffuse						...	
High ang. momentum						...	
...
∞	<i>HF Limit</i>					...	Schrödinger Equation

1.1.6.1 CHOICE OF THEORY AND BASIS SET FOR MODEL SYSTEM

For a model system where the *ab initio* calculation will be applied, the appropriate choice of level of theory depends on the problem to be solved, especially the type on the type of bonding involved.¹⁹ In some cases, Hartree-Fock theory is too simple to model a system accurately. In other cases, the use of high level electron correlation is

unnecessary. Similarly, the discretion from the computational chemist is also required for the choice of basis set. In some cases, a small basis set is not sufficient for accurate results. In other cases, the use of too large of a basis set will not really improve the accuracy of the results while it does lead to a substantially longer calculation. Finding an effective tradeoff between desired accuracy and the finite available computing resources is very important for a computational chemist.

1.1.6.2 HYBRID CALCULATION WITH ONIOM MODEL

High accuracy model chemistry scales unfavorably with the size of the molecule, which gives rise to a practical limit on how large a system can be studied and therefore places many systems of chemical and biological interest out of reach of traditional approaches. In order to overcome these limitations, a hybrid method called ONIOM²⁰ (*Our own N-layered Integrated molecular Orbital and molecular Mechanics*) has been devised. In principle, ONIOM is a kind of QM/MM method, in which atoms that are most important are treated with quantum mechanics (QM) and the rest by molecular mechanics (MM). In practice, ONIOM, this onion skin-like extrapolation method, divides the large molecules into two or three layers that are treated at different levels of accuracy, and the results are then automatically combined into the final predicted results. For instance, for a two-layer ONIOM system shown below, the energy of the real system at the high level can be estimated as:

$$E(\text{high}, \text{real}) \approx E(\text{ONIOM}, \text{real}) = E(\text{high}, \text{model}) + E(\text{low}, \text{real}) - E(\text{low}, \text{model})$$

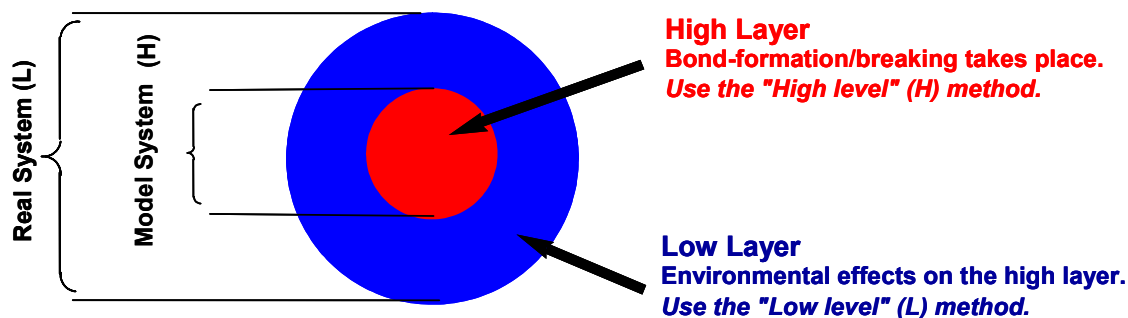


Figure 1.1 Diagram of two-layer ONIOM model

It has been shown that the predictions from ONIOM method are essentially equivalent to those that would be produced by the high accuracy method alone on the entire large system.

1.2 CALCULATION OF CHEMICAL SHIFT

In this section, we will briefly discuss the quantum chemical nuclear magnetic resonance (NMR) chemical shift calculation, which facilitates interpretation of the NMR spectroscopy and provides the missing connection between the experimental measure NMR shifts and the structural parameters of interest.

1.2.1 BASIC ASPECTS OF CHEMICAL SHIFT

The chemical shift has its origin in the magnetic shielding²¹ produced by electrons. As magnetic particles, electrons' motion is influenced by the imposition of an external field (B). According to Lenz's law, this motion induced by an applied field is in a

direction as to oppose that field. Therefore, the magnetic field at the nucleus can be written as:

$$B_{nucleus} = B - \sigma B = (1 - \sigma)B$$

where σ is the shielding factor. Based on Lamb's equation, this shielding factor is related to the electron density ρ at a distance r from the nucleus:

$$\sigma = \frac{4\pi e^2}{3mc^2} \int_{-\infty}^{\infty} r \rho(r) dr$$

Since the ability of the magnetic factor to influence the motion of electrons depends on the orientation of the molecule relative to the external field B , we can define three mutually orthogonal axes within the molecule such that σ may be expressed in terms of three principal components, σ_{11} , σ_{22} , and σ_{33} . Rapid, random tumbling of molecules will lead to an averaging of the shielding interactions to an isotropic shift tensor, which is given by:

$$\sigma_{iso} = \frac{1}{3}(\sigma_{11} + \sigma_{22} + \sigma_{33})$$

Although the shielding tensor is the most physically fundamental object in NMR theory, relative shifts are the quantities actually used in interpreting spectra, and these relative shifts are defined by:

$$\delta = \sigma_{ref} - \sigma$$

where σ_{ref} is the shielding of the chosen reference compounds, e.g., tetramethylsilane (TMS) for ^1H , ^{13}C , and ^{29}Si NMR.

1.2.2 CALCULATION METHODS FOR CHEMICAL SHIFT

For the splitting of the nuclear spin energy levels in the presence of an external magnetic field, we can obtain:

$$\Delta E = -m_J B_{nucleus} = -m_J(1 - \sigma)B$$

where m_J is the nuclear magnetic moment. This splitting is not only proportional to the external field B but also to the shielding tensor σ . As the shielding tensor is a second-order property with respect to the two “perturbations” B and m_J , we can obtain this shielding tensor by the corresponding second derivative of the electronic energy²²⁻²⁴:

$$\sigma = \left(\frac{dE_{electronic}}{dB dm_J} \right)_{B, m_J=0}$$

In practice, Ramsey used second-order perturbation theory to develop a formula that in principle accounts for the shielding factor:

$$\sigma = \sigma_D + \sigma_p$$

where σ_D represents diamagnetic shielding, the first-order term which can be calculated from the ground electronic state, while σ_p represents paramagnetic shielding, the second-order term which requires the knowledge of excited state wave function and energies of those excited states. In this theory, the external magnetic field is represented by a magnetic vector potential, and attention should be paid that σ is gauge-invariant, independent of the origin of the magnetic vector potential (gauge origin). GIAO (gauge-including atomic orbitals) method is the most popular one which satisfies the gauge-origin independence by including the gauge factor in the basis sets. On the other hand,

CSGT (continuous set of gauge transformations) method circumvents the gauge-origin dependence by using a continuous set of gauge transformations. In CSGT method, the nuclear magnetic tensor, expressed in terms of the induced current density, is written as:

$$\sigma_{\alpha\beta} = -\frac{1}{cB} \int d\vec{r}_N [\vec{r}_N \times j_{\beta}^{(1)}(\vec{r}_N) / r_N^3]_{\beta}$$

where $j_{\beta}^{(1)}(\vec{r})$ represents the induced first-order current density, and r_N represents the position vector of electron from nuclear N.

1.2.3 PRACTICAL CONSIDERATION

Just like the calculation of the energy of a molecule using *ab initio* techniques, computational chemist needs to choose the level of theory and basis set to calculate the chemical shift. In most case, the calculation of chemical shift requires a more elaborate representation of the electronic structure to accurately represent the shielding of the nucleus. Consequently, the computational level of theory applied must be sufficient, and the basis set employed must be of adequate size. As noted before, the calculation of paramagnetic shielding σ_p incorporates both ground and excited state. So very often, DFT is employed in the calculation of chemical shift as it has been demonstrated to calculate excited states more accurately than standard Hartree-Fock procedure. Furthermore, a basis set of at least triple split valence and at least one set of polarization function is needed.

REFERENCES

- (1) Schiff, L. I., *Quantum Mechanics*; McGraw-Hill, New York, **1968**.
- (2) Levine, I. N., *Quantum Chemistry*; 4th ed., Prentice-Hall, Englewood Cliffs, NJ, **1991**.
- (3) Grant, G.; Richards, W., *Computational Chemistry*; Oxford, New York, **1994**.
- (4) Hinchliffe, A., *Modelling Molecular Structure*; John Wiley and Sons, New York, **1994**.
- (5) Atkins, P. W.; Freidman, R. S., *Molecular Quantum Mechanics*; 3rd ed., Oxford, New York, **1997**.
- (6) Szabo, A.; Osterlund, N., *Modern Quantum Chemistry*; Dover, Mineola, **1996**.
- (7) Schrödinger E., *Ann. Physik* **1926**, 79,361.
- (8) Born, M.; Oppenheimer, J. R., *Ann. Physik* **1927**, 84, 457.
- (9) Davidson, E. R.; Feller, D., *Chem. Rev.* **1986**, 86, 681.
- (10) Huzinaga, S.; Andzeim, J.; Klobukowski, M.; Radzio-Andzeim, E.; Sakai, Y.; Tatewaki, H., *Gaussian Basis Sets for Molecular Calculations*; Elsevier, Amsterdam, **1984**.
- (11) Roothaan, C. C. J, *Rev. Mod. Phys.*, **1951**, 23, 69.
- (12) Hall, G. G., *Proc. Roy. Soc. (London)* **1951**, A205, 541.
- (13) Cizek, J., *Adv. Chem. Phys.* **1969**, 14, 35.
- (14) Purvis, G. D.; Bartlett, R. J., *J. Chem. Phys.* **1982**, 76, 1910.
- (15) Pople, J. A.; Head-Gordon, M.; Raghavachari, K., *J. Chem. Phys.* **1987**, 87, 5968.
- (16) Moller, C.; Plesset, M. S., *Phys. Rev.* **1934**, 46, 618.
- (17) Hohenberg, P.; Kohn, W., *Phys. Rev.* **1964**, 136, B864.
- (18) Kohn, W.; Sham, L. J., *Phys. Rev.* **1965**, 140, A1133.

- (19) Foresman, J.; Frisch, A., *Exploring Chemistry with Electronic Structure Methods*; 2nd ed., Gaussian Inc., Pittsburg, **1996**.
- (20) Dapprich, S.; Komáromi, I.; Byun, K. S.; Morokuma, K.; Frisch, M. J., *J. Mol. Struct. (Theochem)* **1999**, 462, 1.
- (21) Becker, E. D., *High Resolution NMR Theory and Chemical Application*; 3rd ed., Academic Press, London, **2000**.
- (22) Helgaker, T.; Jaszunski, M.; Ruud, K., *Chem. Rev.* **1999**, 99, 293.
- (23) O'Reilley, D. E., *Prog. Nucl. Magn Reson. Spectrosc.* **1967**, 2, 1.
- (24) Gauss, J.; Stanton, J. F., *Adv. Chem. Phys.* **2002**, 123, 355

CHAPTER II

CHARACTERIZATION OF ENZYMATIC INTERMEDIATES IN TRYPTOPHAN SYNTHASE VIA SOLID-STATE NMR, X-RAY CRYSTALLOGRAPHY AND AB INITIO CALCULATIONS

ABSTRACT

The pyridoxal-phosphate(PLP)-dependent tryptophan synthase $\alpha_2\beta_2$ bienzyme complex catalyses the last two steps in the synthesis of L-Trp. The absence of a synthetic pathway for L-Trp in higher animals and in humans makes the tryptophan synthase nanomachine a potential target both for the development of herbicides, and for the design of drugs to treat infectious disease. Understanding the molecular basis of substrate channeling and the catalytic mechanisms of the α - and β -subunits could provide useful insights for developing tryptophan synthase as an important target for drug design, or for the development of herbicides, while chemical level details such as protonation and hybridization states are critical for understanding enzymatic mechanism and function. In this study, we make use of solid-state NMR, X-ray crystallography, and *ab initio* theory to characterize enzymatic quinonoid intermediate in tryptophan synthase. The substrate ^{13}C and ^{15}N chemical shifts allow unambiguous identification of this key species for which various models of charge and protonation states can be distinguished by their calculated effect on the observed chemical shifts, allowing us to choose the chemical

species most consistent with the experimental results. These support the ketoenamine and dipolar forms that are in fast exchange to each other in quinonoid intermediate, which we believe has mechanistic implications.

2.1 INTRODUCTION

The pyridoxal-phosphate (PLP)-dependent tryptophan synthase (TS) $\alpha_2\beta_2$ holoenzyme complex (Figure 2.1) catalyses the last two steps in the synthesis of L-Trp¹ (Figure 2.2A), consecutive processes that require channeling of the common metabolite, indole, between the α - and β -subunits (Figure 2.2B). Indole channeling is regulated by allosteric interactions that switch the enzyme between open, low activity, and closed, high activity, states during the catalytic cycle.^{2, 3} In the α -site, 3-indole-D-glycerol-3'-phosphate (IGP) is cleaved to D-glyceraldehyde-3-phosphate (G3P) and indole. In stage I of the β -reaction (Figure 2.2A), L-Ser reacts with the internal aldimine, E(Ain), giving in sequence gem-diamine, E(GD₁), L-Ser external aldimine, E(Aex₁), quinonoid, E(Q₁), and aminoacrylate Schiff base, E(A-A), species and a water molecule. In stage II (Figure 2.2A), indole, channeled from the α -site, makes a nucleophilic attack on E(A-A) giving E(Q₃), E(Aex₂), E(GD₂) intermediates and finally product, L-Trp. Nucleophilic analogues of indole, such as indoline⁴ and 2-aminophenol⁵ (2-AP) will substitute for indole in the formation of quinonoid species. 2-AP reacts with E(A-A) to give a stable

quinonoid species, $E(Q)_{2-AP}$, which does not appear to appear to turnover to the corresponding amino acid⁶. The allosteric regulation of substrate channeling has been investigated extensively^{3, 7-13}. Allosteric interactions are mediated by substrate binding to the α -site and the interconversion of covalent intermediates, $E(Aex_1)$, $E(A-A)$, $E(Q)$, and $E(Aex_2)$ at the β -site and by the binding of a monovalent cation (MVC) to the β -subunit. The function of this allosteric signaling is to achieve synchronization of the activities of the α - and β -sites by switching the α - and β -subunits between open conformations of low activity and closed conformations of high activity, and to prevent the escape of the channeled intermediate, indole.

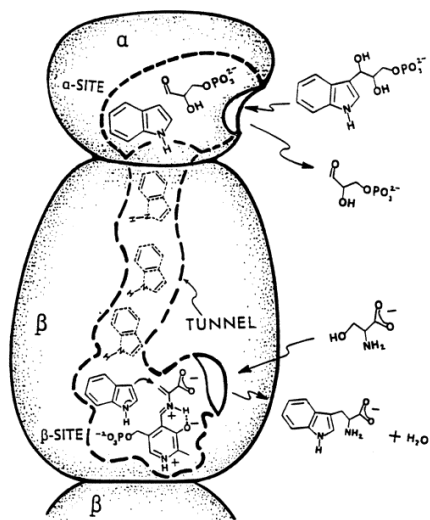
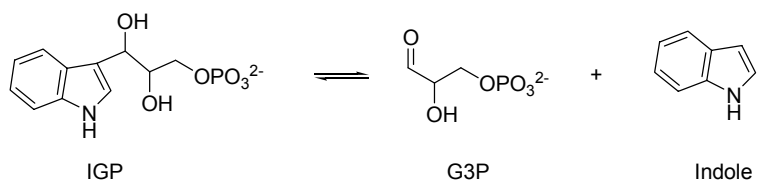


Figure 2.1. α - and β -subunits of an $\alpha\beta$ -dimeric unit of the tryptophan synthase tetramer

A α site reaction



B β site reaction

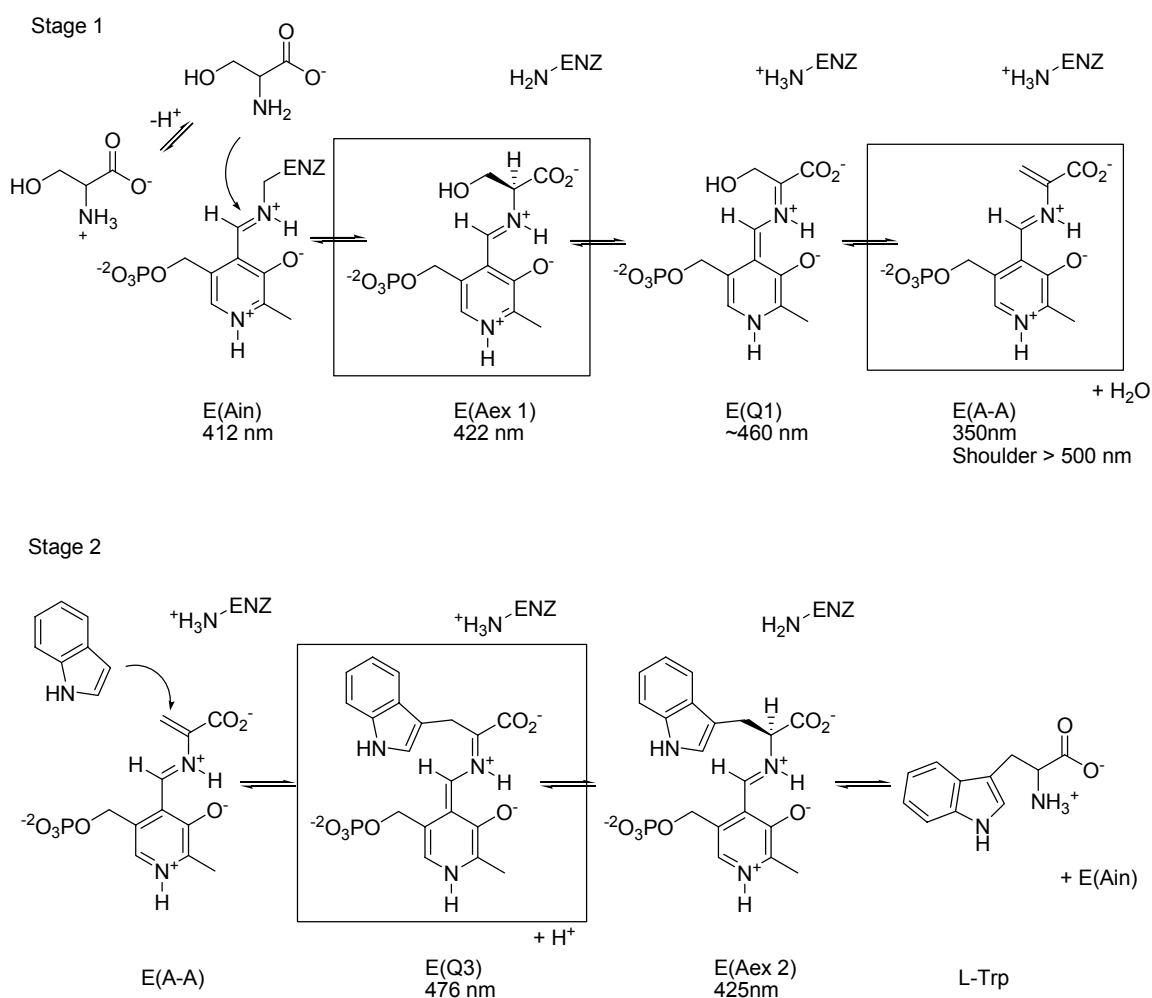


Figure 2.2. Organic structures of reactants, products, and intermediates identified in the tryptophan synthase α - and β -reaction. Equilibria favoring the boxed intermediates can be established by varying the experimental conditions of pH and α -site ligand.

Recent X-ray structure determinations of complexes with substrates, intermediates, and substrate analogues^{2, 3, 6} have resulted in a significant break through concerning identification of the linkages between the bienzyme complex structure, catalysis at the α - and β -active sites, and the allosteric regulation of substrate channeling. This effort combined organic synthetic work and solution kinetic/spectroscopic studies with X-ray crystal structure determinations of 10-15 different ligand complexes with tryptophan synthase^{4, 10}. Despite these successes, significant chemical questions remain as the resolution of the X-ray structure does not allow for a detailed chemical mechanism to be established for the substrate transformation.

Solid-state NMR is particularly promising for studying the chemical structure of enzymatic intermediates^{14, 15} as it allows for NMR data to be acquired under the same conditions that are used for X-ray crystallography, and complementary structural information to be obtained. Initial work by Schaefer¹⁶ showed that by supplying labeled L-[3-¹³C]Ser as a substrate, solid-state ¹³C NMR spectroscopy could identify the aminoacrylate E(A-A) Schiff base intermediate in the crystalline state. Here we show that the additional intermediates, E(Q)_{indoline} and E(Q)_{2-AP}, can be characterized by solid-state NMR under conditions identical to those used to solve for the X-ray crystal structure. While the analysis of the chemical shifts and absorption maxima for intermediates derived from reaction of ¹³C and ¹⁵N-substituted L-Ser gives unambiguous identification of E(Q) species, further insights into the protonation state and distribution of these species can be obtained by combining both the X-ray and spectroscopic data with *ab initio* calculations. In this case, various models of charge and protonation states can be

distinguished by their calculated effect on the observed chemical shifts, allowing us to choose the chemical species for each intermediate that is most consistent with the experimental results. These calculations support the the ketoenamine and dipolar forms that are in fast exchange to each other, which we believe has mechanistic implications.

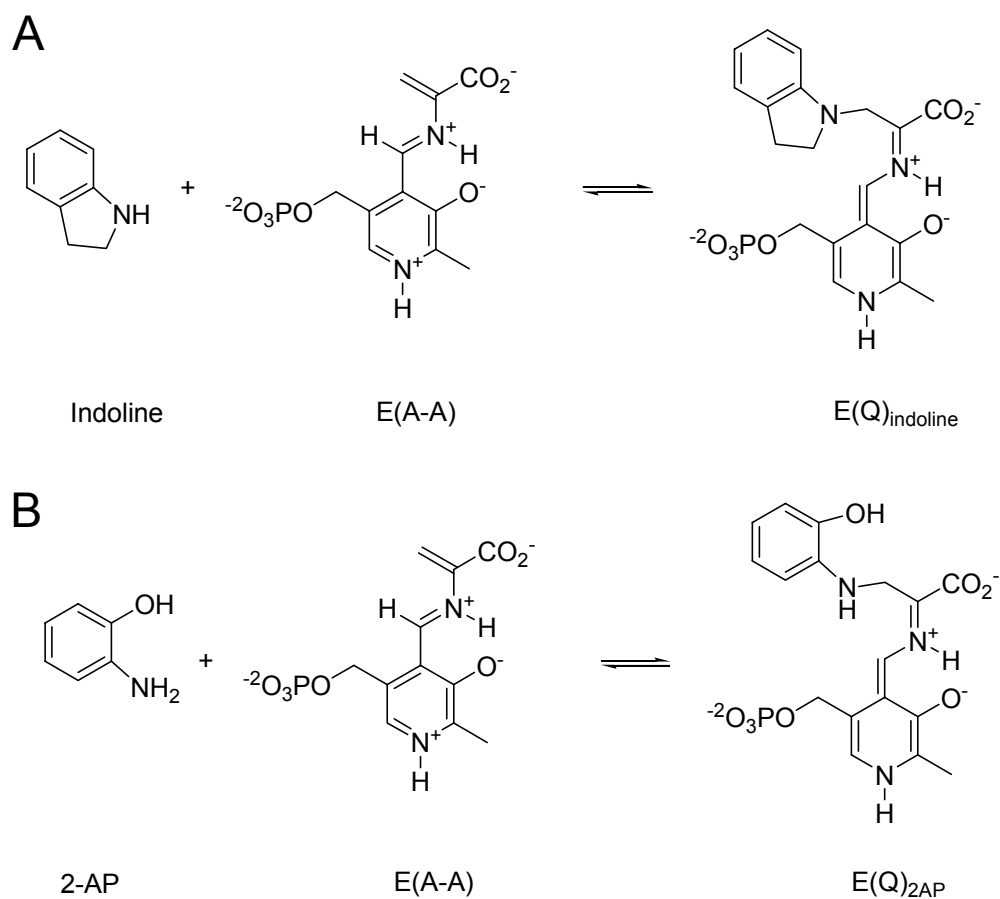


Figure 2.3. Quinonoid intermediates. Reaction of the indole analogue, indoline and 2-aminophenol, with E(A-A) to give the indoline quinonoid and 2-AP quinonoid intermediates.

2.2 MATERIALS AND METHODS

2.2.1 MATERIALS

Tryptophan synthase was purified as previously described¹⁷. Microcrystals were prepared by diluting enzyme solution 1:1 with T-buffer containing 12-14% Polyethylene Glycol 8000 (PEG 8000) and 1.5 mM Spermine. Microcrystals were collected and washed with 50 mM Triethanolamine (TEA), pH 7.8 containing 20% PEG 8000, 1.5 mM Spermine, and supplemented with ligands unique to each experiment, i.e. NaCl, CsCl, N-(4'-trifluoromethoxybenzoyl)-2-aminoethyl phosphate (F9), indoline, or 2-AP. Magic-angle-spinning rotors were packed with approximately 16-19 mg of protein. A concentrated solution of unlabeled (Sigma) or labeled (Cambridge Isotope Labs) L-Ser in 50 mM TEA, pH 7.8 was added immediately prior to data collection.

2.2.2 SOLID-STATE NMR

Magic-angle-spinning (MAS) NMR spectra were acquired on a Bruker DSX 400 Spectrometer (400.42 MHz ¹H; 100.70 MHz ¹³C) using a double resonance 4 mm MAS probe (sample volume ~ 80 μ l) and a MAS rate of 8 kHz. Sample temperatures were maintained using a Kinetics XRII851 Sample Cooler. 83 kHz ¹H and 50 kHz ¹³C $\pi/2$ pulses were used along with either low power (20 kHz) or high-power (83 kHz) ¹H decoupling during acquisition. 1D ¹³C spectra were acquired beginning with either a single carbon channel pulse and low-power decoupling (64 scans in 4 min 40 sec) or

cross-polarization from ^1H with high-power decoupling (4096 scans in 4 hours 36 min 50 sec or 2048 scans in 2 hours 18 min 25 sec; CP: 1 ms contact time, 50 kHz ^1H spin-lock, 50% - 100% linearly ramped ^{13}C match). These experiments were alternated for at least 24 hrs with the former reporting predominantly on free ligand and reaction products in solution, and the later reporting on immobilized (solid) species. In both experiments, 2048 complex time points were sampled with a spectral width of 50 kHz and averaged with a relaxation delay of 4 s. Data sets were zero-filled to 4k complex time points and processed with 50 Hz exponential line broadening for the cross-polarization experiments. No line broadening was used for the one-pulse experiments. Spectra were graphically aligned to the unlabeled control spectrum which was referenced via an external adamantane standard with a downfield shift of 38.48 ppm from TMS. As well, 1D ^{15}N spectra were acquired beginning with cross-polarization from ^1H with high-power decoupling, and referenced to NH_4Cl with downfield shift of 39.27 ppm from ammonia.

2.2.3 AB INITIO CALCULATIONS

Molecules were optimized to their ground state geometries using ONIOM calculations¹⁸, in which the protein side chains near the active site are modeled with semi-empirical methods and the substrate is treated with full *ab initio* methods. PM3 was selected for the semi-empirical calculation, and *ab initio* calculations were performed at the density functional theory (DFT) using the B3LYP functional¹⁹⁻²¹ with standard 6-31G(d,p) basis. In the ONIOM calculations, all non-hydrogen atoms in the protein side-

chains are fixed at their crystallographic coordinates, while the protons on the side chains and minimal constraints derived from the X-ray crystal structure were implemented to substrate as discussed below. NMR chemical shifts were calculated at B3LYP/6-311++G(d,p) level with the gauge-including atomic orbital (GIAO) method. Calculated ^{13}C and ^{15}N chemical shifts were reference to benzene (^{13}C chemical shift at 128.0 ppm from TMS) and urea (^{15}N chemical shift at 79.4 ppm from NH_3), optimized and calculated at the same level of theory and basis sets. All the calculations were performed with Gaussian 03 software package²².

2.3 RESULTS AND DISCUSSION

2.3.1 BACKGROUND

Recent studies have advanced our understanding of the relationship between the conformational states of the tryptophan synthase α - and β -subunits, the catalytic mechanisms of the α - and β -sites, and the allosteric regulation of substrate channeling⁷. Structures of the wild-type enzyme are now available for the open conformations of the E(Ain) and E(Aex₁) species with a variety of ligands bound to the α -site, and for the closed conformation of the $\alpha\beta$ -dimeric unit of E(A-A) species with GP bound to the α -site³. Additionally, there are structures available for several mutant enzymes and their complexes^{6, 23, 24}. Of particular note are the structures of the E(Aex₁) form of βK87T mutant with closed $\alpha\beta$ -dimeric units²⁴. However, the structures of quinonoid species

have eluded determination, and thus these structures are an important missing component of the tryptophan synthase structure-function puzzle. Surprisingly, although there are numerous examples of near atomic resolution structures of PLP-enzyme-bound chemical intermediates (principally Schiff base species), there are few examples of quinonoid intermediates. The determination of structures of E(Q) species at or near atomic resolution with the β -subunit in the closed conformation is critically important for understanding both the chemical mechanism of catalysis and the regulation of channeling. To stabilize crystalline E(Q) intermediates in the closed β -subunit conformation, we adopted a strategy that involves the use of Cs^+ in combination with a tight-binding α -site ligand, N-(4'-trifluoromethoxybenzenesulfonyl)-2-aminoethyl phosphate (F9) to shift the equilibrium distribution of species in favor of the closed conformations³. As was shown, the Cs^+ form of the E(Q)_{indoline} species with F9 bound to the α -site, gives a protein complex with both the α - and the β -subunits in the closed conformation allowing us to report the X-ray structure of the tryptophan synthase E(Q) species, E(Q)_{indoline}⁴.

As for other PLP-requiring enzymes, the identification of intermediates in the β -reaction catalyzed by tryptophan synthase has principally relied upon the comparison of UV/Vis absorption spectra of model compounds with the spectra observed for enzyme-bound species. UV/Vis spectroscopy conducted in combination with kinetic methods (e.g., rapid-scanning stopped-flow), made possible relatively unambiguous assignments of the chemical structures of intermediates along the reaction pathway²⁵.

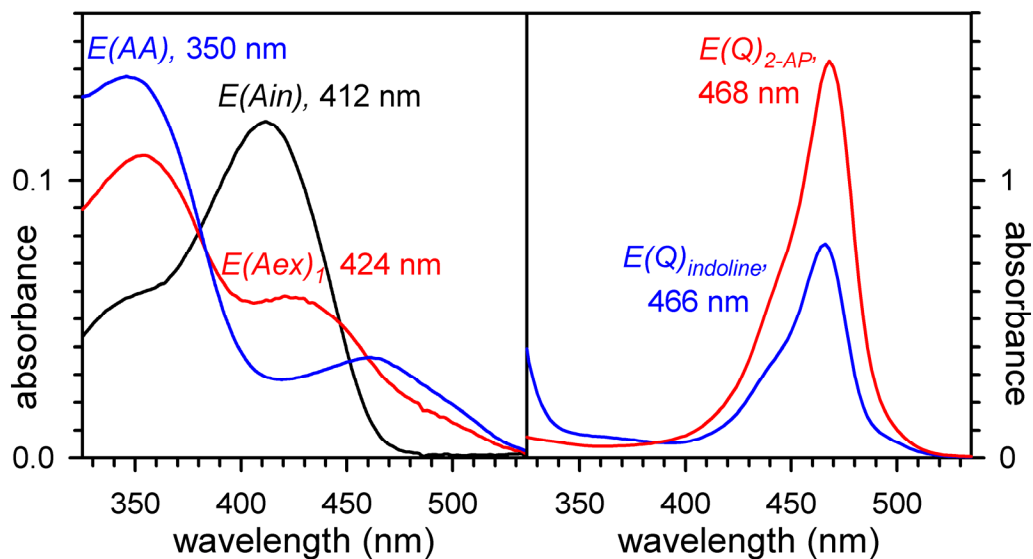


Figure 2.4. UV/Vis spectra of intermediates. Solution UV/Vis spectra for the reaction of 15 μM tryptophan synthase E(Ain) with 50 mM L-Ser (left panel) in the presence of 100 mM NaCl (red spectrum) or 100 mM CsCl and 2 mM F9 (blue spectrum). The right panel shows the reaction of enzyme with L-Ser and either 5 mM Indoline (blue spectrum) or 2 mM 2-AP (red spectrum), both in the presence of 100 mM CsCl and 2 mM F9

The solution UV/Vis spectra depicted in Figure 2.4 compare the reaction of TS with 50 mM L-Ser measured in the presence of 100 mM NaCl with the same reaction measured in the presence of 100 mM CsCl and 2 mM F9 (left panel). The figure illustrates that the binding of Cs^+ in combination with a tight-binding ASL (i.e. F9) shifts the equilibrium of enzyme-bound intermediates at the β -site in favor of the α -aminoacrylate Schiff base, E(A-A), species with $\lambda_{\text{max}} \sim 350$ nm. The right panel shows that in the presence of Cs^+ and F9, both indoline and 2-Aminophenol (2-AP) react with E(A-A) to produce almost

exclusively quinonoidal intermediates, $E(Q)_{\text{indoline}}$ and $E(Q)_{2\text{-AP}}$, with λ_{max} at 466 and 468 nm, respectively.

While providing insight into the chemical species present, the protonation states and/or tautomeric states of the critical quinonoid intermediate remain ambiguous, particularly regarding protonation of the PLP ring N, the position of the proton shared between the pyridine hydroxyl O and the Schiff base N in aldimine species, and the carboxylic acid. In this study, we identify conditions that cause quinonoid intermediate in the solid (crystalline) state to persist over long time periods with high site occupancy. These are the indoline quinonoid species, $E(Q)_{\text{indoline}}$ (Figures 2.5) and the 2-AP quinonoid species, $E(Q)_{2\text{-AP}}$ (Figures 2.6). Furthermore, the NMR chemical shifts allow us to identify the chemical species and to make reasonable conclusions about the protonation states in this intermediate.

2.3.2 THE PYRUVATE SIDE REACTION AND STRATEGY FOR ASSIGNING THE MAS ^{13}C NMR SPECTRA

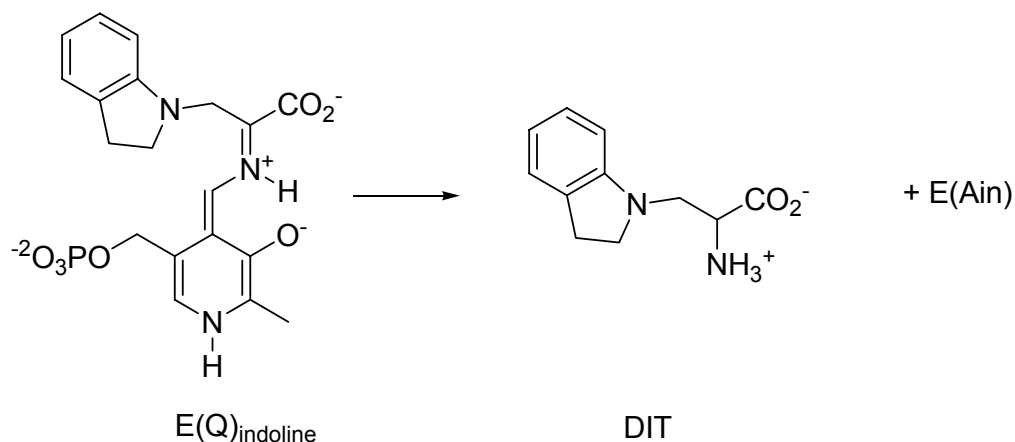
Efforts to prepare stable intermediates in stages I and II of the tryptophan synthase β -reaction for structural analysis are complicated by the side reaction in which L-Ser is converted to pyruvate and NH_4^+ . In the absence of indole, the $E(\text{A-A})$ intermediate formed from reaction of L-Ser with $E(\text{Ain})$ undergoes a slow conversion to pyruvate, ammonium ion¹²:

species immobilized in the microcrystals are necessary for rigorous assignment. Non-specifically bound species almost always lack kinetic competence; therefore, kinetic studies can distinguish between the intermediates of interest and non-specifically bound species. During the course of the experiments reported here, the mother liquor component of the NMR sample rotor was monitored both to insure that ample L-Ser was available to saturate the enzyme sites, and to monitor progression of pyruvate and pyruvate-derived side-product accumulation during data acquisition. These time courses were then compared to those for the changes in the amplitudes of peaks detected in the solid-state spectra to assist identification of enzyme-bound intermediates. The necessary time courses were obtained by alternating solid-state acquisitions (2.3-4.6 hr blocks) with analysis of the mother liquor (~5 min blocks) as outlined in the MATERIALS AND METHODS section.

2.3.3 ASSIGNMENTS OF QUINONOID INTERMEDIATE VIA SOLID-STATE NMR SPECTROSCOPY

The tryptophan synthase catalytic mechanism has long been known to involve quinonoid intermediates²⁶⁻²⁸ in stages I and II of the β -reaction (Figure 2.2 B). The unusually intense ($\epsilon_{\max} > 30,000 \text{ M}^{-1}\text{cm}^{-1}$) absorbance bands make these species easily detectable by UV/Vis spectroscopy. However, until recently⁴, no X-ray structure of a tryptophan synthase quinonoid species has been published. The L-Ser quinonoid and L-Trp quinonoid species are transient species that rapidly form and decay, and these species do not accumulate as stable species in either stage I or stage II of the β -reaction. Roy et

al.²⁹ reported that the indole analogue, indoline, undergoes a rapid reaction with E(A-A) to give a quasi-stable quinonoid species, E(Q)_{indoline}, which only slowly turns over to the corresponding amino acid, dihydroiso-L-Trp (DIT).



The indoline reaction has been used extensively to test the mechanism of nucleophile reaction with E(A-A)^{2, 3, 13, 25} and to investigate the allosteric regulation of substrate channeling^{9, 13, 25, 30-32}. Aniline^{12, 13, 23, 25} and 2-aminophenol (2-AP)⁶ also form quinonoid species. The 2-AP system is particularly interesting in that this indole analogue exhibits the highest affinity of any reported nucleophile for the E(A-A), giving a quinonoid, E(Q)_{2-AP}, with an $\epsilon_{\text{max}} > 40,000 \text{ M}^{-1} \text{ cm}^{-1}$ (manuscript in preparation). We have been unable to demonstrate any turnover of E(Q)_{2-AP} to the corresponding new amino acid.

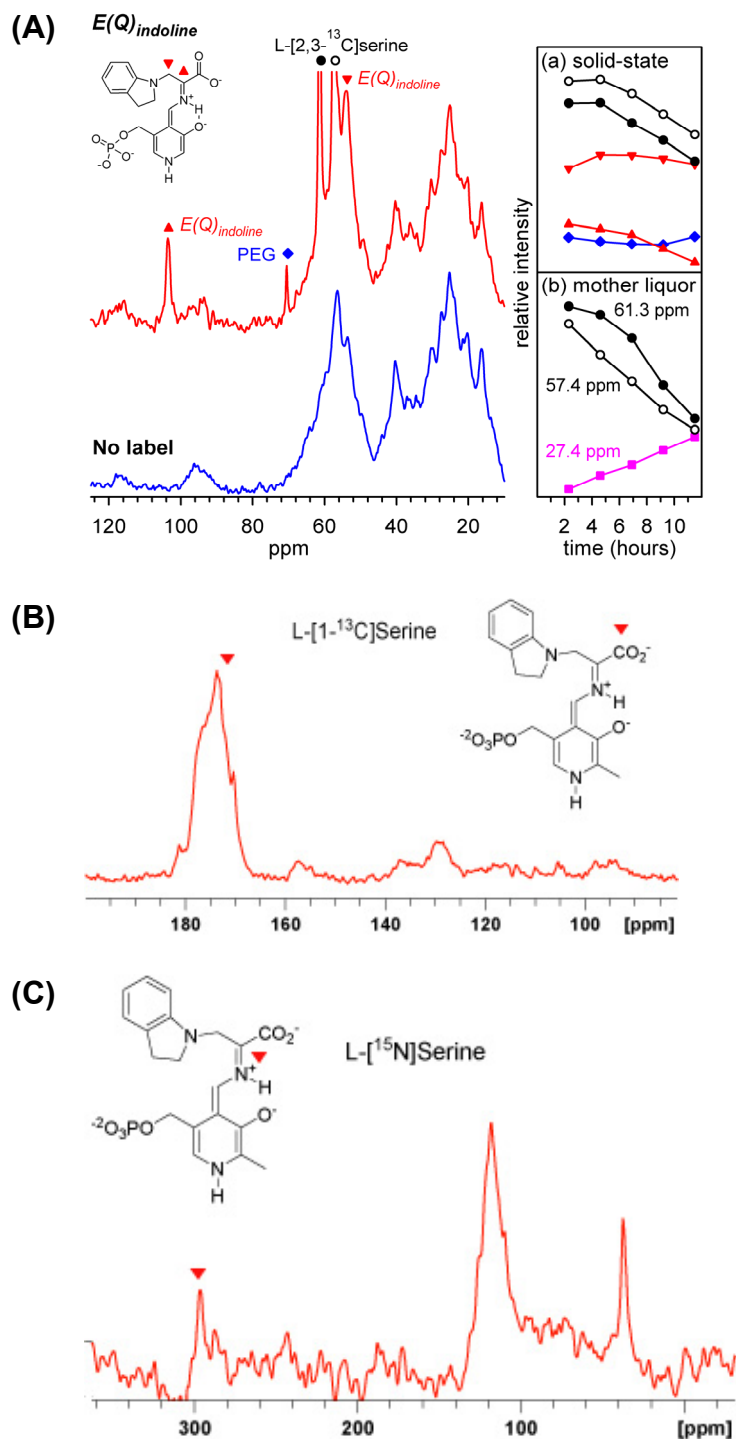


Figure 2.5. The solid-state NMR spectra (red) of *E(Q)*_{indoline}. (A) from L-[2,3-¹³C]Ser Vs. unlabeled L-Ser, (B) from L-[1-¹³C]Ser, and (C) from L-[¹⁵N]Ser

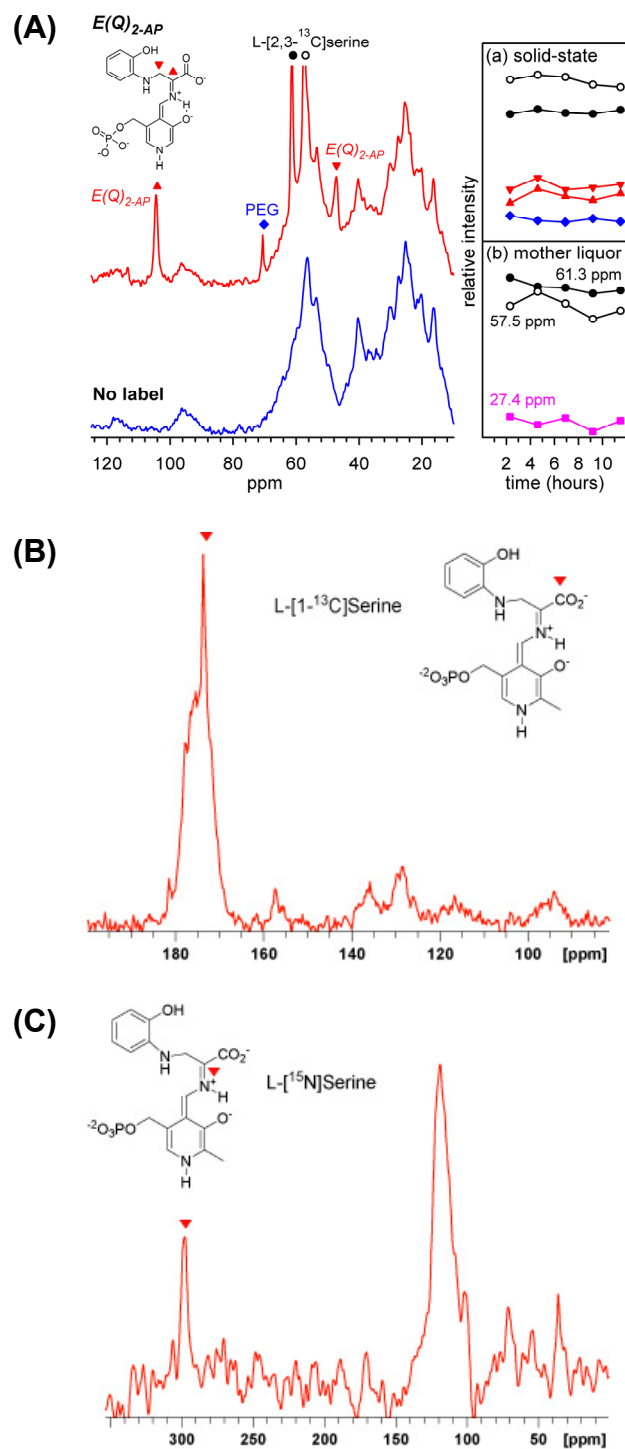


Figure 2.6. The solid-state NMR spectra (red) of *E(Q)*_{2-AP}. (A) from L-[2,3-¹³C]Ser Vs. unlabeled L-Ser, (B) from L-[1-¹³C]Ser, and (C) from L-[¹⁵N]Ser

Chemical Species	Chemical Shift (ppm)			
	CA	CB	CO	N
E(Q) _{indoline}	103.6	54.1	173.0	296.5
E(Q) _{2-AP}	104.4	47.3	173.1	296.9

Table 2.1. Summary of Solid-state NMR Chemical Shifts of E(Q)_{indoline} and E(Q)_{2-AP} Species

Figure 2.5(A) (main panel) shows the solid-state ¹³C-NMR spectrum of the reaction of tryptophan synthase microcrystals with 100 mM L-[2,3-¹³C]Ser and ~12 mM indoline measured in the presence of 2-3 mM F9 and 100 mM CsCl (top spectrum) collected at -10°C and averaged over 11.6 hrs. These conditions favor accumulation of the enzyme-bound quinonoid intermediate, E(Q)_{indoline} species. The resonances from the enzyme-bound intermediate appear in the spectrum together with several resonances from immobilized species. Assignments are summarized in Table 2.1. Time courses for both the solid-state and mother liquor peaks (Figure 2.5A minor panel) allowed assignment of the peaks (Table 2.1). The resonance at 103.6 ppm (red triangle) and 54.1 ppm (inverted red triangles) are identified as the sp²-hybridized 2-¹³C and the sp³-hybridized 3-¹³C of E(Q)_{indoline} intermediate, respectively. The resonances assigned to E(Q)_{indoline} are stable only as long as sufficient L-Ser and indoline are present. On longer timescales the peaks at 103.6 ppm and 53.9 ppm disappear as substrates are depleted. The disappearance of labeled L-Ser (white and black circles) occurs at a much faster rate than the appearance of pyruvate (pink squares, 27.4 ppm). This behavior is consistent both with turnover of indoline to dihydroiso-L-Trp (DIT), and with maintenance of the E(Q)_{indoline} intermediate

in the closed conformation, which suppresses the pyruvate side reaction. Resonances at 70.6 ppm (blue diamonds), at 57.4 ppm (black open circles) and 61.3 ppm (black circles) (main panel) are identified as natural abundance PEG8000 and 2-¹³C/3-¹³C labeled L-Ser, respectively, non-specifically bound to the microcrystals.

Figure 2.5(B) shows a solid-state ¹³C-NMR spectrum of E(Q)_{indoline} intermediate collected under conditions similar to those used in Figure 2.5(A), but with 100 mM L-[1-¹³C]Ser. The resonance at 173.0 ppm has been identified as the 1-¹³C E(Q)_{indoline} intermediate through the same assignment strategy. Figure 2.5(C) is the solid-state ¹⁵N-NMR spectrum of E(Q)_{indoline} intermediate, in which the resonance at 296.5 ppm has been assigned to the ¹⁵N E(Q)_{indoline} intermediate.

Figure 2.6(A) (main panel) shows the solid-state ¹³C-NMR spectrum of the reaction of tryptophan synthase microcrystals with 40 mM L-[2,3-¹³C]Ser and 20 mM 2-AP in the presence of 2-3 mM F9 and 100 mM CsCl (top spectrum) collected at -10°C and averaged over 11.6 hrs. Accumulation of the enzyme-bound quinonoid, E(Q)_{2-AP}, intermediate is favored by these conditions. The identity and assignment of resonances derived from the bound and immobilized species are summarized in Table 2.1. The resonances at 104.4 ppm (red triangles) and 47.3 ppm (inverted red triangles) are identified as the sp²-hybridized 2-¹³C and the sp³-hybridized 3-¹³C of the E(Q)_{2-AP}, respectively, from the reaction time courses. The stability of E(Q)_{2-AP} is only affected by the turnover of L-Ser to pyruvate; no turnover for the E(Q)_{2-AP} to a new amino acid derived from 2-AP has been observed. Peaks at 70.6 ppm (blue diamonds), 57.5 ppm, (white open circles) and 61.4 ppm (black circles (main panel) are identified as natural

abundance PEG8000 and 2-¹³C/3-¹³C labeled L-Ser, respectively, non-specifically bound to the microcrystals. Again, the resonance at 27.6 ppm (magenta squares) has been assigned to pyruvate. The unassigned peak at 25.5 ppm increases in amplitude with a similar rate that is similar to the appearance of pyruvate and the disappearance of labeled L-Ser. This finding is consistent with a species derived from the pyruvate side-reaction.

The 2-AP reaction with tryptophan synthase was repeated by using L-[1-¹³C]Ser and L-[¹⁵N]Ser, respectively, and the corresponding NMR spectra have been shown in Figure 2.6(B) and Figure 2.6(C). Using the same assignment strategy, we identified the ¹³C resonance at 173.1 ppm as the 1-¹³C E(Q)_{2-AP} intermediate, and assigned the ¹⁵N resonance at 296.9 ppm to the ¹⁵N E(Q)_{2-AP} intermediate.

2.3.4 AB INITIO CALCULATIONS

As shown in Figures 2.5 and 2.6, reaction of the Cs⁺ form of E(Ain) with L-Ser and either indoline or 2-AP converts the crystalline enzyme essentially completely to the corresponding quinonoid species. Further analysis of the time courses for appearance of the ¹³C and ¹⁵N resonances in bound species resulting from ¹³C and ¹⁵N labeled L-Ser provide unequivocal identifications of these species. While the chemical shifts show the presence of the quinonoid intermediate E(Q), the empirical correlation of shift with structure does not provide a complete chemical model. By combining the spectroscopic data with *ab initio* calculations of structures and NMR chemical shifts³³⁻⁴², a significantly more detailed model of charge and protonation states can be proposed and tested by comparison with experimental chemical shifts. For these calculations, both the X-ray

crystal structure and the NMR chemical shifts provide important constraints. The complete protein system is too large to be fully modeled using *ab initio* methods, so heavy atom constraints are derived from the crystal structure to provide a framework for examining the substrate conformation and chemistry. The quality of the model is judged by how well *ab initio* calculations of chemical shifts for these structures agree with the experimental NMR shifts. This combination of X-ray, NMR and *ab initio* data has become quite popular for assigning chemical shifts and refining crystal structures of small organic molecules. Here we show that this approach has remarkable promise for providing chemical level detail of large enzymatic complexes.

The quality of chemical shift calculation depends on both the geometrical parameters and level of theory performed. At first, *ab initio* GIAO calculation shows a great sensitivity of absolute nuclear shielding over the change in geometry, therefore the geometry must be optimized to give rise to a model structure that closely resembles the real structure. Here the computational models investigated are based on the X-ray crystal structure of indoline quinonoid whose PDB ID is 3CEP⁴. The substrate together with the side chains within 8 Å around this substrate are cut out from X-ray crystal structure. The side chains will mimic the whole enzyme system and provide constraints to the optimization of substrate. The protonation of all amino acids of the cut-out side chains is standard. The optimization is calculated at the ONIOM (B3LYP/6-31G**:*PM3*) level of theory. In ONIOM calculations, the full cut-out system is partitioned into two layers, as shown in Figure 2.7. The high layer (ball & stick) corresponds to the interested indoline quinonoid intermediate, which is modeled with *ab initio* methods. The low layer

(wireframe) corresponds to the side chains around the indoline quinonoid, which is treated with semi-empirical methods. The interactions between two layers are included at the PM3 level of theory.

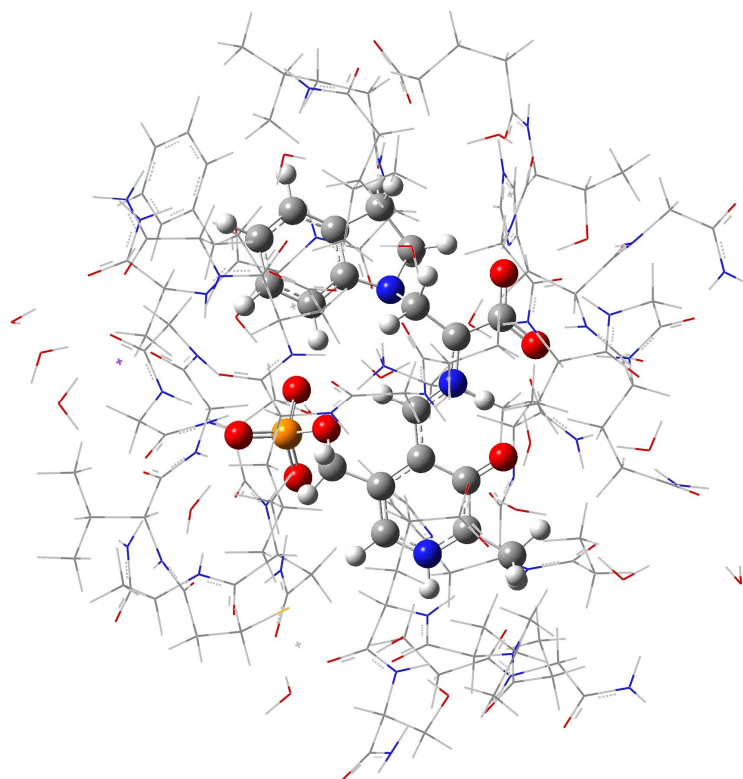
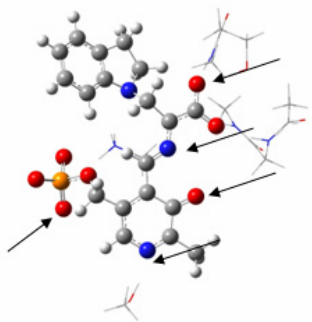


Figure 2.7. ONIOM structure model of indoline quinonoid cut out from X-ray crystal structure (PDB ID: 3CEP). Substrate is shown in ball & stick type, and the side chains are shown in wireframe.

Secondly, the quality of chemical shift calculation is sensitive to the level of theory applied. Therefore, larger basis sets are required to obtain results that are comparable with experiment. In this work, a polarized triple split valence basis sets with diffuse functions, i.e. 6-311++G(d,p), has been used. As is well known, the NMR

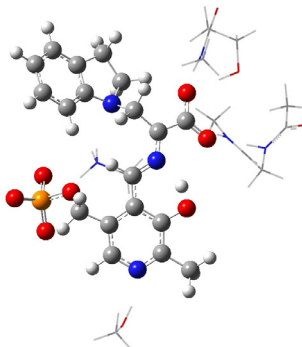
chemical shifts are highly correlated with π electron densities. For that reason, it is not surprising to observe⁴² that the computed shifts are highly sensitive to the presence of nearby hydrogen-bonding partners, which change the π electron density, influencing the formal charge and the shielding. All of these highlight the importance of including hydrogen-bond partners to better describe the interactions between the substrate and its neighbor side chains. On this account, the side chains which are hydrogen-bonding to substrate and will affect the conjugated PLP system are all included. To correctly represent the important interactions between substrate and its hydrogen-bonding side chains in the GIAO calculation, all the atoms are calculated at B3LYP/6-311++G(d,p) level of theory.

Figure 2.8 summarizes the calculations at B3LYP/6-311++G(d,p) level of theory for the quinonoid intermediate (ball & stick) with its hydrogen-bond partners (wireframe). Here we examine protonation states at 5 possible sites, the protonation of the PLP phosphate, the protonation of the pyridine ring N, the position of the proton shared between the pyridine hydroxyl O and the Schiff base N, and protonation of the carboxylate, reflecting 24 possible combinations. In the models presented, the number of “0” represents deprotonated state, and the number of “1” represents protonated state, in the order of the PLP phosphate, the pyridine ring nitrogen, the pyridine hydroxyl oxygen, the Schiff base nitrogen, and the carboxylate. For instance, model 0-1010 corresponds to the structure with the pyridine ring nitrogen and the Schiff base nitrogen protonated, while the PLP phosphate, the pyridine hydroxyl oxygen, and the carboxylate unprotonated.



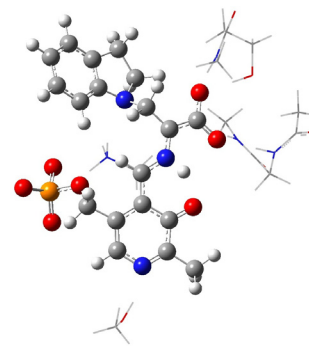
Model: 0-0000

CA = 101.28 ppm
 CB = 55.73 ppm
 CO = 176.03 ppm
 N = 402.21 ppm



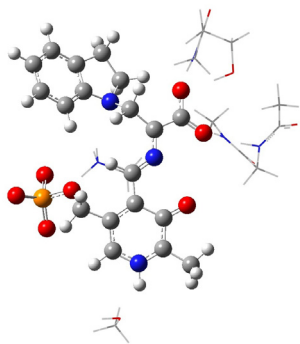
Model: 0-0100

CA = 105.73 ppm
 CB = 55.14 ppm
 CO = 175.08 ppm
 N = 338.58 ppm



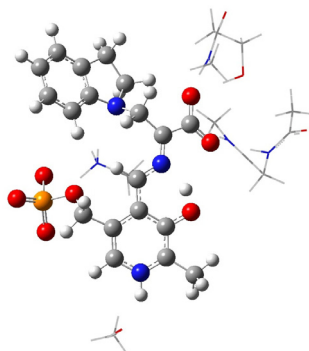
Model: 0-0010

CA = 92.35 ppm
 CB = 56.53 ppm
 CO = 170.94 ppm
 N = 219.24 ppm



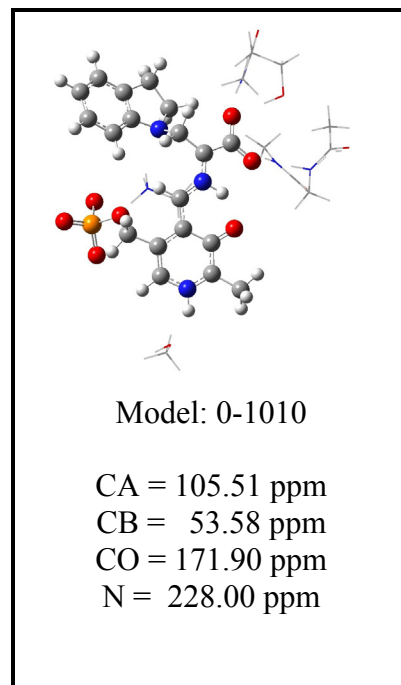
Model: 0-1000

CA = 111.17 ppm
 CB = 52.12 ppm
 CO = 176.88 ppm
 N = 411.45 ppm



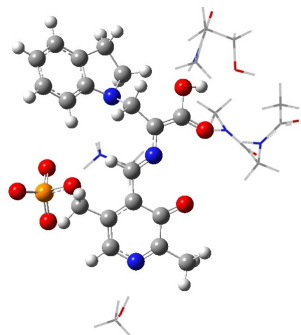
Model: 0-1100

CA = 124.29 ppm
 CB = 52.26 ppm
 CO = 175.15 ppm
 N = 334.64 ppm



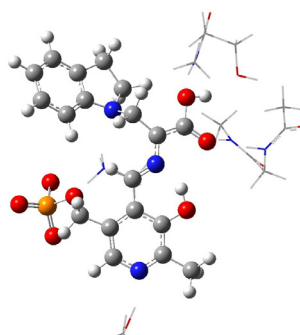
Model: 0-1010

CA = 105.51 ppm
 CB = 53.58 ppm
 CO = 171.90 ppm
 N = 228.00 ppm



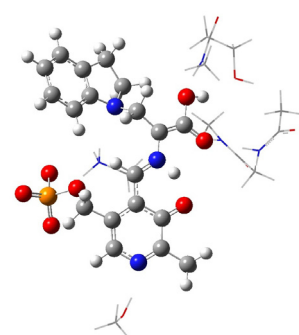
Model: 0-0001

CA = 97.69 ppm
 CB = 52.60 ppm
 CO = 159.59 ppm
 N = 357.98 ppm



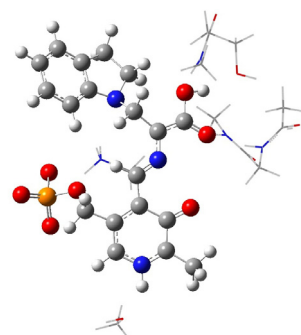
Model: 0-0101

CA = 97.37 ppm
 CB = 52.61 ppm
 CO = 162.51 ppm
 N = 325.53 ppm



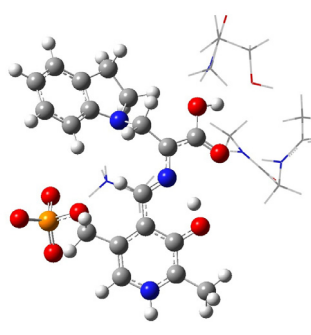
Model: 0-0011

CA = 87.74 ppm
 CB = 52.88 ppm
 CO = 158.15 ppm
 N = 195.42 ppm



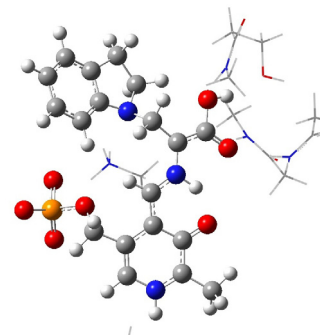
Model: 0-1001

CA = 100.82 ppm
 CB = 54.75 ppm
 CO = 163.46 ppm
 N = 397.44 ppm



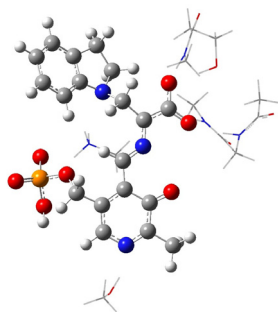
Model: 0-1101

CA = 105.34 ppm
 CB = 51.11 ppm
 CO = 164.25 ppm
 N = 335.65 ppm



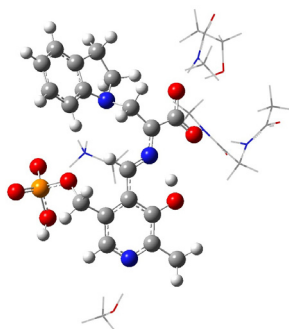
Model: 0-1011

CA = 92.87 ppm
 CB = 51.81 ppm
 CO = 161.03 ppm
 N = 207.90 ppm



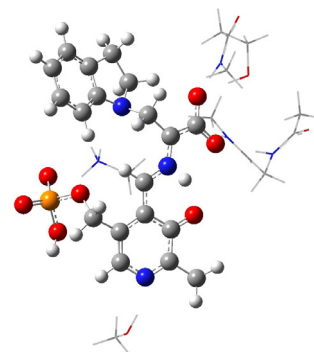
Model: 1-0000

CA = 104.52 ppm
 CB = 54.90 ppm
 CO = 175.83 ppm
 N = 406.21 ppm



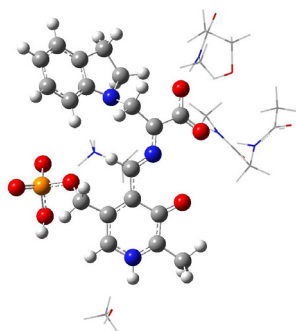
Model: 1-0100

CA = 110.64 ppm
 CB = 54.87 ppm
 CO = 175.20 ppm
 N = 339.54 ppm



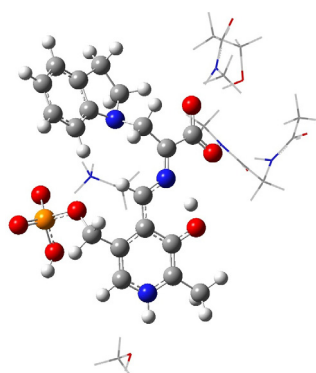
Model: 1-0010

CA = 96.77 ppm
 CB = 56.56 ppm
 CO = 171.28 ppm
 N = 225.79 ppm



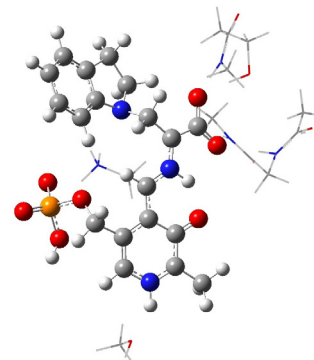
Model: 1-1000

CA = 116.99 ppm
 CB = 51.83 ppm
 CO = 176.60 ppm
 N = 411.16 ppm



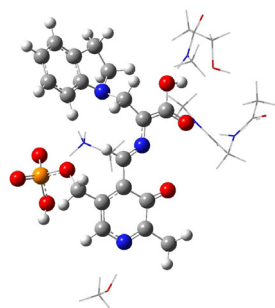
Model: 1-1100

CA = 132.26 ppm
 CB = 52.03 ppm
 CO = 173.72 ppm
 N = 329.05 ppm



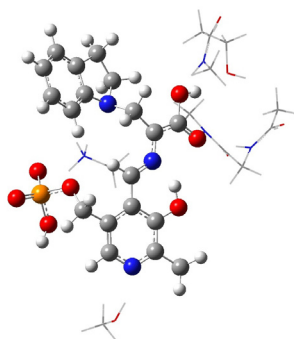
Model: 1-1010

CA = 111.84 ppm
 CB = 53.20 ppm
 CO = 170.81 ppm
 N = 229.18 ppm



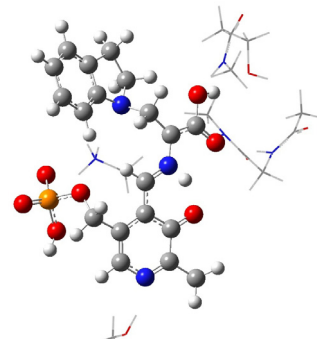
Model: 1-0001

CA = 96.92 ppm
 CB = 52.56 ppm
 CO = 161.13 ppm
 N = 373.66 ppm



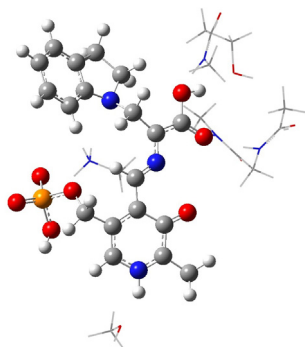
Model: 1-0101

CA = 99.14 ppm
 CB = 52.42 ppm
 CO = 164.21 ppm
 N = 335.76 ppm



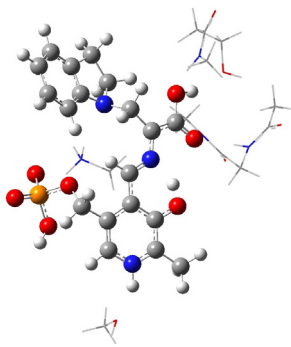
Model: 1-0011

CA = 88.60 ppm
 CB = 52.86 ppm
 CO = 160.02 ppm
 N = 207.22 ppm



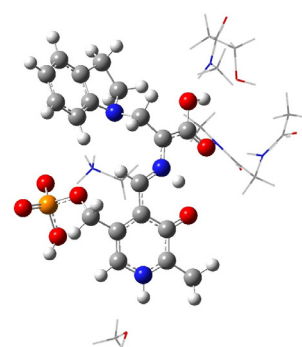
Model: 1-1001

CA = 102.98 ppm
 CB = 54.46 ppm
 CO = 164.59 ppm
 N = 408.35 ppm



Model: 1-1101

CA = 111.58 ppm
 CB = 51.10 ppm
 CO = 166.86 ppm
 N = 344.45 ppm



Model: 1-1011

CA = 97.85 ppm
 CB = 49.05 ppm
 CO = 164.47 ppm
 N = 236.58 ppm

Figure 2.8. Models of indoline quinonoid. 24 possible *ab initio* minimized structures and chemical shifts (B3LYP/6-311++G**) exploring protonation states at 5 sites (shown by arrows) in the indoline quinonoid intermediate. The boxed intermediate gives the best agreement with the experimental ^{13}C shifts. CA refers to the carbon that originated at the serine alpha carbon, CB refers to the carbon from the serine beta carbon, CO refers to the carbon from the serine carboxylate carbon, and N refers to the nitrogen from the serine nitrogen.

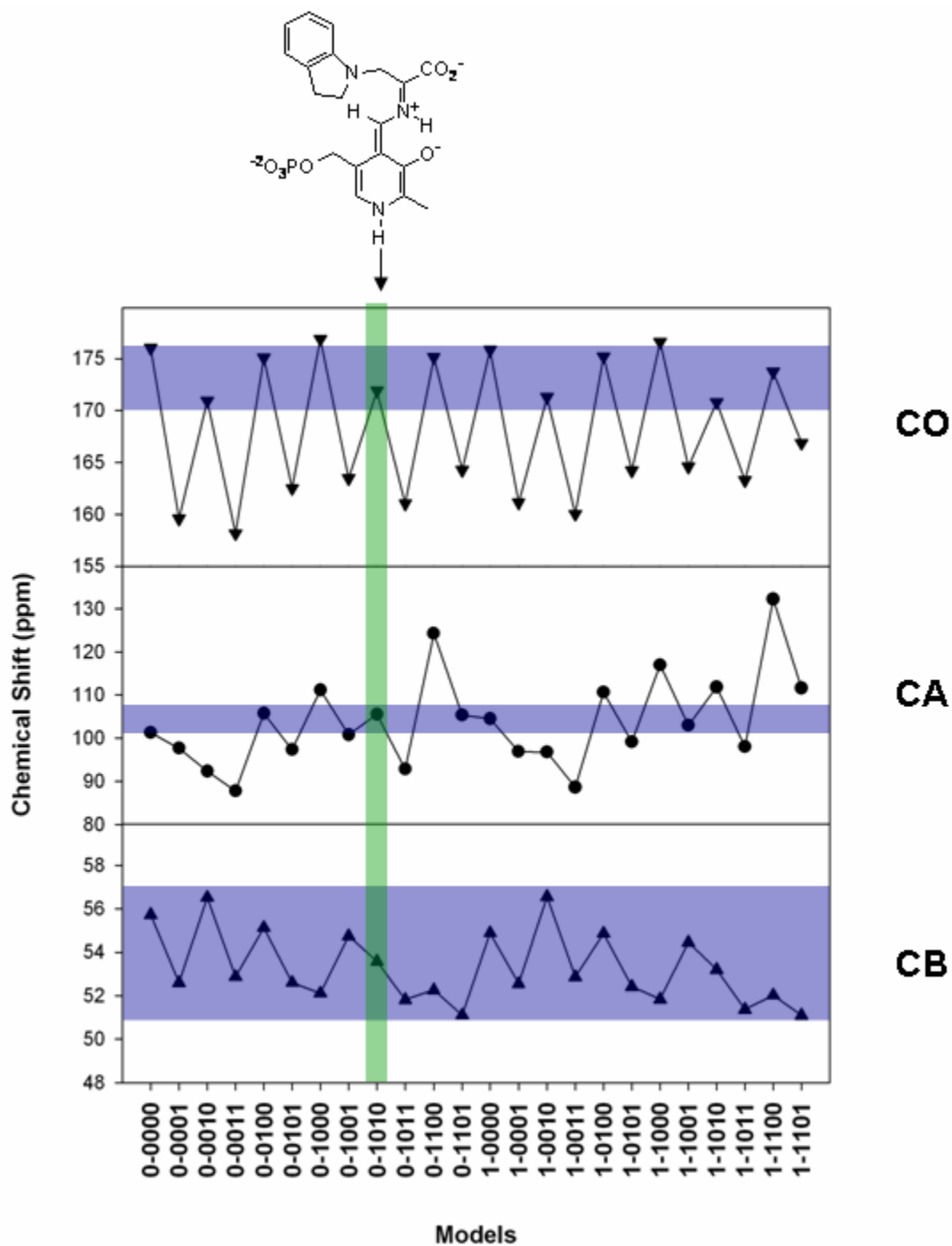


Figure 2.9. Comparison of the calculated ^{13}C chemical shifts of indoline quinonoid with experimental results

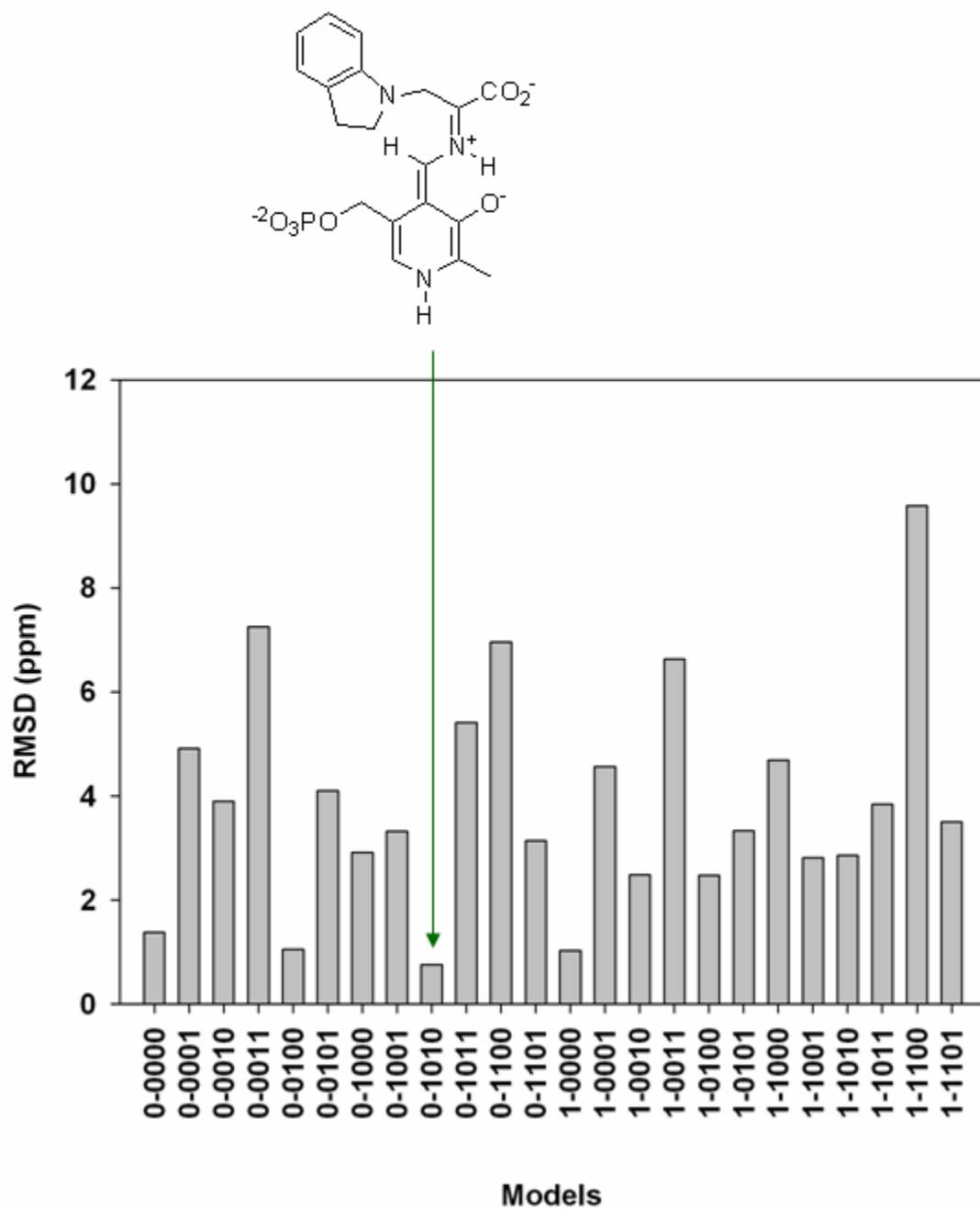


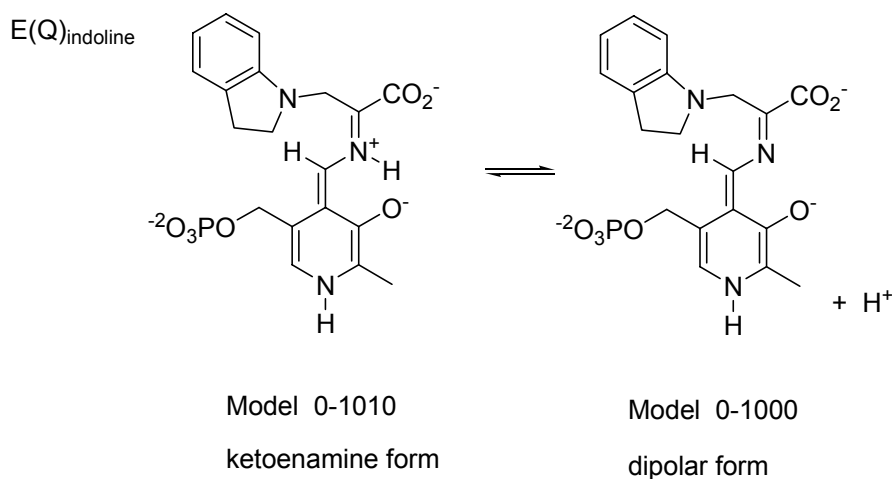
Figure 2.10. The root mean square deviation (RMSD) of the calculated ^{13}C chemical shifts from the experimental results

Attention should be paid that the structures are derived from the optimized structures using ONIOM method. In the ONIOM calculation, all non-hydrogen atoms in the protein side-chains are fixed at their crystallographic coordinates. In addition, indoline and pyridine ring planes of substrate remain fixed at their relative crystallographic orientations, a weak constraint necessary to mimic the effect of the surrounding protein residues on the substrate structure. These structures were minimized subject to the constraint that the indoline and pyridine ring planes remain fixed at their relative crystallographic orientations, a weak constraint necessary to mimic the effect of the surrounding protein residues on the substrate structure. Actually we also tried the calculation with all the coordinates of substrate fully optimized. The results (data not shown) provide similar CA, CO and N chemical shifts but worse CB chemical shifts, which highlights the importance of constraint of relative orientations of the indoline and pyridine ring planes in substrate.

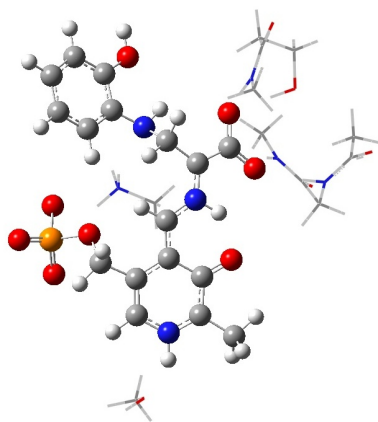
Figure 2.9 compares the calculated ^{13}C chemical shifts, including CA, CB, and CO shifts, with the experimental results. The blue shade areas represent the confidence range within 3 ppm deviation from the experimental shifts. For better comparison, the root mean square deviation (RMSD) of the calculated ^{13}C chemical shifts from the experimental shifts has been also shown in Figure 2.10. From Figure 2.9 and Figure 2.10, it's straightforward to choose the ketoenamine form, model 0-1010, as the best candidate for quinonoid species. The calculated chemical shifts of model 0-1010 entirely fall in the confidence range (Figure 2.9), in accordance with the experimental shifts. Furthermore, its RMSD is only 0.76 ppm (Figure 2.10), smallest among all the possible models.

Essentially, this ketoenamine form with the pyridine ring nitrogen and the Schiff base nitrogen protonated is also the canonical protonation state proposed by biochemist⁴³ but without proof.

Further comparison of the ¹⁵N chemical shift of 228.0 ppm for model 0-1010 with the experimental result of 296.5 ppm, a difference of 68.5 ppm has been found. This finding strongly suggests that another model with Schiff base nitrogen deprotonated also exists and is in fast exchange with the canonical ketoenamine form. This second candidate can only be the model 0-1000, dipolar form. In this model, the pyridine N is again protonated while all the other protonation states are unprotonated. Because of the fast exchange between the ketoenamine form and dipolar form, the observed chemical shifts are actually the weight average of the chemical shifts of both model 0-1010 and 0-1000. To ensure the lowest RMSD, an equilibrium of 63% of model 0-1010 and 37% of model 0-1000 will give rise to chemical shifts of CA at 107.6 ppm, CB at 53.0 ppm, CO at 173.7 ppm and N at 295.9 ppm, which match the experimental results of CA at 103.6 ppm, CB at 54.1 ppm, CO at 173.0 ppm and N at 296.5 ppm.



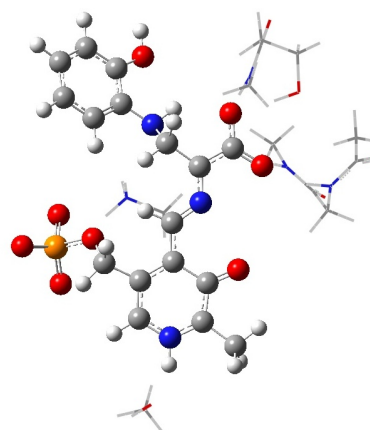
In fact, the importance of the existence of the dipolar form can be illustrated in the pathway of β -reaction shown in Figure 2.2. In the final synthesis of L-Trp, quinonoid intermediate will take a proton from nearby β -lysine 87 to form E(Aex₂) first, and this E(Aex₂) will finally produce L-Trp together E(Ain). The presence of the model 0-1000 in the quinonoid species will make the whole quinonoid intermediate more negative charged, and consequently easier to attract the positive proton from the β -lysine 87.



Model 0-1010 of E(Q)_{2-AP}

ketoenamine form

CA = 105.63 ppm
 CB = 49.62 ppm
 CO = 171.97 ppm
 N = 225.68 ppm



Model 0-1000 of E(Q)_{2-AP}

dipolar form

CA = 112.94 ppm
 CB = 45.37 ppm
 CO = 177.73 ppm
 N = 408.23 ppm

Figure 2.11. *Ab initio* minimized structures and chemical shifts (B3LYP/6-311++G**) of the 2-AP quinonoid intermediate. Only the two best candidates are shown.

To further test this model, the chemical shifts of 2-AP quinonoid have also been calculated using the same constraints from indoline quinonoid, and the calculated results are shown in Figure 2.11. Again, a combination of 63% of model 0-1010 and 37% of model 0-1000 will give rise to chemical shifts of CA at 108.3 ppm, CB at 48.0 ppm, CO at 174.1 ppm and N at 293.2 ppm, which match the experimental results of CA at 104.4 ppm, CB at 47.3 ppm, CO at 173.1 ppm and N at 296.9 ppm

2.5 CONCLUSION

Chemical level details such as protonation and hybridization states are critical for understanding enzymatic mechanism and function. Even under moderately high resolution, these are difficult to determine from X-ray crystallography. The chemical shift, however, is extremely sensitive to these effects and here we make use of a combined solid-state NMR, X-ray crystallography, and *ab initio* approach to characterize the enzymatic quinonoid intermediates in the PLP-dependent tryptophan synthase. The analysis of the chemical shifts for intermediates derived from reaction of ^{13}C - and ^{15}N substituted L-Ser gives unambiguous identification of several intermediate species, while further insights into the protonation state and distribution of these species can be obtained by combining both the X-ray and NMR data with *ab initio* calculations of chemical shift. In this case, various models of charge and protonation states can be distinguished by their calculated effect on the observed chemical shifts, allowing us to choose the chemical species most consistent with the experimental results. These support the ketoenamine

and dipolar forms that are in fast exchange to each other in quionoid intermediate, which we believe has mechanistic implications.

REFERENCE

- (1) Pan, P.; Woehl, E.; Dunn, M. F., *Trends Biochem.Sci.* **1997**, *22*, 22.
- (2) Ngo, H.; Harris, R.; Kimmich, N.; Casino, P.; Niks, D.; Blumenstein, L.; Barends, T. R.; Kulik, V.; Weyand, M.; Schlichting, I.; Dunn, M. F., *Biochemistry* **2007**, *46*, 7713.
- (3) Ngo, H.; Kimmich, N.; Harris, R.; Niks, D.; Blumenstein, L.; Kulik, V.; Barends, T. R.; Schlichting, I.; Dunn, M. F., *Biochemistry* **2007**, *46*, 7740.
- (4) Barends, T. R. M.; Domratcheva, T.; Kulik, V.; Blumenstein, L.; Niks, D.; Dunn, M. F.; Schlichting, I., *ChemBioChem* **2008**, *9*, 1024.
- (5) Kulik, V.; Hartmann, E.; Weyand, M.; Frey, M.; Gierl, A.; Niks, D.; Dunn, M. F.; Schlichting, I., *J. Mol. Biol.* **2005**, *352*, 608.
- (6) Blumenstein, L.; Domratcheva, T.; Niks, D.; Ngo, H.; Seidel, R.; Dunn, M. F.; Schlichting, I., *Biochemistry* **2007**, *46*, 14100.
- (7) Dunn, M. F.; Niks, D.; Ngo, H.; Barends, T. R. M.; Schlichting, I., *Trends Biochem.Sci.* **2008**, *33*, 254.
- (8) Barends, T. R. M.; Dunn, M. F.; Schlichting, I., *Curr. Opin. Chem. Biol.* **2008**, *12*, 593.
- (9) Brzovic, P. S.; Ngo, K.; Dunn, M. F., *Biochemistry* **1992**, *31*, 3831.
- (10) Casino, P.; Niks, D.; Ngo, H.; Pan, P.; Brzovic, P.; Blumenstein, L.; Barends, T. R.; Schlichting, I.; Dunn, M. F., *Biochemistry* **2007**, *46*, 7728.
- (11) Dunn, M. F.; Woehl, E.; Pan, P., *Faseb J.* **1995**, *9*, A1285.
- (12) Ferrari, D.; Niks, D.; Yang, L. H.; Miles, E. W.; Dunn, M. F., *Biochemistry* **2003**, *42*, 7807.
- (13) Leja, C. A.; Woehl, E. U.; Dunn, M. F., *Biochemistry* **1995**, *34*, 6552.
- (14) McDermott, A.; Polenova, T., *Curr. Opin. Struct. Biol.* **2007**, *17*, 617.
- (15) Jakeman, D. L.; Mitchell, D. J.; Shuttleworth, W. A.; Evans, J. N. S., *Biochemistry* **1998**, *37*, 12012.

- (16) McDowell, L. M.; Lee, M. S.; Schaefer, J.; Anderson, K. S., *J. Am. Chem. Soc.* **1995**, *117*, 12352.
- (17) Schneider, T. R.; Gerhardt, E.; Lee, M.; Liang, P. H.; Anderson, K. S.; Schlichting, I., *Biochemistry* **1998**, *37*, 5394.
- (18) Dapprich, S.; Komaromi, I.; Byun, K. S.; Morokuma, K.; Frisch, M. J., *Theochem-J. Mol. Struct.* **1999**, *461*, 1.
- (19) Becke, A. D., *Phys. Rev. A* **1988**, *38*, 3098.
- (20) Becke, A. D., *J. Chem. Phys.* **1993**, *98*, 5648.
- (21) Lee, C. T.; Yang, W. T.; Parr, R. G., *Phys. Rev. B* **1988**, *37*, 785.
- (22) Frisch, M. J.; Trucks, G. W.; Schlegel, H. B.; Scuseria, G. E.; Robb, M. A.; Cheeseman, J. R.; Montgomery, J., J. A.; Vreven, T.; Kudin, K. N.; Burant, J. C.; Millam, J. M.; Iyengar, S. S.; Tomasi, J.; Barone, V.; Mennucci, B.; Cossi, M.; Scalmani, G.; Rega, N.; Petersson, G. A.; Nakatsuji, H.; Hada, M.; Ehara, M.; Toyota, K.; Fukuda, R.; Hasegawa, J.; Ishida, M.; Nakajima, T.; Honda, Y.; Kitao, O.; Nakai, H.; Klene, M.; Li, X.; Knox, J. E.; Hratchian, H. P.; Cross, J. B.; Bakken, V.; Adamo, C.; Jaramillo, J.; Gomperts, R.; Stratmann, R. E.; Yazyev, O.; Austin, A. J.; Cammi, R.; Pomelli, C.; Ochterski, J. W.; Ayala, P. Y.; Morokuma, K.; Voth, G. A.; Salvador, P.; Dannenberg, J. J.; Zakrzewski, V. G.; Dapprich, S.; Daniels, A. D.; Strain, M. C.; Farkas, O.; Malick, D. K.; Rabuck, A. D.; Raghavachari, K.; Foresman, J. B.; Ortiz, J. V.; Cui, Q.; Baboul, A. G.; Clifford, S.; Cioslowski, J.; Stefanov, B. B.; Liu, G.; Liashenko, A.; Piskorz, P.; Komaromi, I.; Martin, R. L.; Fox, D. J.; Keith, T.; Al-Laham, M. A.; Peng, C. Y.; Nanayakkara, A.; Challacombe, M.; Gill, P. M. W.; Johnson, B.; Chen, W.; Wong, M. W.; Gonzalez, C.; Pople, J. A. *Gaussian 03*, E.01; Gaussian Inc., Wallingford CT: 2004.
- (23) Ferrari, D.; Yang, L. H.; Miles, E. W.; Dunn, M. F., *Biochemistry* **2001**, *40*, 7421.
- (24) Rhee, S.; Parris, K. D.; Hyde, C. C.; Ahmed, S. A.; Miles, E. W.; Davies, D. R., *Biochemistry* **1997**, *36*, 7664.
- (25) Dunn, M. F.; Aguilar, V.; Brzovic, P.; Drewe, W. F.; Houben, K. F.; Leja, C. A.; Roy, M., *Biochemistry* **1990**, *29*, 8598.
- (26) Lane, A. N.; Kirschner, K., *Eur. J. Biochem.* **1981**, *120*, 379.
- (27) Drewe, W. F.; Dunn, M. F., *Biochemistry* **1985**, *24*, 3977.
- (28) Drewe, W. F.; Dunn, M. F., *Biochemistry* **1986**, *25*, 2494.

- (29) Roy, M.; Miles, E. W.; Phillips, R. S.; Dunn, M. F., *Biochemistry* **1988**, *27*, 8661.
- (30) Brzovic, P. S.; Hyde, C. C.; Miles, E. W.; Dunn, M. F., *Biochemistry* **1993**, *32*, 10404.
- (31) Harris, R. M.; Dunn, M. F., *Biochemistry* **2002**, *41*, 9982.
- (32) Harris, R. M.; Ngo, H.; Dunn, M. F., *Biochemistry* **2005**, *44*, 16886.
- (33) Mao, J. H.; Mukherjee, S.; Zhang, Y.; Cao, R.; Sanders, J. M.; Song, Y. C.; Zhang, Y. H.; Meints, G. A.; Gao, Y. G.; Mukkamala, D.; Hudock, M. P.; Oldfield, E., *J. Am. Chem. Soc.* **2006**, *128*, 14485.
- (34) Le, H. B.; Oldfield, E., *J. Phys. Chem.* **1996**, *100*, 16423.
- (35) Pearson, J. G.; Wang, J. F.; Markley, J. L.; Le, H. B.; Oldfield, E., *J. Am. Chem. Soc.* **1995**, *117*, 8823.
- (36) Oldfield, E., *Annu. Rev. Phys. Chem.* **2002**, *53*, 349.
- (37) Bai, S.; Hu, J. Z.; Pugmire, R. J.; Grant, D. M.; Taylor, C. M. V.; Rubin, J. B.; Peterson, E. J., *Macromolecules* **1998**, *31*, 9238.
- (38) Harper, J. K.; Barich, D. H.; Heider, E. M.; Grant, D. M.; Franke, R. R.; Johnson, J. H.; Zhang, Y. G.; Lee, P. L.; Von Dreele, R. B.; Scott, B.; Williams, D.; Ansell, G. B., *Cryst. Growth Des.* **2005**, *5*, 1737.
- (39) Harper, J. K.; Facelli, J. C.; Barich, D. H.; McGeorge, G.; Mulgrew, A. E.; Grant, D. M., *J. Am. Chem. Soc.* **2002**, *124*, 10589.
- (40) Harper, J. K.; Grant, D. M., *J. Am. Chem. Soc.* **2000**, *122*, 3708.
- (41) Liu, F.; Phung, C. G.; Alderman, D. W.; Grant, D. M., *J. Am. Chem. Soc.* **1996**, *118*, 10629.
- (42) Mukkamala, D.; Zhang, Y.; Oldfield, E., *J. Am. Chem. Soc.* **2007**, *129*, 7385.
- (43) Hur, O.; Niks, D.; Casino, P.; Dunn, M. F., *Biochemistry* **2002**, *41*, 9991.

CHAPTER III

INFLUENCE OF PERIPHERAL GROUPS ON THE PHYSICAL AND CHEMICAL BEHAVIOR OF CINCHONA ALKALOIDS

ABSTRACT

While cinchona alkaloids play a key role in many applications, from medicine to catalysis, there is not yet a complete understanding of the reasons for their unique chemical behavior. Past studies have identified the chiral pocket formed by the two main constituting moieties of the cinchona, the quinoline and quinuclidine rings, as the main factor determining their physiological and enantioselective reactivity. That explanation, however, does not account for the differences observed among similar cinchona alkaloids. Here we show that subtle changes in the position of the substituent groups outside the central chiral pocket explain the disparities observed in basic physicochemical properties between pairs of near-enantiomers (quinine vs. quinidine, cinchonidine vs. cinchonine) such as crystal structure, solubility, and adsorption equilibrium. Both energetic and entropic factors need to be considered to fully account for the trends observed.

3.1 INTRODUCTION

Cinchona alkaloids, natural products typically extracted from the bark of *Cinchona ledgeriana* trees, have proven quite versatile. They are used to treat malaria^{1,2} and cardiac arrhythmias,³ as flavors in food and drinks,⁴ as catalysts or co-catalysts in both homogeneous^{5,6} and heterogeneous systems,^{7,8} and as chiral resolving agents.⁹ The utility of these molecules has been traced to the unique chiral pocket formed by their two main moieties, an aromatic quinoline ring and a rigid quinuclidine bicyclic amine, as they hinge around an alcoholic chiral linker (Figure 3.1).

Structure of Cinchona Alkaloids

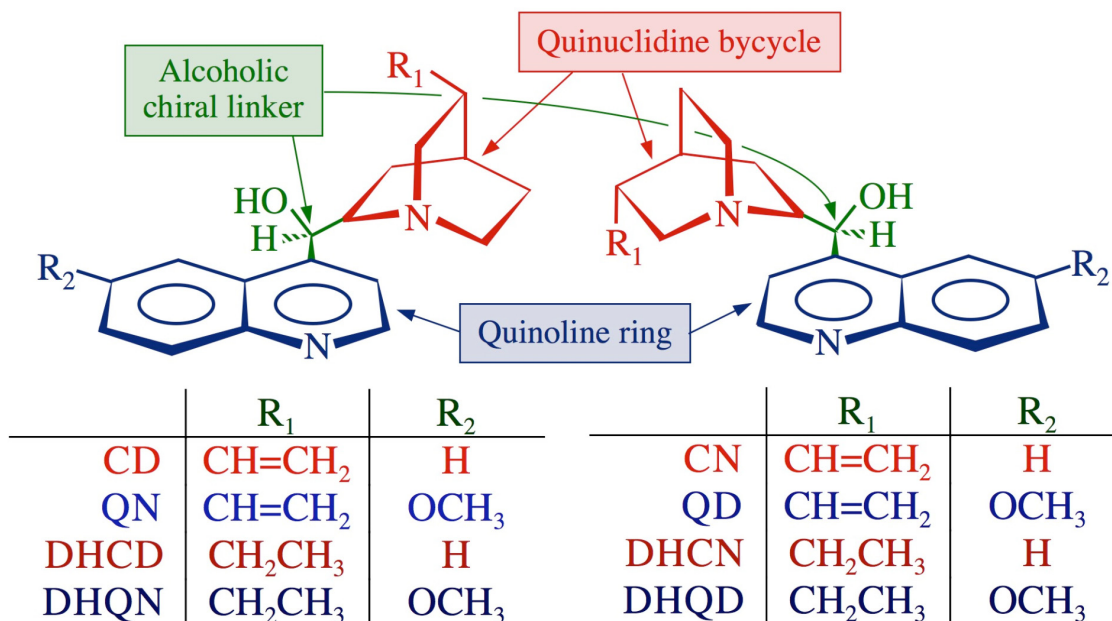


Figure 3.1. Structure of the eight cinchona alkaloids discussed in this chapter. The three main functional moieties identified as responsible for most of their unique chemistry, namely, a quinoline aromatic ring, a quinuclidine amine bicyclic, and an alcoholic chiral linker, are highlighted.

However, neither that basic structural argument nor relative differences in the ability of the cinchona to form intermolecular hydrogen bonds around the chiral pocket¹⁰⁻¹³ can account for the variations in pharmacological efficiency,^{14, 15} enantioselectivity in catalysis,^{16, 17} or other chemistry¹⁸ seen between near-enantiomers such as quinine vs. quinidine or cinchonidine vs. cinchonine.

Surprisingly, while many aspects of the chemistry of individual cinchona alkaloids have been extensively studied in the past, comparative studies among similar cinchona are much more sparse. In search for an explanation of the differences mentioned in the preceding paragraph, here we focus on contrasting some fundamental physicochemical properties of the four pairs of near enantiomers shown in Figure 3.1. In each of these pairs, both the two carbons that define the chiral pocket and the chirality of the pocket itself are inverted, and only the chiral atoms in the rigid quinuclidine bicycle maintain the same stereo configuration. Preservation of the chirality of the quinuclidine moiety while switching the handedness of the carbon atoms around the alcoholic linker leads to a different stereo orientation of the R_1 ligand. We show that the resulting differences in position of the peripheral groups causes the combination of energetic and entropic changes ultimately responsible for the variations in properties observed.

3.2 EXPERIMENTAL SECTION

Quantum mechanics calculations of the minimum-energy crystal structures were carried out using a plane-wave based density functional theory (DFT) within the

CASTEP code.¹⁹ The popular Perdew–Burke–Ernzerhof (PBE) density functional of generalized gradient approximation (GGA) was adopted.²⁰ Ultrasoft pseudopotentials were used with a plane-wave basis energy cutoff of 300 eV.²¹ Gaussian 03 (DFT-B3LYP; 6-31G**) was used for the gas-phase calculations.²²⁻²⁴ 2D NOESY NMR spectra were acquired on a 11.7 T Varian Inova spectrometer (¹H frequency 500.14 MHz) equipped with a triple-resonance triple-axis gradient probe.²⁴ The relative intensities of the 2D NOESY ¹H NMR cross-peaks were estimated by Gibbs-free-energy weight-averaging of the calculated $1/r^6$ values for the same 27 most stable conformations of each cinchona used for the entropy calculations. Solubilities were measured using established reported methods.^{25,26} Infrared spectra were taken in transmission mode for the solid samples and in-situ at the solid-liquid interface in single reflection mode (RAIRS) for the adsorbed cinchona alkaloids using a setup developed in our laboratory.²⁷

3.3 RESULTS

The first property to be explored in this report is the crystallographic structure of the solid cinchona alkaloids. Cinchonine forms monoclinic crystals with a $P2_1$ space group,²⁸ whereas cinchonidine crystallizes in an orthorhombic, $P2_12_12_1$ space group instead. Our quantum-mechanics calculations, summarized in Figure 3.2, indicate that this difference can be explained by differences in the energetics of the two molecules in their crystal structures.

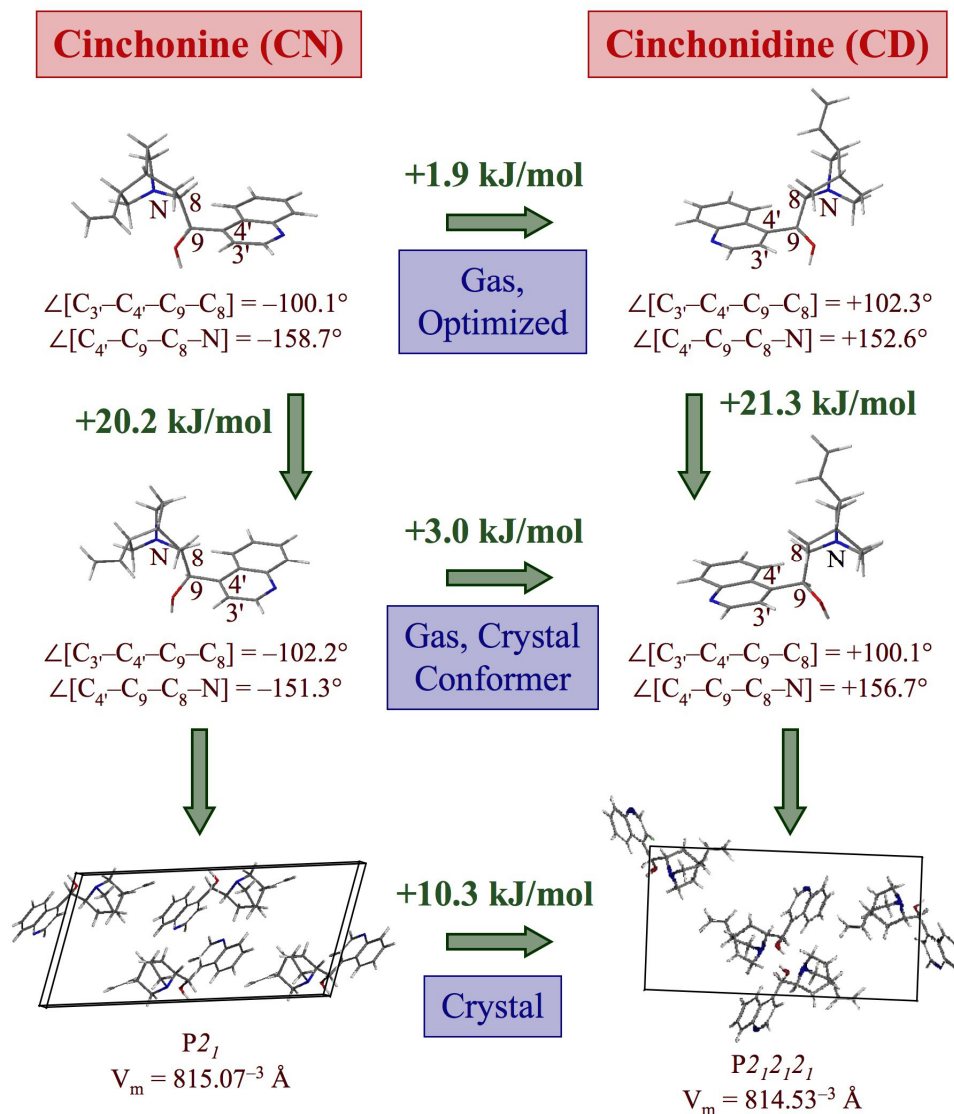


Figure 3.2. Comparative quantum-mechanics calculations of the energy of crystallization of cinchonine (left) versus cinchonidine (right). These energies have been divided into two components: (1) the intramolecular energy needed for the molecules to adopt the rotational conformation seen in the crystal (first step going down), and (2) the intermolecular energy involved in holding the molecules together within the crystal (second step). Most of the energy differences between cinchonine and cinchonidine are associated with the second term.

It was found that the crystal of cinchonine is more stable than that of cinchonidine, by 10.3 kJ/mol, and that most of this energy difference is ascribed to intermolecular interactions within the crystalline structure; the energy difference between cinchonine and cinchonidine in gas phase amounts to only 1.9 kJ/mol. It was also determined that the molecules assume essentially the same rotational configuration in gas and solid phases, with the dihedral angles of the two free-rotating bonds within the alcoholic linker, $\angle[C_3-C_4-C_9-C_8]$ and $\angle[C_4-C_9-C_8-N]$ ²⁹ varying by only a few degrees (compare the structures and energies in the top and middle rows of Figure 3.2, which correspond to the conformers in gas and solid phases, respectively). It appears that the different position adopted by the peripheral vinyl group in cinchonine allows that molecule to pack with a slightly better pairing of the quinoline rings than cinchonidine. Interestingly, most of the energy difference between the cinchonine and cinchonidine crystals disappears if the molecules are placed in the crystalline form of the other (cinchonidine in a monoclinic crystal and cinchonine in an orthorhombic structure; data in Figure 3.3). Differences in energy of crystallization lead to differences in melting point ($T_m = 484$ and 538 K for cinchonidine and cinchonine, respectively),³² and may be expected to also correlate with energies of dissolution. However, the latter assertion can be called into question because of the fact that the solubilities of cinchona alkaloids can vary by several orders of magnitude depending on the solvent used (Figure 3.4, left).²⁶ These variations have been correlated to changes in the average conformation of the molecule in solution, in particular to the average $\angle[C_3-C_4-C_9-C_8]$ dihedral angle in the alcoholic chiral linker.³³ On the other hand, our measurements indicate that all cinchona alkaloids follow similar

solubility trends as a function of solvent, and that the ratios of solubilities among those compounds are approximately constant regardless of solvent (Figure 3.4).

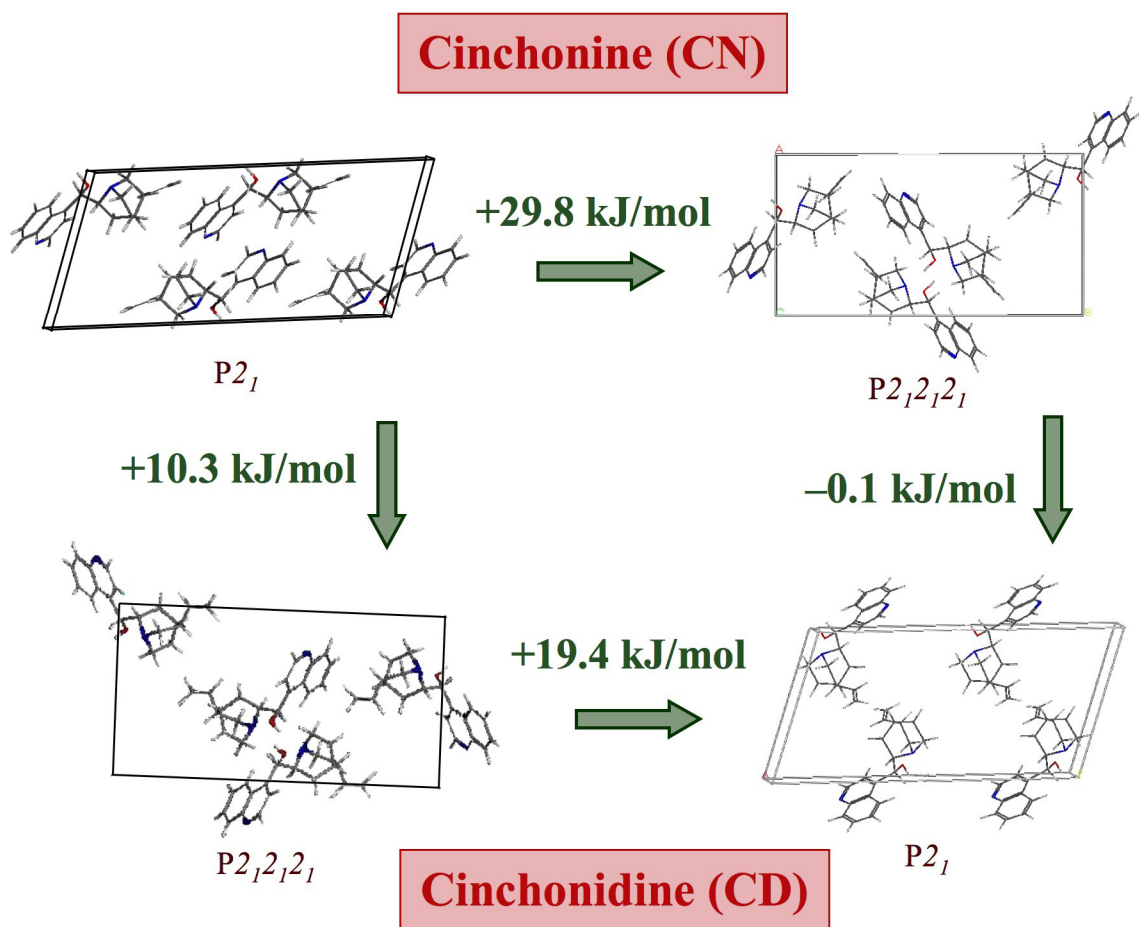


Figure 3.3. Quantum-mechanics calculations of the energetics of CD and CN in each other's crystalline structures. Estimates of the energy needed to crystallize cinchonine (CN) and cinchonidine (CD) in $P2_12_12_1$ and $P2_1$ structures, respectively. The additional stability of CN in its natural crystal monoclinic structure when compared with CD in its orthorhombic structure is lost upon forcing the CN molecules into an orthorhombic arrangement (compared to CD in a monoclinic crystal). These results further point to the key importance of intermolecular forces in determining the differences in energy of crystallization between CN and CD.

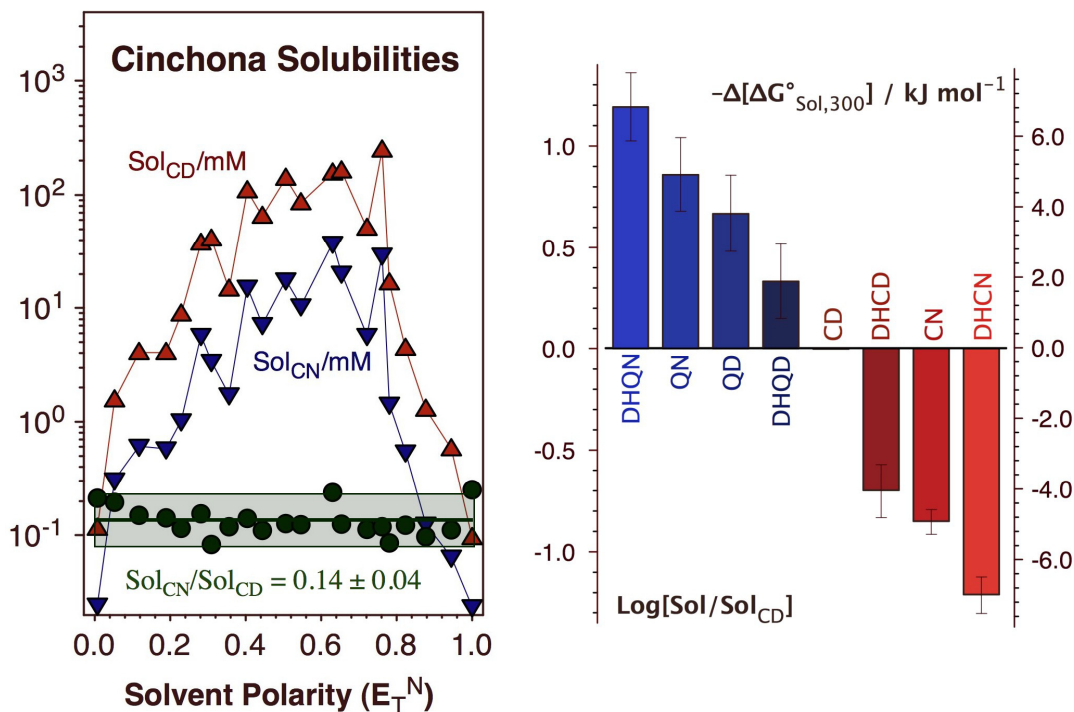


Figure 3.4. Comparative solubility studies with cinchona alkaloids. Left: Solubility of cinchonidine (CD, red upper triangles) and cinchonine (CN, blue down triangles) in a number of different solvents, arranged as a function of their empirical polarity. Also shown are the corresponding Sol_{CN}/Sol_{CD} solubility ratios (green circles) to highlight the fact that those are approximately constant regardless of the solvent used. Right: Average solubilities, relative to those of cinchonidine, for several cinchona alkaloids (cinchonine, quinine –QN–, quinidine –QD–, and the 10,11-dihydro analogs of all four original cinchona), obtained as illustrated in the left. The right y-axis of this plot provides a scale for the corresponding differences in standard Gibbs free energy referred to 1 M solutions.

In general, our data indicate that: (1) the addition of a methoxy group to the quinoline ring (e.g., to make quinine, QN, out of cinchonidine, CD) increases solubility; (2) cinchona with the chirality of cinchonidine (CD, DHCD, QN, DHQN) are more soluble than those with the opposite chirality (CN, DHCN, QD, DHQD); and (3) substitution of

the vinyl moiety by an ethyl group at the R₁ position most often leads to a decrease in solubility. These observations hold true regardless of the solvent used, and are therefore inherent to the nature of the cinchona and due to changes in the positions of the peripheral R₁ and R₂ groups.

Cinchona/CD₃OD 2D NOESY ¹H NMR

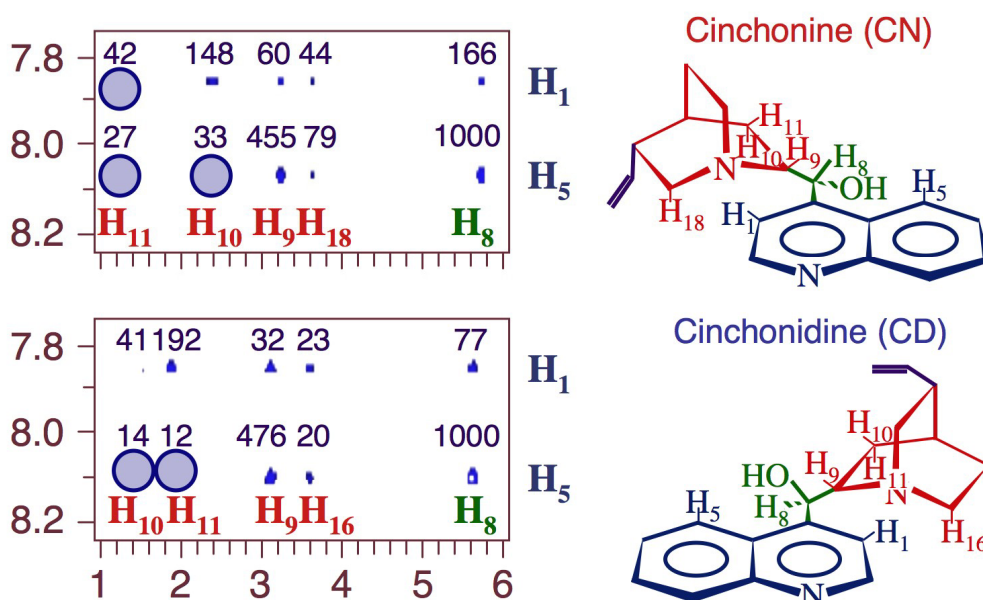


Figure 3.5. Detail of 2D NOESY ¹H NMR data for **cinchonine (top)** and **cinchonidine (bottom)** dissolved in perdeuteromethanol. The absence of some specific cross peaks, highlighted in the figure by the blue circles, points to restrictions in the rotational conformation space of these molecules. However, according to quantum-mechanics calculations, the non-accessible conformations are quite energetic, and therefore not important. The numbers above the experimental peaks in these spectra correspond to their calculated intensities. They match the experimental values reasonably well in spite of the fact that they do not include any solvent effects.

Trends in solubility may not be directly related to trends in energy of crystallization because in solution the molecules are free to rotate around the C₄–C₉ and C₉–C₈ bonds in the chiral linker and to adopt many rotational conformers. Indeed, the 2D NOESY ¹H NMR data reported in Figure 3.5 show a high degree of rotational freedom for the cinchona alkaloids in solution: reasonably intense cross peaks are seen between most of the hydrogen atoms in the bottom ring of the quinuclidine ring (H₉, H₁₀ and H₁₈ in cinchonine, H₉, H₁₁ and H₁₆ in cinchonidine) and both of the top hydrogens in the quinoline moiety (H₁ and H₅), indicating the existence of configurations where those atoms are in close proximity. The only telling absences in the spectra are the cross-peaks between H₁₁ in cinchonine or H₁₀ in cinchonidine and both H₁ and H₅. For those hydrogen atoms to approach each other, the ∠[C₄–C₉–C₈–N] dihedral angle would need to reach values close to zero, and that requires the quinuclidine and quinoline rings to be in close proximity to each other (a high-energy state, as seen in the energy surfaces provided in Figure 3.6).

Further support for the similarity in energetics among cinchona alkaloids in solution comes from quantum-mechanics calculations. For one, published results have identified similar most-stable conformers for several individual cinchona.^{10, 12, 34} Moreover, our comparative calculations, summarized in the two-dimensional map of the energy differences between cinchonidine and cinchonine as a function of the ∠[C₃–C₄–C₉–C₈] and ∠[C₄–C₉–C₈–N] dihedral angles provided in Figure 3.7, point to the similarities between those two molecules.

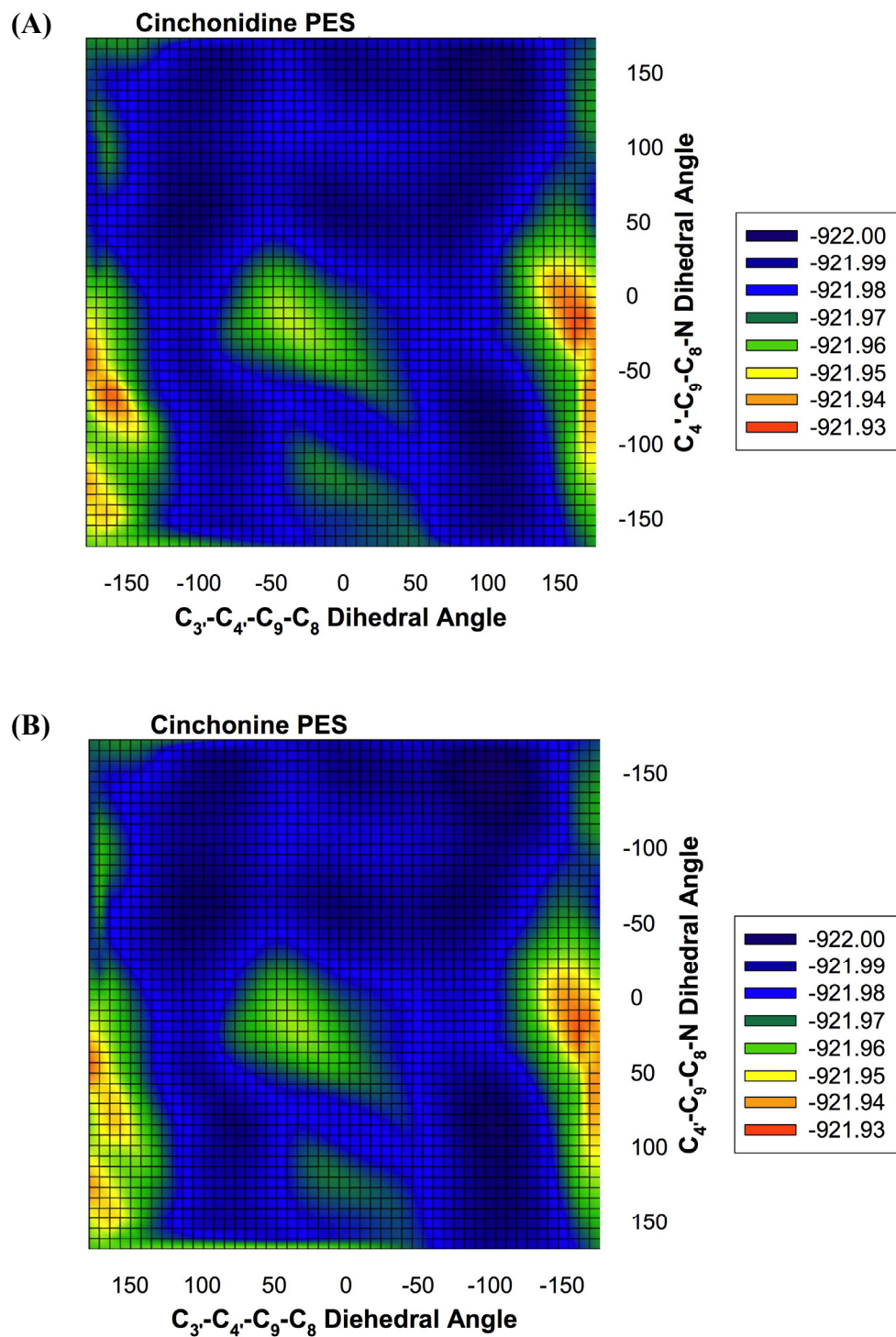


Figure 3.6. 2D potential energy surfaces (PES) as a function of rotations around the two central bonds within the alcohol linker (energy scale in atomic units): (A) cinchonidine; (B) cinchonine .

Energy Difference Between CN and CD vs. Rotational Angles

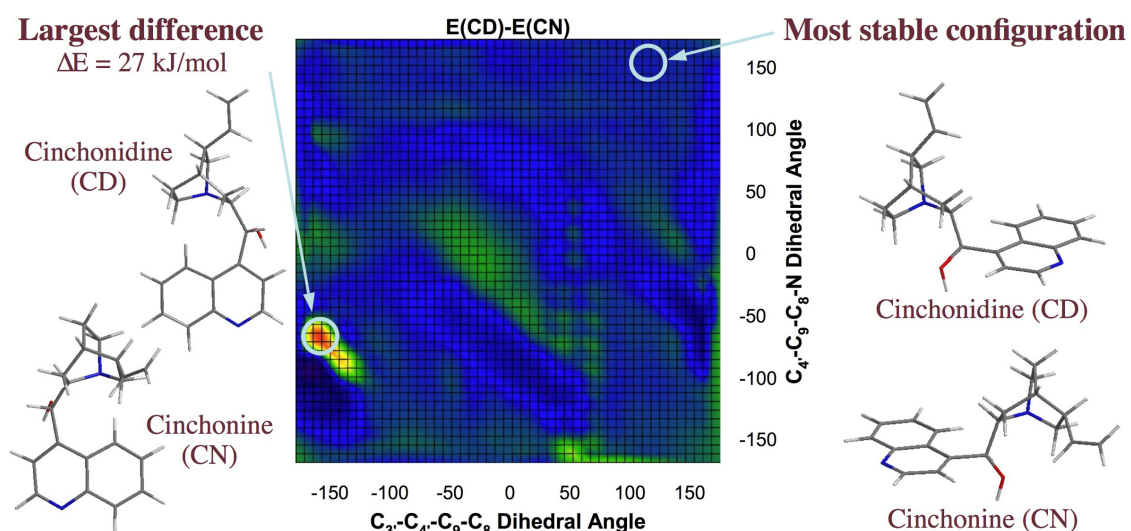


Figure 3.7. Quantum-mechanics calculations for the differences in energy between cinchonidine (CD) and cinchonine (CN) as a function of the values of the $\angle[C_3-C_4-C_9-C_8]$ and $\angle[C_4-C_9-C_8-N]$ dihedral angles associated with the chiral pocket. The light and dark blue colors that cover most of this 2D plot correspond to energy differences of less than 5 kJ/mol, and the green areas to $E(\text{CD}) - E(\text{CN})$ values between 5 and 10 kJ/mol. Only in the lower left corner the orange and yellow areas associated with higher energy differences are seen. They amount to $E(\text{CD}) - E(\text{CN})$ values between 10 and 20 kJ/mol, but correspond to the high-energy and unimportant configurations depicted on the left. The most stable configurations of cinchonidine and cinchonine, the so-called Open 3 structures associated with the upper right corner (depicted on the right side),⁴⁸ are almost isoenergetic.

Their energetics are indeed quite similar over most of their internal-rotation conformer space, and only show significant deviations for configurations where the peripheral vinyl moiety is close to the quinoline ring. Since those geometries are quite energetic (see Figure 3.6), they are not expected to contribute significantly to the overall behavior of these molecules in solution. It should also be said that the relative intensities of the 2D NOESY ^1H NMR cross peaks estimated using the Gibbs free energies as a function of dihedral angles from our quantum-mechanics calculations (the numbers above the corresponding peaks in Figure 3.5) agree reasonably well with the experimental data, even though they do not include any effects due to the solvent. Clearly, the differences in solubility reported above cannot be justified solely, or even mainly, by differences in energetics, as is the case with the crystal structures; an entropic term must be considered as well. This is made particularly evident by the van't Hoff plots of solubility versus temperature shown in Figure 3.8: at least for the case of cinchonidine versus cinchonine in ethanol, the differences in solubility, which amount to almost two orders of magnitude, can be ascribed almost exclusively to entropic effects. The explanation for such entropy prominence is suggested by statistical-mechanics averaging of the quantum-mechanics results obtained for the energetics of the cinchonidine and cinchonine molecules (see Figure 3.9 and Table 3.1-3.3).

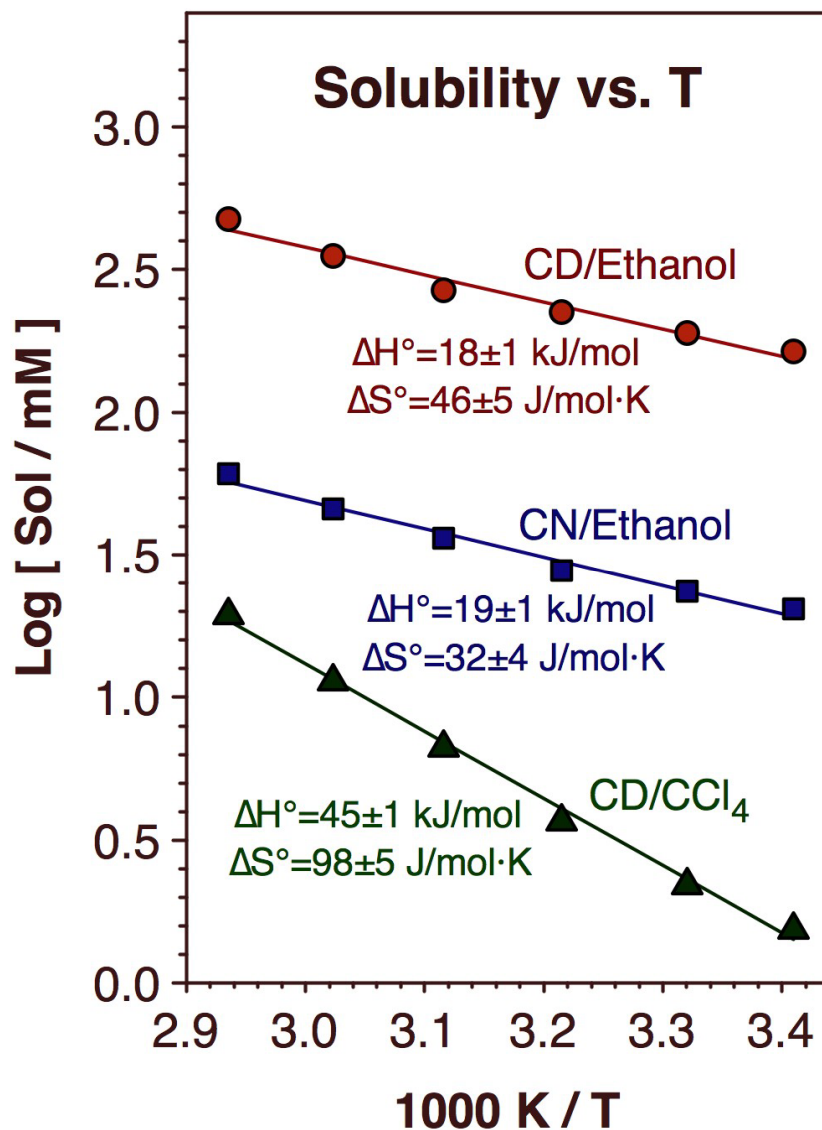


Figure 3.8. Temperature dependence of the solubilities of cinchonidine (red circles) and cinchonine (blue squares) in ethanol and of cinchonidine in carbon tetrachloride (green upper triangles). Plotted in van't Hoff fashion in order to extract the corresponding thermodynamic parameters (included in the figure). The data indicate that, when using the same solvent, the changes in solubility among different cinchona are due mainly to entropic factors. Both the entropy and the enthalpy of solution do vary for each cinchona alkaloid as a function of the solvent used.

Entropy Differences

CD vs. CN most stable configurations

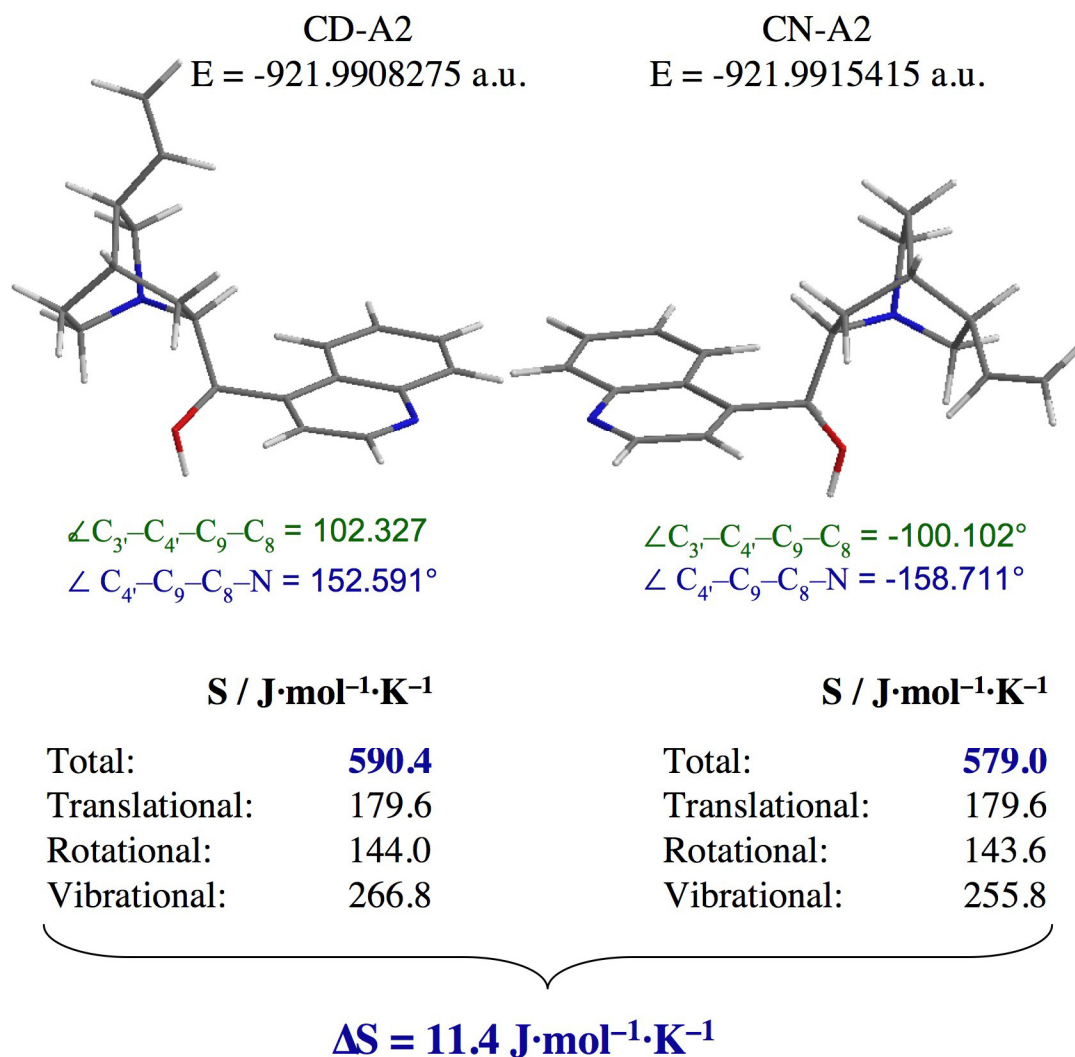


Figure 3.9. Calculations of entropy contributions from the different vibrational and rotational modes of CD vs. CN.

Vibration Number	$S_{CD} / \text{J}\cdot\text{mol}^{-1}\cdot\text{K}^{-1}$	$S_{CN} / \text{J}\cdot\text{mol}^{-1}\cdot\text{K}^{-1}$	$S_{CD} - S_{CN} / \text{J}\cdot\text{mol}^{-1}\cdot\text{K}^{-1}$
1	34.3	23.5	10.9
2	22.8	26.9	-4.1
3	22.2	20.3	1.9
4	18.1	18.2	-0.1
5	16.9	15.7	1.2
6	12.2	12.1	0.1
7	11.5	9.9	1.6
8	9.7	9.7	0.0
9	8.8	8.8	-0.1
10	8.1	8.3	-0.2
11	7.2	7.6	-0.5
12	7.0	6.9	0.1
13	6.6	6.4	0.2
14	6.4	6.2	0.3
15	5.2	5.4	-0.1
16	4.9	5.1	-0.1
17	4.6	4.8	-0.2
18	4.5	4.4	0.1
19	3.9	3.8	0.1
20	3.6	3.6	0.0
TOTAL	218.7	207.6	11.1

Vibration Number 1

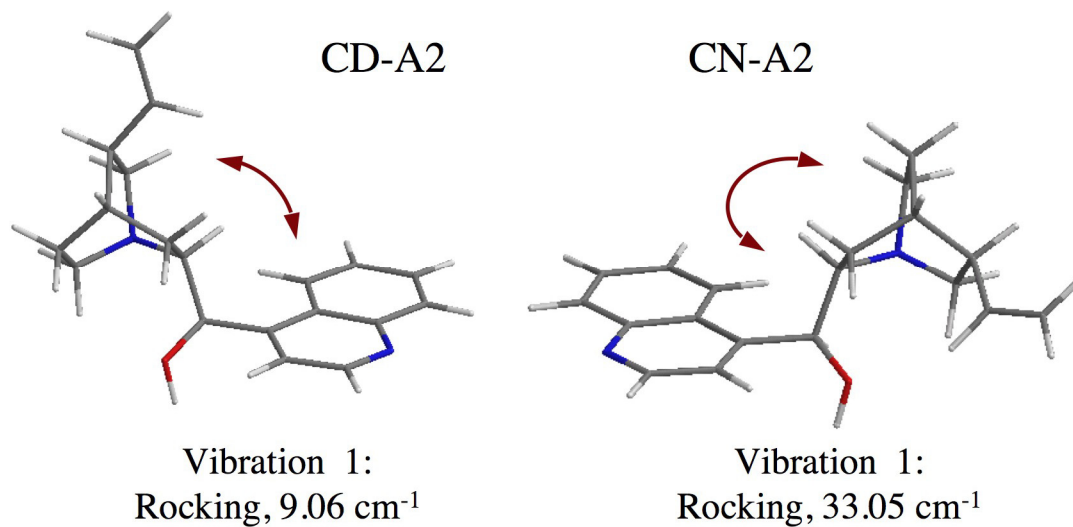


Table 3.1. Entropy Contributions from Each Vibrational Mode in the Most Stable Configurations of CD and CN.

Configuration	$\angle[\text{C}_3\text{--C}_4\text{--C}_9\text{--C}_8]$	$\angle[\text{C}_4\text{--C}_9\text{--C}_8\text{--N}]$	$\angle[\text{H--C}_5\text{--C}_V\text{--H}]$	$E_{\text{Rel}} / \text{kJ}\cdot\text{mol}^{-1}$	Relative Population	$S / \text{J}\cdot\text{mol}^{-1}\cdot\text{K}^{-1}$
CD-A2	102.3	152.6	-176.9	0.0	0.6849	590.4
CD-B2	101.5	-85.4	-175.6	6.2	0.0553	572.7
CD-C2	84.1	68.8	-176.5	9.1	0.0172	580.4
CD-A1(i)*	-87.8	151.1	-176.2	11.0	0.0000	558.7
CD-B1	-81.1	-88.1	-175.3	14.1	0.0023	573.2
CD-C1	-105.3	58.3	-176.4	6.4	0.0527	585.5
CD-A3	16.5	153.1	-177.2	13.4	0.0031	591.3
CD-B3	2.0	-86.3	-176.2	30.1	0.0000	566.8
CD-C3	12.2	54.3	-178.3	12.4	0.0046	587.6
CD-A2-2	102.1	154.1	60.5	5.1	0.0888	583.5
CD-A2-3	102.1	151.8	-72.9	6.6	0.0478	579.9
CD-B2-2	101.3	-86.0	61.1	9.8	0.0131	568.9
CD-B2-3	101.0	-84.8	-77.1	11.1	0.0076	569.6
CD-C2-2	82.7	68.3	62.4	13.3	0.0031	580.6
CD-C2-3	83.1	67.7	-75.1	14.8	0.0018	579.6
CD-A1-2	-88.0	150.4	62.5	16.0	0.0011	585.9
CD-A1-3	-87.3	153.6	-75.4	17.3	0.0006	582.2
CD-B1-2	-81.6	-88.9	60.7	18.2	0.0004	568.7
CD-B1-3	-81.7	-88.3	-76.4	19.3	0.0003	570.3
CD-C1-2	-104.8	60.3	59.2	10.9	0.0085	584.3
CD-C1-3	-104.5	61.1	-74.2	12.3	0.0047	581.6
CD-A3-2	17.7	152.9	61.8	17.6	0.0006	594.4
CD-A3-3	15.8	153.4	-71.6	19.3	0.0003	583.5
CD-B3-2	1.9	-86.4	60.6	33.6	0.0000	570.2
CD-B3-3	1.7	-86.0	-75.8	35.6	0.0000	566.7
CD-C3-2	13.3	54.1	64.3	17.2	0.0007	590.7
CD-C3-3	13.7	53.3	-68.6	18.6	0.0004	583.4

* Imaginary frequency

$$S_{\text{CD,Total}} = \sum [S \cdot (\text{Relative Population})] = 587.3 \text{ J}\cdot\text{mol}^{-1}\cdot\text{K}^{-1}$$

Table 3.2. Entropies for Each of the 27 Most Stable Configurations, Cinchonidine.

Configuration	$\angle[\text{C}_3\text{-C}_4\text{-C}_9\text{-C}_8]$	$\angle[\text{C}_4\text{-C}_9\text{-C}_8\text{-N}]$	$\angle[\text{H-C}_5\text{-C}_v\text{-H}]$	$E_{\text{Rel}} / \text{kJ}\cdot\text{mol}^{-1}$	Relative Population	$S / \text{J}\cdot\text{mol}^{-1}\cdot\text{K}^{-1}$
CN-A2	-100.1	-158.7	-174.6	0.0	0.6782	579.0
CN-B2	-101.2	85.8	-178.5	5.3	0.0811	570.0
CN-C2	-83.5	-67.5	178.6	8.0	0.0266	587.7
CN-A1	88.5	-149.6	-174.5	10.7	0.0092	581.4
CN-B1	81.5	87.4	-177.0	13.8	0.0026	569.7
CN-C1	104.0	-61.6	179.6	6.1	0.0574	584.4
CN-A3	-18.0	-151.9	-174.0	13.7	0.0027	581.4
CN-B3	-3.0	87.1	173.2	35.5	0.0000	566.4
CN-C3	-12.8	-57.0	-180.0	13.0	0.0036	587.3
CN-A2-2	-100.6	-156.4	42.5	6.3	0.0525	578.6
CN-A2-3	-101.2	-157.3	-68.9	7.5	0.0324	576.5
CN-B2-2	-100.8	83.6	57.6	9.1	0.0171	567.0
CN-B2-3	-100.6	84.9	-67.5	11.4	0.0068	563.9
CN-C2-2	-84.2	-67.7	66.5	12.3	0.0048	580.7
CN-C2-3	-83.4	-66.1	-65.7	13.3	0.0032	578.5
CN-A1-2	87.7	-155.7	42.3	16.2	0.0010	575.9
CN-A1-3	88.6	-154.2	-68.5	17.1	0.0007	578.3
CN-B1-2	82.2	88.8	58.8	17.2	0.0006	571.9
CN-B1-3	82.7	88.0	-68.0	19.5	0.0003	566.6
CN-C1-2	103.9	-61.2	66.8	10.2	0.0112	586.1
CN-C1-3	104.3	-60.0	-66.4	11.4	0.0068	579.0
CN-A3-2	-16.9	-152.9	41.5	20.6	0.0002	588.3
CN-A3-3	-16.3	-152.9	-69.6	22.1	0.0001	586.2
CN-B3-2	-1.1	86.9	76.0	36.2	0.0000	562.8
CN-B3-3	-0.1	86.2	-68.4	35.6	0.0000	562.7
CN-C3-2	-14.3	-55.1	66.9	17.1	0.0007	592.3
CN-C3-3	-13.6	-54.7	-67.9	18.6	0.0004	583.7

$$S_{\text{CN,Total}} = \sum [S \cdot (\text{Relative Population})] = 578.6 \text{ J}\cdot\text{mol}^{-1}\cdot\text{K}^{-1}$$

Entropy difference, CD minus CN:

$$S_{\text{CD,Total}} - S_{\text{CN,Total}} = (587.3 - 578.6) \text{ J}\cdot\text{mol}^{-1}\cdot\text{K}^{-1} = 8.7 \text{ J}\cdot\text{mol}^{-1}\cdot\text{K}^{-1}$$

Table 3.3. Entropies for Each of the 27 Most Stable Configurations, Cinchonine.

The entropies associated with the internal vibrations and rotations of the two cinchona were estimated to differ by approximately 11.4 J/mol·K between the most stable conformers, and by 8.7 J/mol·K between energy-weighted values using their nine most stable conformers (and three rotational positions for the vinyl moiety for each conformer). Those numbers are within the same order of magnitude of the $\Delta S = 14 \pm 9$ J/mol·K difference observed experimentally (Figure 3.8). Moreover, most of this difference ($\Delta S = 11.1$ J/mol·K) could be ascribed to one particular molecular internal vibration, a "clam" like motion with the alcoholic linker acting as the hinge in cinchonidine ($\nu = 9$ cm⁻¹) that becomes more of a twisting motion in cinchonine ($\nu = 33$ cm⁻¹). It appears that the change in position of the vinyl group within the quinuclidine ring between the two (cinchonidine vs. cinchonine) molecules leads to a significant change in the moment of inertia of the overall quinuclidine-vinyl moiety relative to the alcoholic linker, and therefore to noticeable variations in the density of states for this mode that determines the entropy of dissolution.

It should be noted that the data in Figure 3.8 also indicate vastly different values for both the entropy and the enthalpy of dissolution with different solvents: witness the contrast between cinchonidine in ethanol versus carbon tetrachloride. Nevertheless, within the same solvent, the solubility differences among cinchona alkaloids are mostly due to changes in entropy. This is in contrast with the properties in solid state, where the rotational conformations may be locked and energetic factors dominate. In fact, similar rotational limitations may in some instances play a role in solution as well. At an extreme, acidic solvents are known to lock specific cinchona conformers by fixing the

quinoline and quinuclidine rings together via hydrogen-bond bridges.^{24, 35} Additional molecular-rotation restrictions are expected in heterogeneous catalysis, where the cinchona need to bond to the solid (typically platinum dispersed in a high-surface-area oxide). This is believed to occur via bonding of the quinoline ring to the surface of the metal, and to be optimum for a flat ring orientation.³⁶⁻³⁸

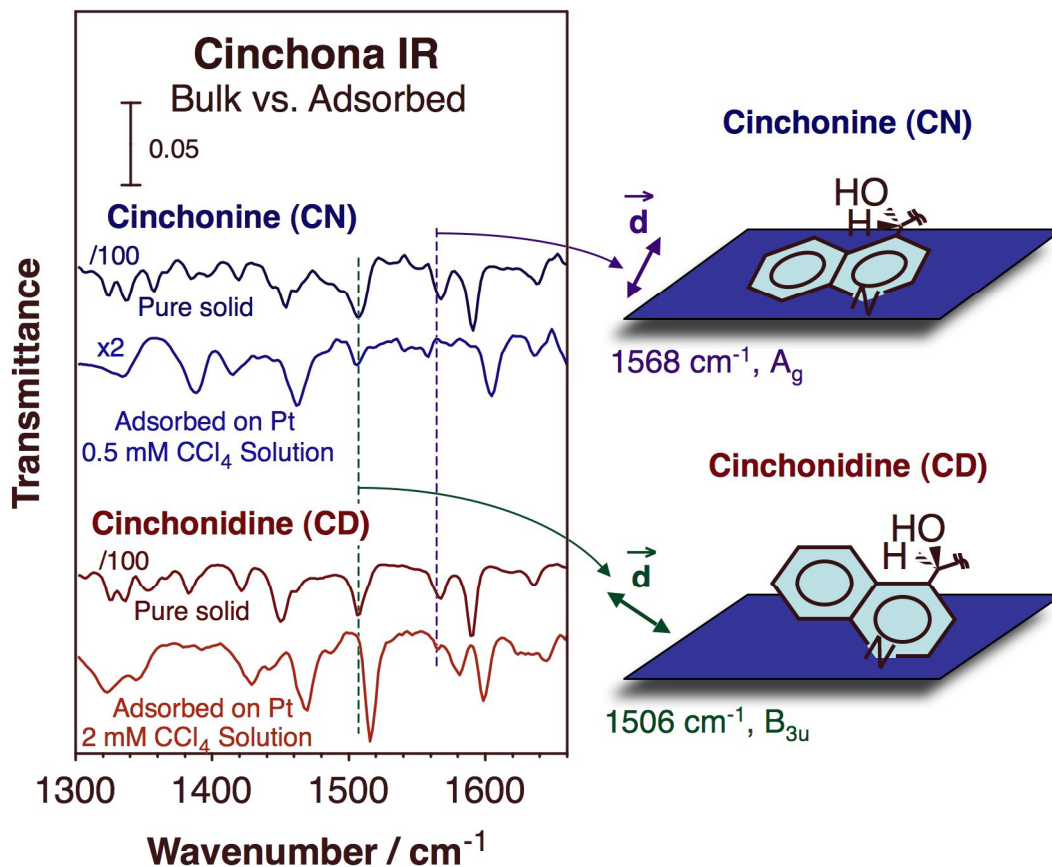


Figure 3.10. Adsorption geometries of cinchona alkaloids on platinum surfaces. Infrared absorption spectra for cinchonine (blue, top two traces) and cinchonidine (red, bottom two traces), both as pure solids (taken in transmission mode, top traces in each pair) and adsorbed onto a platinum polished foil from carbon tetrachloride solutions (acquired in situ in reflection-absorption mode, bottom traces of each pair). Both the shifts in frequencies and the changes in relative intensities seen between the spectra of the solid versus those of the adsorbed species provide information about bonding to the surface, which proved to be different with each cinchona alkaloid.

Our in-situ infrared characterization data indicate different modes of adsorption for different cinchona alkaloids, at least at high coverages.^{33, 39} Figure 3.10 provides infrared absorption spectra for cinchonine and cinchonidine both as solids and adsorbed on Pt from CCl₄ solutions to illustrate this point. A number of observations are worth highlighting here: (1) with both molecules, the peaks associated with the deformation of the quinoline ring are blue-shifted upon adsorption, corroborating the idea of bonding through that moiety; (2) the spectra of cinchonidine and cinchonine solids are quite similar, but those of the adsorbed species are quite different, presumably because each molecule adopts a different mode of adsorption; (3) the peak at 1568 cm⁻¹, due to a quinoline A_g mode, is blue-shifted in the spectrum of adsorbed cinchonidine (to 1581 cm⁻¹), a sign of adsorption via the N–C₂ bond (conversely, that peak becomes invisible in the spectrum of adsorbed cinchonine); (4) the feature at 1506 cm⁻¹, a quinoline B_{3u} mode with its dynamic dipole along the long axis, becomes blue-shifted and quite intense upon adsorption for cinchonidine, again indicating that the ring stands on the N–C₂ bond;⁴⁰ (5) for cinchonine that mode is weak and has the same frequency as in the solid, so the long axis of the ring is likely to be aligned close to the plane of the surface; (6) the peak at 1451 cm⁻¹, associated mainly with CH₂ scissoring motions within the non-vinyl-substituted ring of the quinuclidine bicyclic system, also blue-shifts upon adsorption (more in the cinchonidine case).

The overall conclusion is that the quinoline ring of cinchonine tilts along its long axis, perhaps to optimize π – π intermolecular interactions, whereas in cinchonidine the ring tilts along the short axis and binds mainly through the lone electron pair of the

nitrogen atom. There seems to be a better proximity of the quinuclidine ring to the surface with cinchonine, most likely because of the different placement of the vinyl moiety. These arguments mimic those used to explain the higher stability of cinchonine crystals. However, it should also be noted that the data in Figure 6 and our previous reports indicate that cinchonine monolayers reach saturation at lower solution concentrations (~0.5 mM) than cinchonidine monolayers (~2 mM).^{39, 41, 42} The ultimate adsorption behavior of these cinchona is determined by a balance between the weaker cinchonidine bond to the surface and its higher solubility, that is, between energetic and entropic factors. Certainly, cinchonidine can still displace cinchonine from the surface (the opposite not being true),⁴¹ and is more effective at imparting chirality in heterogeneous catalysis.⁴³⁻⁴⁵

3.4 DISCUSSION

The typical cinchona alkaloids readily available as natural products all share a common central structure with an alcoholic linker holding quinuclidine and quinoline rings together, and display similar chemical and physiological behavior. Nevertheless, they also show a number of significant differences in basic physicochemical properties, as highlighted by the results reported here. We traced back these differences to the substitutions in the peripheral positions of each individual molecule, specifically the vinyl (or ethyl) moiety bonded to the quinuclidine bicycle, which is placed in sterically different positions in cinchonidine and quinine versus cinchonine and quinidine, and the

added methoxy group in quinine and quinidine (compared to cinchonidine and cinchonine, respectively).

Our studies indicate that those groups alter the fundamental properties of these molecules via a combination of energetic and entropic effects, which influence the corresponding rotational conformation spaces. Accordingly, the different crystallographic structures adopted by cinchonidine versus cinchonine are explained by a more optimized packing in the latter, which presumably allows for better intermolecular interactions. Cinchonine is also less soluble than cinchonidine, but that difference is mostly ascribed to entropic, not energetic, factors: both energetic and entropic terms in the solubility of cinchona alkaloids are highly dependent on the nature of the solvent, but the energetic variations appear to be similar for all the cinchona molecules. Finally, additional rotational restrictions are imposed on these molecules upon adsorption on solid surfaces, forcing them to adopt significantly different configurations. The combined variations in adsorption geometry and solubility account for the differences in adsorption equilibrium seen with different members of this cinchona alkaloids family.

These differences in physicochemical properties translate into the differences in chemical reactivity that make each molecule so unique. For instance, quinidine (where the C₈ and C₉ atoms have S and R chiral configurations, respectively) has been reported to be more than twice as active as an antimalarial agent as quinine (which has the opposite 8R, 9S configuration in the chiral pocket), and over two orders of magnitude more effective than 9-epiquinine and 9-epiquinidine (the 8S, 9S and 8R, 9R alkaloids).¹⁴ The relative inactivity of the latter 9-epi isomers has been justified in terms of differences

in the relative positioning of the hydroxyl group versus the quinuclidine nitrogen atom, which allegedly controls the relative strengths of the hydrogen bonds that need to be formed with haematin in the vacuole of the parasite (an interaction central to the antimalarial activity),¹⁴ but that cannot explain the differences between quinine and quinidine. Those are more likely due, at least in part, to differences in the distribution ratio (D) of the cinchona between aqueous and lipid phases, because a larger D increases the transfer rate of the drug through the erythrocyte membrane (a lipid) into the parasite's vacuole.¹⁵ The experimental values for these partition ratios at a pH of 7.4 vary from 92:1 with quinine to 44:1 with quinidine and ~5:1 with the 9-epi compounds,¹⁵ a trend that correlates well with the solubilities reported in Figure 3 ($Sol_{QN}/Sol_{QD} = 1.6$). This still does not fully explain all the antimalarial activity trends, because partition of the cinchona into the lipid erythrocyte membrane also depends on energetic factors akin to those seen in adsorption. Nevertheless, our observations indicate that entropic, in addition to bond-strength, factors need to be considered in this discussion.

Another key property affected by the configuration of the cinchona alkaloids is their enantioselective promoting capacity in heterogeneous catalysis. In particular, cinchonidine and cinchonine promote the formation of opposite enantiomers during the hydrogenation of α -ketoesters such as ethyl pyruvate on platinum catalysts (to produce (R)- and (S) hydroxoesters, respectively), as expected, but with significantly different enantioselectivities: cinchonidine is more enantioselective than cinchonine.^{44, 46} Bartók and coworkers have justified these trends in terms of different adsorption geometries for cinchonidine versus cinchonine on the platinum surface⁴⁷, but Baiker et al. dismissed

such an explanation in favor of differences in adsorption strength.⁷ Our data indicate not only that the two effects are in fact related,³³ but that differences in solubilities contribute to the adsorption equilibria as well.^{41, 42} Again, both energetic and entropic factors, associated both with the geometries and strengths of bonding and with solubilities, contribute to the overall performance of the cinchona-platinum catalytic system.

3.5 CONCLUSION

In conclusion, it is our contention that the specific position of the peripheral substitutions explains most of the differences in performance among related cinchona alkaloids. We were able to correlate the variations in basic properties among these different cinchona alkaloids with their specificity in medical and chemical applications. Now that these compounds can be made synthetically,¹ they may be tailor-designed for the use of interest by applying the basic structure-function understanding revealed by our work. Furthermore, subtle structural changes such as those illustrated here, leading to changes in both energetic and entropic terms, could be also used to tune specific fundamental properties in many other systems, and to guide, for instance, the synthesis of new molecules with targeted properties.

REFERENCES

- (1) Kaufman, T. S.; Rúveda, E. A., *Angew. Chem. - Int. Ed.* **2005**, *44*, 854.
- (2) Ashley, E.; McGready, R.; Proux, S.; Nosten, F., *Travel. Med. Infect. Dis.* **2006**, *4*, 159.
- (3) White, N. J., *Lancet Infect. Dis.* **2007**, *7*, 549.
- (4) Meyer, C. G.; Marks, F.; Hay, J., *Trop. Med. Int. Health* **2004**, *9*, 1239.
- (5) Wynberg, H., *Top. Stereochem.* **1986**, *16*, 87.
- (6) Kacprzak, K.; Gawroński, J., *Synthesis* **2001**, 961.
- (7) Mallat, T.; Orglmeister, E.; Baiker, A., *Chem. Rev.* **2007**, *107*, 4863.
- (8) Ma, Z.; Zaera, F., Chiral Modification of Catalytic Surfaces. In *Design of Heterogeneous Catalysis: New Approaches Based on Synthesis, Characterization, and Modelling*; Ozkan, U. S., Ed.; Wiley-VCH: Weinheim, 2009; pp 113-140.
- (9) Lämmerhofer, M.; Lindner, W., *Adv. Chromatog.* **2008**, *46*, 1.
- (10) Oleksyn, B. J.; Suszko-Purzycka, A.; Dive, G.; Lamotte-Brasseur, J., *J. Pharm. Sci.* **1992**, *81*, 122.
- (11) Karle, J. M.; Bhattacharjee, A. K., *Bioorg. Med. Chem.* **1999**, *7*, 1769.
- (12) Caner, H.; Biedermann, P. U.; Agranat, I., *Chirality* **2003**, *15*, 637.
- (13) Debarge, S.; Thibaudeau, S.; Violeau, B.; Martin-Mingot, A.; Jouannetaud, M. P.; Jacquesy, J. C.; Cousson, A., *Tetrahedron* **2005**, *61*, 2065.
- (14) Karle, J. M.; Karle, I. L.; Gerena, L.; Milhous, W. K., *Antimicrob. Agents Chemother.* **1992**, *36*, 1538.
- (15) Warhurst, D. C.; Craig, J. C.; Adagu, I. S.; Meyer, D. J.; Lee, S. Y., *Malaria J.* **2003**, *2*, 1.
- (16) Exner, C.; Pfaltz, A.; Studer, M.; Blaser, H.-U., *Adv. Synth. Catal.* **2003**, *345*, 1253.

- (17) Bartók, M.; Sutyinszki, M.; Balázsik, K.; Szöllödblacsi, G., *Catal. Lett.* **2005**, *100*, 161.
- (18) Braje, W. M.; Wartchow, R.; Hoffmann, H. M. R., *Angew. Chem. - Int. Ed.* **1999**, *38*, 2540.
- (19) Segall, M. D.; Lindan, P. J. D.; Probert, M. J.; Pickard, C. J.; Hasnip, P. J.; Clark, S. J.; Payne, M. C., *J. Phys.: Condens. Matter* **2002**, *14*, 2717.
- (20) Perdew, J. P.; Burke, K.; Ernzerhof, M., *Phys. Rev. Lett.* **1996**, *77*, 3865.
- (21) Vanderbilt, D., *Phys. Rev. B* **1990**, *41*, 7892.
- (22) Lee, C.; Yang, W.; Parr, R. G., *Phys. Rev. B* **1988**, *37*, 785.
- (23) Becke, A. D., *J. Chem. Phys.* **1993**, *98*, 5648.
- (24) Olsen, R. A.; Borchardt, D.; Mink, L.; Agarwal, A.; Mueller, L. J.; Zaera, F., *J. Am. Chem. Soc.* **2006**, *128*, 15594.
- (25) James, K. C., *Solubility and Related Properties*, Marcel Dekker: New York, 1986.
- (26) Ma, Z.; Zaera, F., *J. Phys. Chem. B* **2005**, *109*, 406.
- (27) Kubota, J.; Ma, Z.; Zaera, F., *Langmuir* **2003**, *19*, 3371.
- (28) Oleksyn, B.; Lebioda, L.; Ciecchanowicz-Rutkowska, M., *Acta Crystallogr. B* **1979**, *35*, 440.
- (29) Here we follow the standard nomenclature used to number the carbon and hydrogen atoms, see Figure 2 and refs. 30 and 31
- (30) Dijkstra, G. D. H.; Kellogg, R. M.; Wynberg, H., *Recl. Trav. Chim. Pays-Bas* **1989**, *108*, 195.
- (31) Dijkstra, G. D. H.; Kellogg, R. M.; Wynberg, H., *J. Org. Chem.* **1990**, *55*, 6121.
- (32) Lide, D. R., *CRC Handbook of Chemistry and Physics*. 86th ed.; Taylor & Francis, CRC Press: Boca Raton, 2005.
- (33) Mink, L.; Ma, Z.; Olsen, R. A.; James, J. N.; Sholl, D. S.; Mueller, L. J.; Zaera, F., *Top. Catal.* **2008**, *48*, 120.

- (34) Silva, T. H. A.; Oliveira, A. B.; Dos Santos, H. F.; De Almeida, W. B., *Struct. Chem.* **2001**, *12*, 431.
- (35) Ferri, D.; Bürgi, T.; Baiker, A., *J. Chem. Soc., Perkin Trans. 2* **2002**, 437.
- (36) Kubota, J.; Zaera, F., *J. Am. Chem. Soc.* **2001**, *123*, 11115.
- (37) Ferri, D.; Bürgi, T.; Baiker, A., *Chem. Comm.* **2001**, 1172.
- (38) Chu, W.; LeBlanc, R. J.; Williams, C. T.; Kubota, J.; Zaera, F., *J. Phys. Chem. B* **2003**, *107*, 14365.
- (39) Zaera, F., *J. Phys. Chem. C* **2008**, *112*, 16196.
- (40) Zaera, F., Surface Structural Determinations: Optical Methods. In *Encyclopedia of Chemical Physics and Physical Chemistry*; Moore, J. H.; Spencer, N. D., Eds.; IOP Publishing Inc.: Philadelphia, 2001; Vol. 2, pp 1563 - 1581.
- (41) Ma, Z.; Zaera, F., *J. Am. Chem. Soc.* **2006**, *128*, 16414.
- (42) Ma, Z.; Lee, I.; Zaera, F., *J. Am. Chem. Soc.* **2007**, *129*, 16083.
- (43) Simons, K. E.; Meheux, P. A.; Ibbotson, A.; Wells, P. B., *Stud. Surf. Sci. Catal.* **1993**, *75*, 2317.
- (44) Blaser, H.-U.; Jalett, H. P.; Lottenbach, W.; Studer, M., *J. Am. Chem. Soc.* **2000**, *122*, 12675.
- (45) Meier, D. M.; Mallat, T.; Ferri, D.; Baiker, A., *J. Catal.* **2006**, *244*, 260.
- (46) Slipszenko, J. A.; Griffiths, S. P.; Johnston, P.; Simons, K. E.; Vermeer, W. A. H.; Wells, P. B., *J. Catal.* **1998**, *179*, 267.
- (47) Bartók, M., *Curr. Org. Chem.* **2006**, *10*, 1533.
- (48) Urakawa, A.; Meier, D. M.; Rügger, H.; Baiker, A., *J. Phys. Chem. A* **2008**, *112*, 7250.

CHAPTER IV

THE ROTATIONAL BARRIERS IN PYRIDINE THIOCARBOXAMIDES: DYNAMIC NUCLEAR MAGNETIC RESONANCE AND AB INITIO STUDIES

ABSTRACT

Thiocarboxamides are a class of compounds with many technical applications, *e.g.* as vulcanization promoters, as metal deactivators in petrochemistry, in pest control, and as pharmacologically important substances. In this study, we make use of dynamic nuclear magnetic resonance (NMR) and *ab initio* calculations to investigate amide rotational barriers of a series of pyridine thiocarboxamides. The experimentally determined activation enthalpies and entropies are $\Delta H^\ddagger = +16.7 \pm 0.6$ kcal/mol and $\Delta S^\ddagger = -11.6 \pm 1.5$ cal/mol·K for thionicotinamide, and $\Delta H^\ddagger = +17.4 \pm 0.7$ kcal/mol and $\Delta S^\ddagger = -9.9 \pm 1.6$ cal/mol·K for thioisonicotinamide, respectively. *Ab initio* calculations of the rotational barriers are in a good agreement with the experimentally measured values. A direct comparison between thionicotinamide and thioisonicotinamide highlights the significance of π electron donation from the pyridine ring to thiocarboxamide moieties. Further comparison between thiocarboxamides and their corresponding amide analogues based on NBO analysis supports the canonical amide resonance model, and indicates the important role of the interaction between amide N lone pairs and C=X π^* antibond.

4.1 INTRODUCTION

As the building block of peptides and proteins, amide bonds play a critical role in both chemistry and biology. The most important feature of the amide bonds is the significantly higher barrier of C–N bond rotation than those found in other amines. This hindered rotation is rationalized by the classical resonance model¹ (Figure 4.1). In this model, it's proposed that the donation of lone-pair electron density from the amide nitrogen to the carbonyl carbon gives rise to partial double bond character of the amide linkage, which in turn raises the rotational barrier.

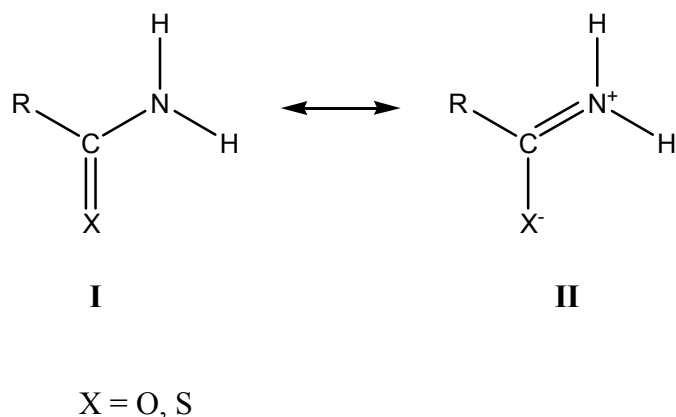


Figure 4.1. Resonance model proposed by Pauling

This barrier determines stability of protein conformation as well as the secondary and the tertiary structure, which consecutively decide the biological activity. On the other hand, this barrier can be modified by a number of structural and electronic properties. On both

accounts, the amide linkage has been extensively investigated both theoretically and experimentally²⁻³¹.

In our previous studies^{2,3}, amide bond rotational barriers of a series of pyridine carboxamides, *i.e.*, picolinamide (2-pyridinylcarboxamide), nicotinamide (3-pyridinylcarboxamide, vitamin B₃), and isonicotinamide (4-pyridinylcarboxamide), have been investigated by dynamic NMR spectroscopy. A substantial difference of 5.4 kcal/mol in their enthalpies of activation has been found. Among those three medicinally important regioisomers, picolinamide's barrier ($\Delta H^\ddagger = +18.3 \pm 0.4$ kcal/mol) is the highest one, followed by isonicotinamide ($\Delta H^\ddagger = +14.1 \pm 0.2$ kcal/mol), and nicotinamide ($\Delta H^\ddagger = +12.9 \pm 0.3$ kcal/mol). *Ab initio* calculations of the rotational barriers agreed well with the experimentally measured values, and further investigation of structures and energetics attributed three major contributions to this significant enthalpy difference. Of principal importance are steric interactions in the ground states of nicotinamide and isonicotinamide, superior π electron donation from the pyridine ring in the transition state of nicotinamide than those of picolinamide and isonicotinamide, and an intramolecular hydrogen bond in the ground state of picolinamide. Furthermore, in our previous paper³, a new least-squares fitting procedure has been introduced, and the strength of this data analysis method is being able to extract the enthalpy and entropy of activation from dynamic NMR data while avoiding imposing a "limiting line width" measured experimentally under conditions of negligible exchange. In specific, we fitted the apparent rate versus temperature profile to a composite curve that includes a constant

term for the limiting line width plus the temperature-weighted exponential rise of transition state theory, so as to avoid the error from poor estimation of the limit line width.

In this work, this simple but reliable fitting procedure will be applied to measurements of the rotational barriers in a series of pyridine thiocarboxamides (Figure 4.2), *i.e.*, thionicotinamide (pyridine-3-thiocarboxamide) and thioisonicotinamide (pyridine-4-thiocarboxamide). These two regioisomers are essentially the thio analogues of nicotinamide and isonicotinamide, correspondingly. This family of compounds shows important biological activity as anticonvulsants, local anesthetics, sedatives, muscle relaxants and enzyme inhibitors. Consequently, they are playing an important role in the pharmaceutical, agricultural, and chemical industries³²⁻³⁵. Here, the rotational barriers of these two pharmaceutically significant pyridine thiocarboxamides are determined by dynamic nuclear magnetic resonance (NMR) spectroscopy, a powerful and well-established method. As the C-N bond rotates, the chemically inequivalent nitrogen protons exchange. The resulting dynamic NMR spectra are quite sensitive to the rate of this exchange, and allow for extraction of the kinetic parameters through variable-temperature NMR experiments without perturbing equilibrium. These experiments show a difference (0.7 kcal/mol) in rotational barriers of thionicotinamide and thioisonicotinamide, primarily due to the variations in π electron donation from the pyridine ring to thiocarboxamide moieties. Of particular importance, a remarkable higher activation energy for bond rotations in thiocarboxamide has been found than that in its corresponding amide analogue by 3-4 kcal/mol. Further NBO analysis recognizes the critical role of the interaction between amide N lone pairs and C=X π^* antibond, and

suggests that chalcogen replacement of O with S strengthens the amide resonance effect, resulting in more double bond character of C-N in thiocarboxamide than its amide analogue, which supports the traditional resonance model and helps shed light on the structural and electronic properties responsible for the differential pharmacological activities of thiocarboxamides and carboxamides.

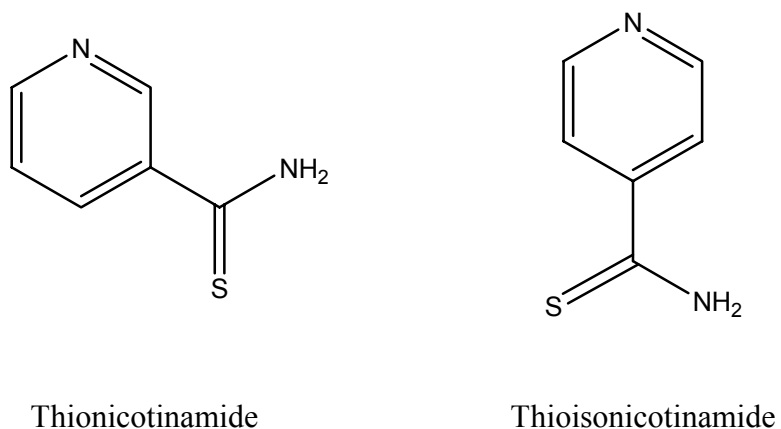


Figure 4.2. The pyridine thiocarboxamides.

4.2 MATERIALS AND METHODS

¹H NMR spectra were recorded on a Bruker Advance 600 spectrometer (¹H frequency 600.13 MHz) equipped with a 5 mm high-resolution double resonance probe with the second channel tuned for ¹⁴N decoupling. Spectra were acquired over a range of temperatures from 76 °C to 144 °C (349 K to 417 K) via an FTS Systems AIRJET

temperature preconditioner. Samples of thionicotinamide (Alfa Aesar), and thioisonicotinamide (AKSci) were prepared in deuterated dimethyl sulfoxide (DMSO, Cambridge Isotope Laboratories) at 5 mg/mL and placed in a 5 mm (OD) NMR tube (Wilmad Glass). A rough estimate of the temperature was provided by the probe thermocouple while the actual temperature was determined by a digital thermocouple. The choice dimethyl sulfoxide (DMSO) as solvent was made on the basis of its ability to accept hydrogen bonds and its convenient liquid-phase temperature range. Aqueous solutions were avoided because of exchange between the amide protons and the water molecules.

A one-pulse experiment with CYCLOPS phase cycling³⁶ was used to obtain the NMR data. Conformer exchange rates were extracted from the real parts of the measured spectra using a complete line shape analysis written within the *Mathematica* programming environment³⁷. Besides the resonance line positions, peak amplitude, half-width, and exchange-induced phase lean, the fitting model incorporated an overall phase correction and a cubic baseline correction as well. Nonexchanging peaks were excluded from the region of the spectrum that was fit whenever possible. In the cases of spectral overlap with nonexchanging peaks, additional Lorentzian lines were integrated into the model to accommodate spectral overlap in the fit window.

The extracted half-widths were used as apparent rates to determine both the entropy and enthalpy of activation associated with the barrier to amide bond rotation based on transition state theory³⁸. This fitting procedure was again performed in *Mathematica*, with the data weighted inversely proportional to numerically estimated

variances of the measured half-widths. The result of the linearized fitting procedure described in our previous study³ was a composite curve composed of a constant along with the temperature-weighted exponential rise of transition-state theory. Error bars for ΔH^\ddagger and ΔS^\ddagger were determined through a numerical calculation of the covariance matrix and are reported as \pm one standard error.

Ab initio calculations were first performed at the restricted density functional (DFT) level of theory using the Gaussian 03 software package³⁹. Molecules were optimized without constraint to their ground and transition state geometries at the B3LYP⁴⁰⁻⁴²/6-311G(d,p) level of theory. Ground and transition states were verified by frequency analysis after optimization, and zero-point energy corrections were applied with the appropriate scaling at the same level. The optimized structures were further analyzed by Weinhold's natural bond orbital (NBO) methods⁴³, which were carried out at the MP2⁴⁴/6-311G(d,p) level of theory using NBO 5.0 interfaced to NWCHEM 4.5 package⁴⁵. Particular attention is focused on the natural population analysis (NPA) and natural resonance theory (NRT) treatment of the calculated charge densities.

4.3 RESULTS AND DISCUSSION

As the C-N bond rotates, chemical exchange of the two thioamide protons has a profound effect on the observed NMR line shapes. Figures 4.3(A) and Figure 4.4(A) show the ¹H NMR spectra of thionicotinamide and thioisonicotinamide at different temperatures, characterized by different rates of chemical exchange. At lower

temperatures where the exchange rate is slow, distinct resonances are observed for the chemically different thioamide protons. As the temperature rises, the exchange rate correspondingly increases. As a result, the lines initially broaden and then eventually coalesce. This region is known as intermediate exchange in which the line shapes are most sensitive to the exchange rates. If the temperature is further increased and the fast exchange happens, this coalesced single peak will become increasingly narrow. Figure 4.3(B) and Figure 4.4(B) show the results of fitting to the two-site exchange model and residuals from the fits for the spectra shown in Figures 4.3(A) and Figure 4.4(A), respectively. The extracted apparent rates as a function of temperature for both compounds are summarized in Table 4.1 and shown graphically in Figure 4.5. Figure 4.5 also includes the best-fit curves to transition state theory by the form of

$$r = \frac{1}{T_2} + \frac{k_B T}{h} e^{+\Delta S^\ddagger/R} e^{-\Delta H^\ddagger/RT}.$$

Here k_B denotes the Boltzmann constant, h denotes Planck's constant, and R denotes the gas constant, $\frac{1}{T_2}$ is the constant term incorporated as the limiting line width with the purpose of avoiding the error from poor estimation of this parameter. The best-fit values are $\Delta H^\ddagger = +16.7 \pm 0.6$ kcal/mol, $\Delta S^\ddagger = -11.6 \pm 1.5$ cal/mol·K, and $T_2 = 49.3 \pm 2.0$ ms for thionicotinamide, and $\Delta H^\ddagger = +17.4 \pm 0.7$ kcal/mol, $\Delta S^\ddagger = -9.9 \pm 1.6$ cal/mol·K, $T_2 = 50.7 \pm 2.0$ ms for thioisonicotinamide (Table 4.2), respectively. A fair difference of 0.7 kcal/mol in the activation enthalpies has been found between thionicotinamide and thioisonicotinamide.

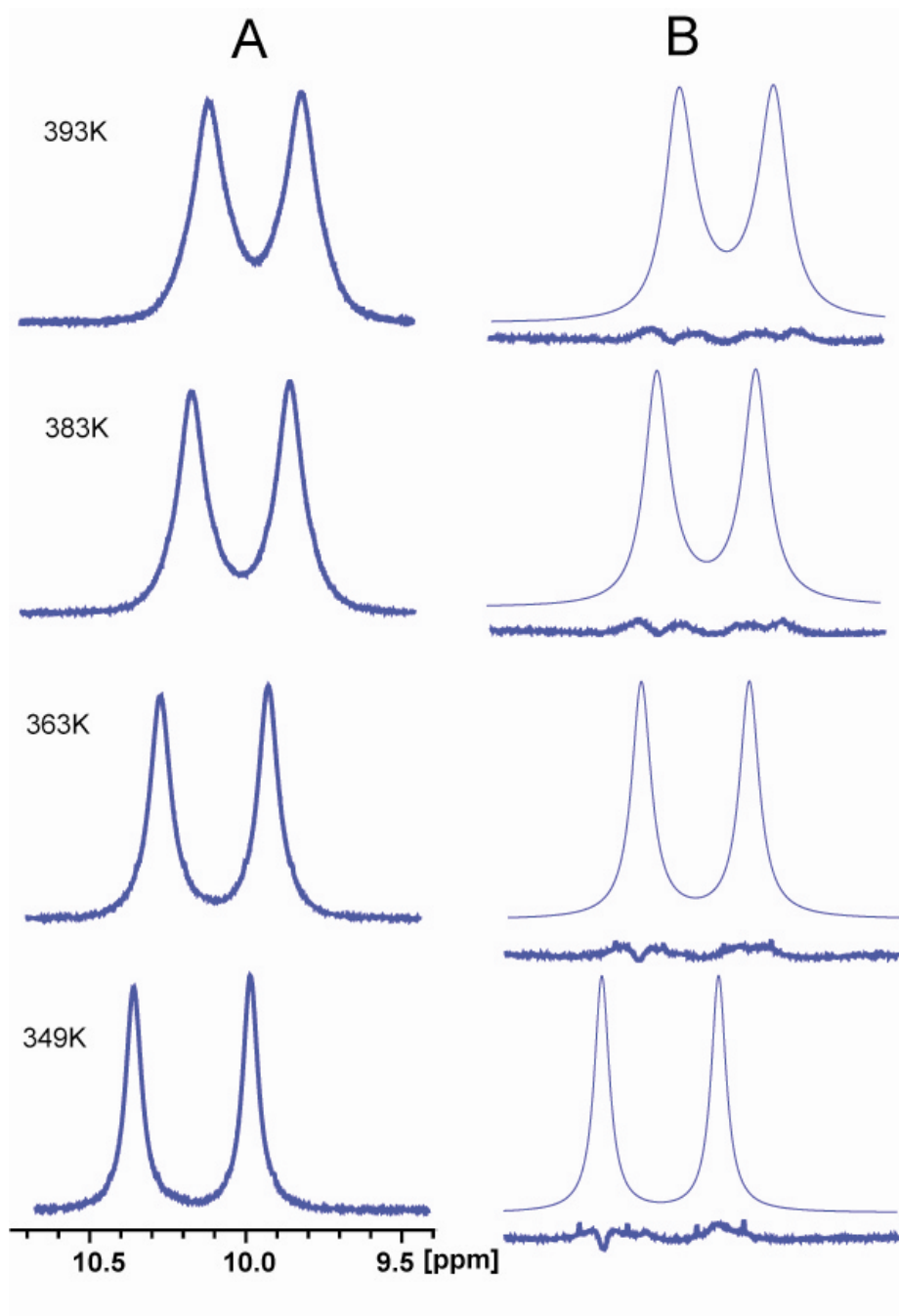


Figure 4.3. Dynamic NMR spectra of thionicotinamide. (A) Only the spectral region of the thioamide protons is shown. Under chemical exchange, the spectral lines broaden and then coalesce into a single peak. In this regime, the line shapes are a sensitive function of the exchange rate. (B) Results of the fitting procedure, including residuals from the fits.

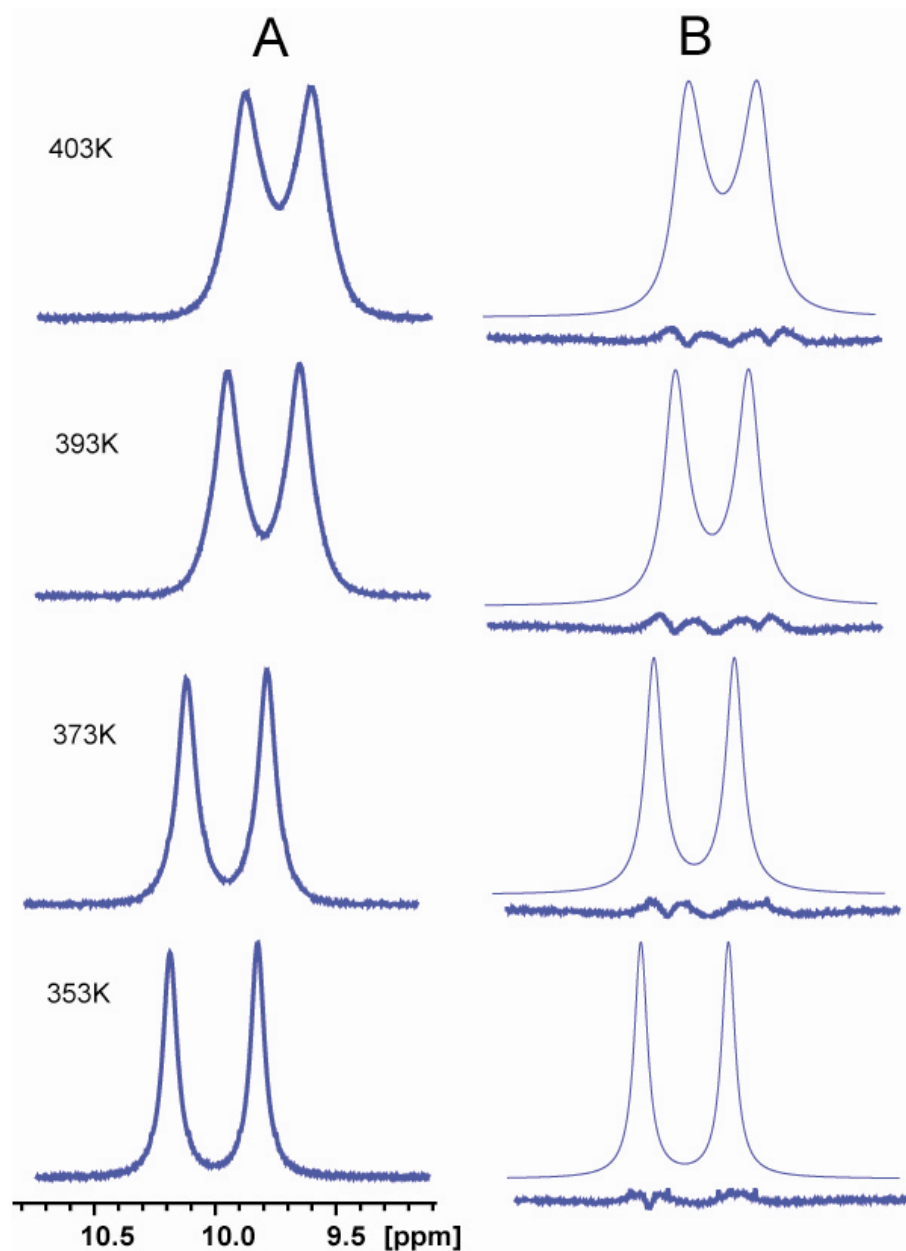
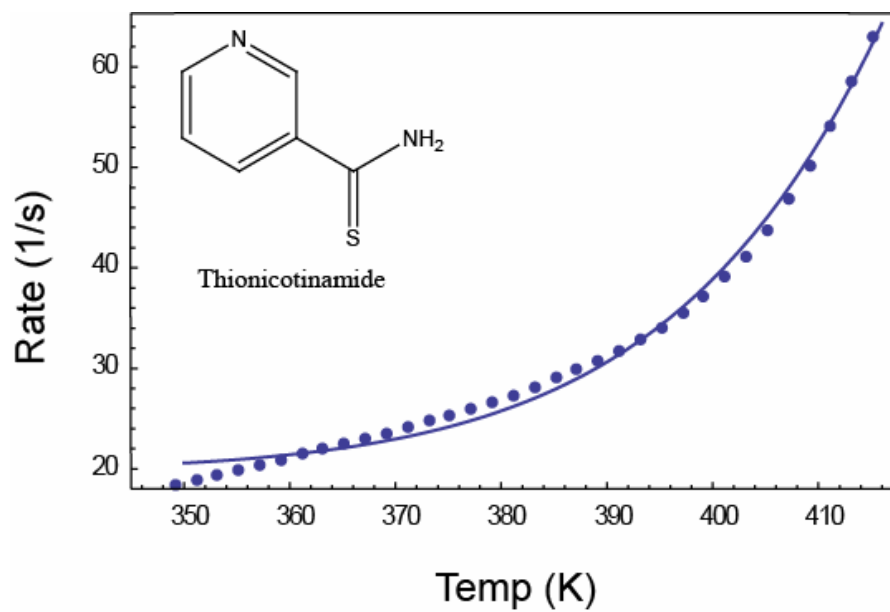


Figure 4.4. Dynamic NMR spectra of thioisonicotinamide. (A) Only the spectral region of the thioamide protons is shown. Under chemical exchange, the spectral lines broaden and then coalesce into a single peak. In this regime, the line shapes are sensitive to the exchange rate. (B) Results of the fitting procedure, together with residuals from the fits.

thionicotinamide		thioisonicotinamide	
T (K)	rate (1/s)	T (K)	rate (1/s)
349.2	18.44	353.2	19.38
351.2	18.91	355.2	19.92
353.2	19.45	357.2	20.44
355.2	19.94	359.2	20.95
357.2	20.41	361.2	21.40
359.2	20.93	363.2	21.98
361.2	21.45	365.2	22.50
363.2	21.97	367.2	23.09
365.2	22.50	369.2	23.61
367.2	23.02	371.2	24.13
369.2	23.55	373.2	24.8
371.2	24.15	375.2	25.44
373.2	24.74	377.2	26.06
375.2	25.35	379.2	26.73
377.2	25.94	381.2	27.41
379.2	26.63	383.2	28.21
381.2	27.35	385.2	29.07
383.2	28.06	387.2	29.91
385.2	29.04	389.2	30.90
387.2	29.87	391.2	31.94
389.2	30.69	393.2	33.08
391.2	31.70	395.2	34.43
393.2	32.82	397.2	35.86
395.2	34.05	399.2	37.57
397.2	35.47	401.2	39.45
399.2	37.12	403.2	41.69
401.2	39.10	405.2	44.26
403.2	41.07	407.2	47.36
405.2	43.81	409.2	50.99
407.2	46.91	411.2	55.30
409.2	50.19	413.2	60.04
411.2	54.11	415.2	65.55
413.2	58.56		
415.2	62.96		
417.2	68.78		

Table 4.1. Experimental Data Points for Thionicotinamide and Thioisonicotinamide

(A)



(B)

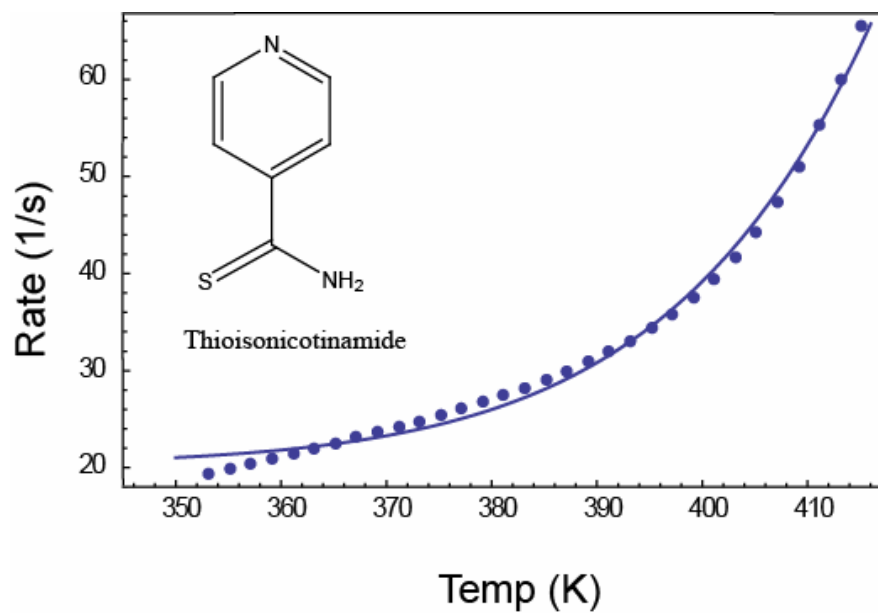


Figure 4.5. The temperature dependence of the apparent rate data fit to transition state theory shown as a nonlinear fit. (A) thionicotinamide. (B) thioisonicotinamide.

	ΔH^\ddagger (kcal/mol)	ΔS^\ddagger (cal/mol·K)	T_2 (ms)
thionicotinamide			
experimental	16.7 ± 0.6	-11.6 ± 1.5	49.3 ± 2.0
B3LYP/6-311G(d,p)	16.2		
thioisonicotinamide			
experimental	17.4 ± 0.7	-9.9 ± 1.6	50.7 ± 2.0
B3LYP/6-311G(d,p)	16.7		
nicotinamide			
experimental ^a	12.9 ± 0.3	-7.7 ± 0.9	
B3LYP/6-311G(d,p)	12.8		
isonicotinamide			
experimental ^b	14.1 ± 0.2	-5.2 ± 1.2	46.7 ± 1.5
B3LYP/6-311G(d,p)	13.1		

^aReference 2. ^bReference 3.

Table 4.2. Rotational Barrier of Pyridine Thiocarboxamides and Pyridine Carboxamides

4.3.1 COMPARISON AMONG REGIOISOMERS AND AB INITIO

CALCULATIONS

The enthalpy of activation for thionicotinamide, $+16.7 \pm 0.6$ kcal/mol, is 0.7 kcal/mol smaller than the value for thioisonicotinamide, $+17.4 \pm 0.7$ kcal/mol. This tendency is comparable to that of pyridine carboxamides found in our earlier studies^{2,3}, in which a difference of 1.2 kcal/mol was reported between the activation enthalpies of nicotinamide ($+12.9 \pm 0.3$ kcal/mol) and isonicotinamide ($+14.1 \pm 0.2$ kcal/mol). In our previous studies, the activation enthalpy of picolinamide ($+18.3 \pm 0.4$ kcal/mol) has also been reported. *Ab initio* calculations detailed in those studies were successful in quantitatively partitioning the enthalpy difference in pyridine carboxamides into its major

contributions: (1) superior π electron donation from the pyridine ring in the transition state of nicotinamide than those of picolinamide and isonicotinamide; (2) steric interactions in the ground states of nicotinamide and isonicotinamide; and (3) an intramolecular hydrogen bond in the ground state of picolinamide.

To thoroughly understand the enthalpy difference in pyridine thiocarboxamides, *ab initio* calculations have also been performed. The results, including rotational pathways and barriers, are shown in Figure 4.8. Here the structures of TN-GS-1 and TI-GS are characterized as the ground states of thionicotinamide and thioisonicotinamide, while the transition states of thionicotinamide and thioisonicotinamide are characterized by structures of TN-TS-1-1 and TI-TS-1, respectively. Their important geometry parameters have been summarized in Table 4.3 as well. As in the case of amides, the ground states of thioamides exhibit a roughly planar geometry for the thioamide nitrogen. The planar geometry allows for delocalization of π electrons between the thioamide nitrogen and the C=S carbon. Steric interactions between the thioamide proton and the pyridine ring protons impose slight (but roughly equivalent) deviations from planarity at the thioamide nitrogen and a twist of the thioamide C-C-N plane relative to the pyridine-ring plane in the ground states of both thionicotinamide and thioisonicotinamide. This twist, characterized by the dihedral angle of C-C-C-N (1-2-3-4 in Figure 4.8), is slightly more pronounced for thioisonicotinamide (by 2.5°) than that for thionicotinamide. The transition states for thionicotinamide and thioisonicotinamide are very similar in structure, where the nitrogens pyramidalize to approximately the same degree and the protons point away from the pyridine ring, again likely owing to steric interactions.

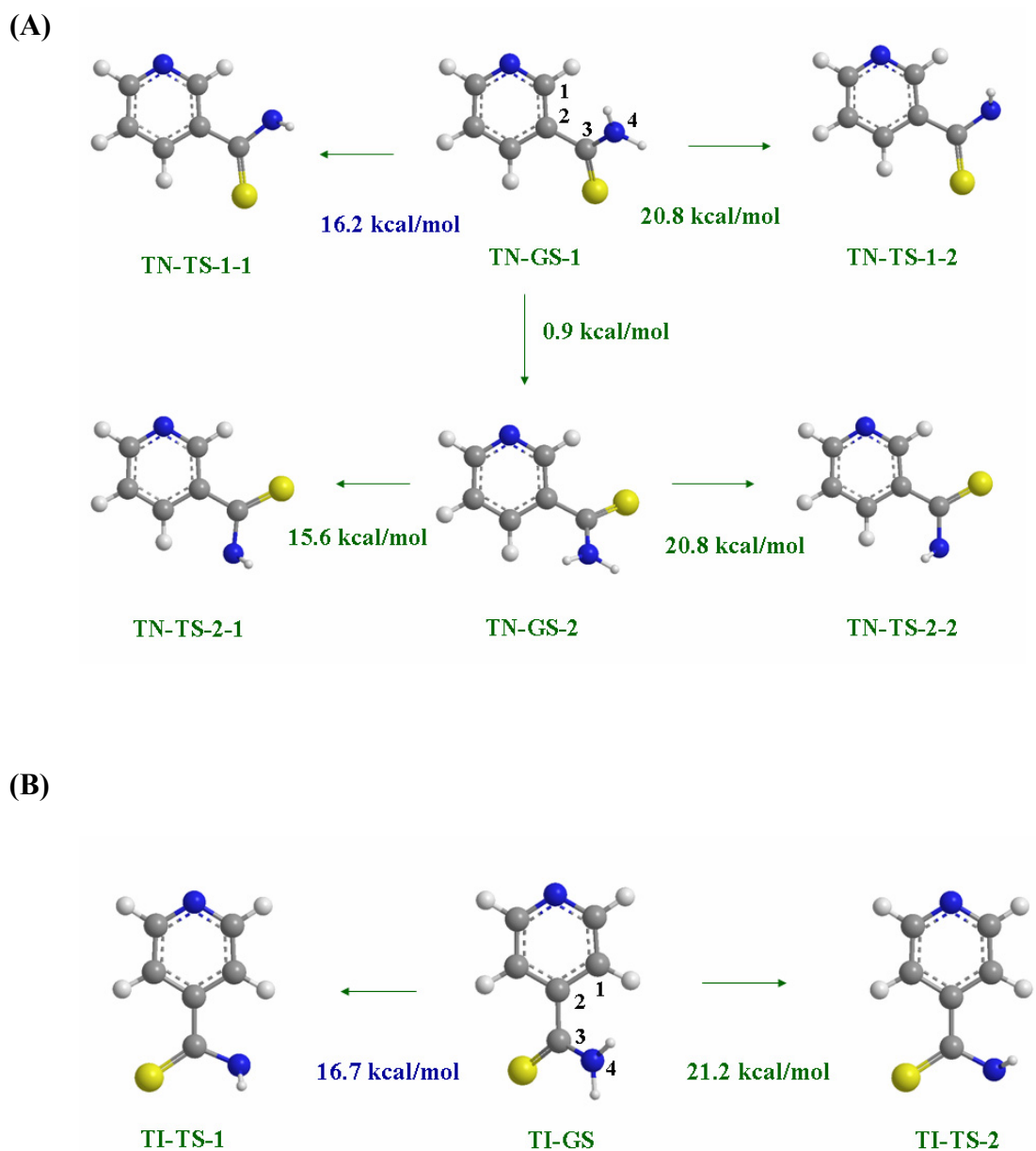


Figure 4.8. Rotational pathways and rotational barriers of pyridine thiocarboxamides reported at the B3LYP/6-311G(d,p) level. (A) thionicotinamide. (B) thioisonicotinamide.

	dihedral angle C-C-C-N ^a	nitrogen pyramidalization angle ^a	C=X bond ^b	C-N bond ^b	dipole moment ^c
thionicotinamide					
ground state	32.8	358.5	1.666	1.350	2.96
transition state	-0.1	320.1	1.649	1.445	0.53
thioisonicotinamide					
ground state	35.3	358.5	1.663	1.349	3.99
transition state	0.0	320.3	1.645	1.444	1.90
nicotinamide					
ground state	18.1	355.1	1.218	1.370	1.87
transition state	-0.1	318.5	1.209	1.452	0.57
isonicotinamide					
ground state	20.2	355.0	1.217	1.369	3.47
transition state	0.0	318.5	1.208	1.451	2.05

^a Angle in degrees. ^b Bond length in angstroms. ^c Dipole moment in Debyes.

Table 4.3. Molecular Parameters Optimized at the B3LYP/6-311G(d,p) Level.

As like the case of pyridine carboxamides, π -electron donation from the pyridine ring to the C=X carbon plays an important role in differentiating the rotational barriers in thionicotinamide and thioisonicotinamide. This kind of delocalization is inclined to stabilize lone-pair electron density on the thioamide nitrogen, and this electronic effect reduces the energy of the transition state for thioamide bond rotation. This reduction in energy of the transition state due to π -electron donation from pyridine is most pronounced when the pyridine nitrogen is disposed in the position meta to the thiocarboxamide as it is in thionicotinamide. Figure 4.9 shows the resonance structures of pyridine thiocarboxamides, which demonstrates how π -electron donation is affected by the position of the relatively electronegative nitrogen. In the roughly planar ground states

of both thionicotinamide and thioisonicotinamide, all three resonance structures shown are important, although **I** and **II** dominate. In the transition state, the thioamide nitrogen is pyramidalized and changes from sp^2 to sp^3 hybridization. At the same time, the thioamide protons are out of the plane defined by the pyridine ring. Consequently, resonance **II** is no longer able to contribute either molecule, and the importance of resonance **III** increases. In this resonance structure, thionicotinamide has distinct advantage as positive charge is distributed over three carbons, while in thioisonicotinamide it is distributed over two carbons and a more electronegative pyridine nitrogen. As a result of this more favorable delocalization, thionicotinamide's transition state is stabilized by resonance **III** to a greater degree than thioisonicotinamide's. Since steric interactions in the ground states of thionicotinamide and thioisonicotinamide are roughly the same, and since intramolecular hydrogen bonding is absent in both molecules, this differential π -electron donation accounts for ~ 1 kcal/mol difference in the barriers to rotation in thionicotinamide and thioisonicotinamide.

The *ab initio* energies characterizing the gas phase rotational barriers are shown in Figure 4.8 and compared to the experimental values in Table 4.2. Generally, the lower energetic barriers calculated with density functional theory are in good agreement with the experimentally determined activation enthalpies for thionicotinamide and thioisonicotinamide, even though solvent interactions is not taken into account in the calculations. The likely similarity of solvent interactions with thionicotinamide and thioisonicotinamide under any circumstances reinforces our primary conclusion that the

~1 kcal/mol greater barrier in thionicotinamide is indeed likely dominated by more favorable delocalization of positive charge over the pyridine ring in the transition state.

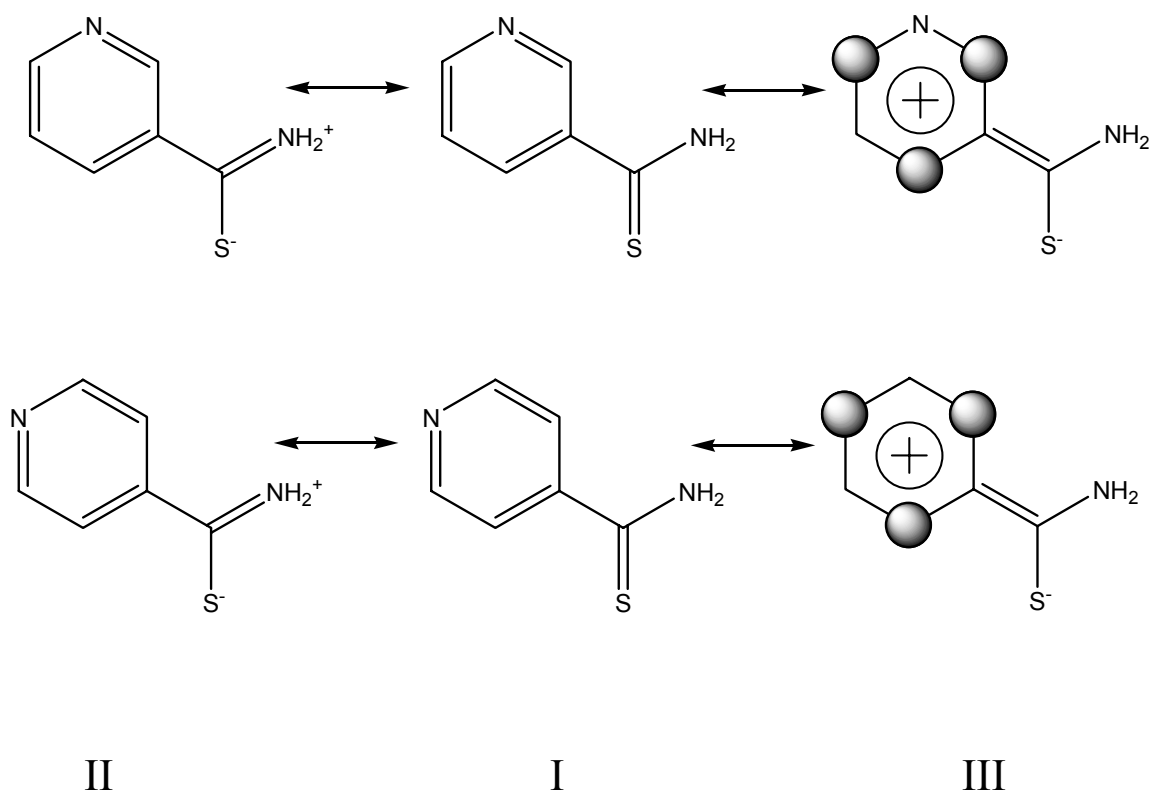


Figure 4.9. Resonance structures for thionicotinamide (top) and thioisonicotinamide (bottom).

4.3.2 COMPARISON TO AMIDE ANALOGUES AND NBO ANALYSIS

It is of particular importance to compare the rotational barrier of thiocarboxamide to its amide analogue since these two classes of compounds show the differential pharmacological activities. Based on our experimental result, higher rotational barriers have been observed for thionicotinamide (16.7 kcal/mol) and thioisonicotinamide (17.4 kcal/mol), compared to their corresponding amide analogues, *i.e.*, nicotinamide (12.9 kcal/mol) and isonicotinamide (14.1 kcal/mol), respectively. *Ab initio* calculations of rotational barriers (Table 4.2) have further verified this tendency, and indicate that chalcogen replacement, from O to S, increases the C-N rotational barrier to certain extent (3-4 kcal/mol) in the system investigated.

Based on the popular resonance model (Figure 4.1), the amide structure is stabilized by the resonance interaction of the p-type N lone pair with C=X π system ($n_N \rightarrow \pi^*_{C=X}$), and the resulting contribution from resonance **II** gives rise to the large rotational barrier. Natural resonance theory (NRT) recognizes this strong $n_N \rightarrow \pi^*_{C=X}$ interaction in the parent Lewis structure **I**, and mixes the dipolar form **II** in its resonance hybrid. This interaction will grant thioamides and amides C-N double-bond character while having a tendency to weaken the C=X π bond. Table 4.4 compares natural resonance weights for the pyridine thiocarboxamides with their amide analogues at the MP2 level. Here only the two main resonances, *i.e.*, the parent Lewis structure **I** and the dipolar form **II**, are shown in the resonance hybrid. As anticipated, the structure of higher weight is the Lewis form **I**.

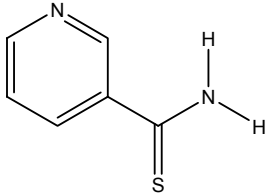
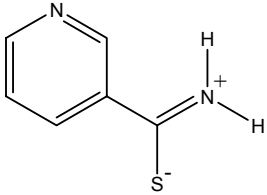
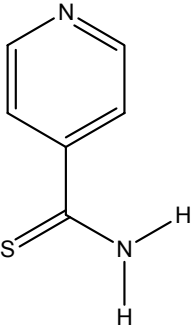
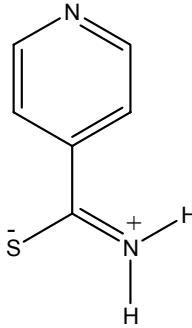
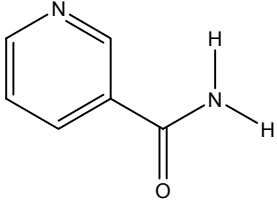
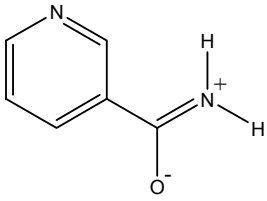
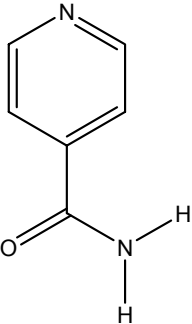
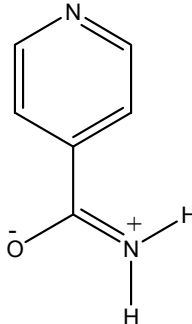
	Resonance I		Resonance II	
	Structure	Weight	Structure	Weight
thionicotinamide		39.81%		27.74%
thioisonicotinamide		42.52%		26.40%
nicotinamide		53.42%		20.71%
isonicotinamide		52.58%		20.03%

Table 4.4. Natural Resonance Weights for Ground States of Thionicotinamide, Thioisonicotinamide, Nicotinamide, and Isonicotinamide at the MP2/6-311G(d,p) Level.

	$\Delta E(\pi^*_{C=X} - n_N)$ [a.u.]	bond order		occupancy	
		b_{C-N}	$b_{C=X}$	n_N	n_X
thionicotinamide	0.62	1.394	1.552	0.623	2.411
thioisonicotinamide	0.59	1.381	1.575	0.634	2.390
nicotinamide	0.65	1.262	1.739	0.746	2.255
isonicotinamide	0.65	1.262	1.747	0.747	2.247

Table 4.5. NBO Analysis of Ground States of Thionicotinamide, Thioisonicotinamide, Nicotinamide, and Isonicotinamide at the MP2/6-311G(d,p) Level

Obviously, replacing the O atom of amides with S atom strengthens the principal $n_N \rightarrow \pi^*_{C=X}$ resonance interaction and increases the contribution from the dipolar form **II**. The weight percent of structure **II** increases from 20.71% in nicotinamide to 27.74% in thionicotinamide. Similarly, the contribution from resonance **II** increases from 20.03% in isonicotinamide to 26.40% in thioisonicotinamide. Such trend is fully in agreement with the increasing rotation barriers from carboxamides to thiocarboxamides shown in Table 4.2.

Table 4.5 shows the natural bond orders of pyridine thiocarboxamides with their amide analogues, which reveals the significant exchange of bonding interaction, the C-N bond gaining double-bond character at the cost of the C=X bonding. For nicotinamide, the C-N bond ($b_{C-N} = 1.262$) has 26.2% double-bond character while the C=O double bond has 26.1% single-bond character ($b_{C=O} = 1.739$). Replacement of O atom in amides with S atom tends to increase the C-N double-bond character, which renders thionicotinamide with 39.4% double-bond character for C-N bond ($b_{C-N} = 1.394$) and 44.8% single-bond character ($b_{C=S} = 1.552$) for C=S bond. Similar higher C-N double-

bond character has also been observed for thioisonicotinamide ($b_{C-N} = 1.381$) compared to isonicotinamide ($b_{C-N} = 1.262$).

The resonance model (Figure 4.1) also implies the transfer of electron density from N to chalcogen atoms, which will be reflected by the electron densities on the nitrogen and chalcogen centers. As anticipated, stronger $n_N \rightarrow \pi^*_{C=X}$ interaction in thiocarboxamides transfers more electron density from nitrogen and therefore leaves less electron density on N shown in Table 4.5. For instance, the n_N occupancy decreases from 0.746 for nicotinamide to 0.623 for thionicotinamide, accompanied by the increase of n_X occupancy from 2.255 for nicotinamide to 2.411 for thionicotinamide. Similar less occupancy of n_N has also been found for thioisonicotinamide ($n_N = 0.634$) relative to isonicotinamide ($n_N = 0.747$). This tendency, together with the natural bond orders discussed above, are fully consistent with the increasing importance of resonance **II** in thiocarboxamides indicated by NRT analysis, which in turn will increase the rotational barriers.

For $n_N \rightarrow \pi^*_{C=X}$ interaction, attention should be paid to the value of $\Delta E(\pi^*_{C=X} - n_N)$, which represents the energy difference between the electron acceptor $\pi^*_{C=X}$ and electron donor n_N . As shown in Table 4.5, $\Delta E(\pi^*_{C=X} - n_N)$ decreases with the replacement of O atom in amides with S atom. For example, the $\Delta E(\pi^*_{C=X} - n_N)$ for nicotinamide is as high as 0.65 a.u. while the thionicotinamide's $\Delta E(\pi^*_{C=X} - n_N)$ is only 0.62 a.u.. Like wise, the $\Delta E(\pi^*_{C=X} - n_N)$ for thioisonicotinamide (0.59 a.u.) is lower than that for isonicotinamide (0.65 a.u.). Such tendency strongly indicates the lower energy of $\pi^*_{C=S}$, compared to $\pi^*_{C=O}$, makes C=S π antibond a better acceptor for resonance

interaction with the N lone pair ($n_N \rightarrow \pi^*_{C=X}$) shown in Figure 4.10, and consequently gives rise to higher rotational barriers of thiocarboxamides than their corresponding amide analogues.

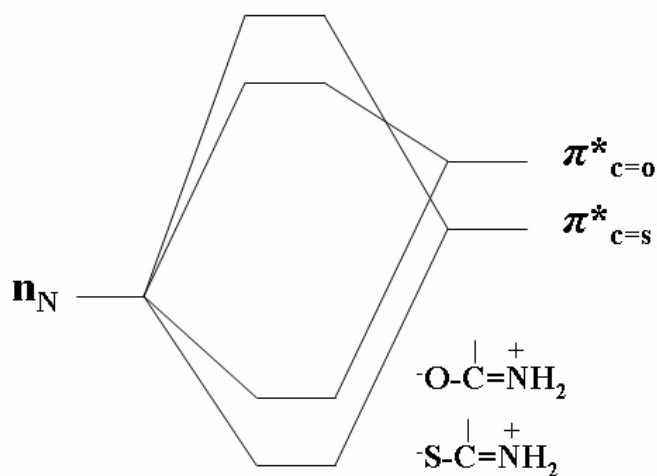


Figure 4.10. Diagram showing the interaction between n_N and $\pi^*_{C=X}$. $n_N \rightarrow \pi^*_{C=S}$ is stronger because ΔE between n_N and $\pi^*_{C=S}$ is smaller.

4.4 CONCLUSION

The C-N rotational barriers of a series of pyridine thiocarboxamides have been investigated by means of dynamic nuclear magnetic resonance (NMR) and *ab initio* calculations. The experimentally measured activation enthalpies and entropies are $\Delta H^\ddagger = +16.7 \pm 0.6$ kcal/mol and $\Delta S^\ddagger = -11.6 \pm 1.5$ cal/mol·K for thionicotinamide, and $\Delta H^\ddagger = +17.4 \pm 0.7$ kcal/mol and $\Delta S^\ddagger = -9.9 \pm 1.6$ cal/mol·K for thioisonicotinamide, respectively. *Ab initio* calculations of the rotational barriers agree well with the experimentally

determined values, and help primarily attribute the 0.7 kcal/mol difference of activation enthalpies between thionicotinamide and thioisonicotinamide to the different π electron donation from the pyridine ring to thiocarboxamide moieties. Particular attention has been paid to 3-4 kcal/mol higher rotational barrier observed for thiocarboxamides compared to their corresponding amide analogues, in which the interaction between amide N lone pairs and C=X π^* antibond ($n_N \rightarrow \pi^*_{C=X}$) plays an important role. Chalcogen replacement of O in amides with S strengthens this interaction, evidenced by the analyses of natural resonance weights, natural bond orders, and electron occupancy. These NBO analyses support the canonical amide resonance model and yield a more detailed picture of structural and electronic properties responsible for the differential pharmacological activities of thiocarboxamides and carboxamides.

REFERENCE

- (1) Pauling, L., *The Nature of the Chemical Bonds*. Cornell University Press: Cornell, 1960.
- (2) Olsen, R. A.; Liu, L.; Ghaderi, N.; Johns, A.; Hatcher, M. E.; Mueller, L. J., *J. Am. Chem. Soc.* **2003**, *125*, 10125.
- (3) Leskowitz, G. M.; Ghaderi, N.; Olsen, R. A.; Pederson, K.; Hatcher, M. E.; Mueller, L. J., *J. Phys. Chem. A* **2005**, *109*, 1152.
- (4) Taha, A. N.; True, N. S., *J. Phys. Chem. A* **2000**, *104*, 2985.
- (5) Stewart, W. E.; Siddall, T. H., *Chem. Rev.* **1970**, *70*, 517.
- (6) Rabinovi, M.; Pines, A., *J. Am. Chem. Soc.* **1969**, *91*, 1585.
- (7) Fontoura, L. A. M.; Rigotti, I. J. D.; Correia, C. R. D., *J. Mol. Struct.* **2002**, *609*, 73.
- (8) Fogarasi, G.; Szalay, P. G., *J. Phys. Chem. A* **1997**, *101*, 1400.
- (9) Basch, H.; Hoz, S., *Chem. Phys. Lett.* **1998**, *294*, 117.
- (10) Bennet, A. J.; Wang, Q. P.; Slebockatilk, H.; Somayaji, V.; Brown, R. S.; Santarsiero, B. D., *J. Am. Chem. Soc.* **1990**, *112*, 6383.
- (11) Berg, U.; Astrom, N., *Acta Chem. Scand.* **1995**, *49*, 599.
- (12) Bain, A. D.; Hazendonk, P.; Couture, P., *Can. J. Chem.-Rev. Can. Chim.* **1999**, *77*, 1340.
- (13) Avalos, J. L.; Boeke, J. D.; Wolberger, C., *Mol. Cell* **2004**, *13*, 639.
- (14) Campomanes, P.; Menendez, M. I.; Sordo, T. L., *J. Phys. Chem. A* **2002**, *106*, 2623.
- (15) Cox, C.; Lectka, T., *J. Org. Chem.* **1998**, *63*, 2426.
- (16) Smith, B. D.; Goodenough-Lashua, D. M.; D'Souza, C. J. E.; Norton, K. J.; Schmidt, L. M.; Tung, J. C., *Tetrahedron Lett.* **2004**, *45*, 2747.
- (17) Wiberg, K. B.; Laidig, K. E., *J. Am. Chem. Soc.* **1987**, *109*, 5935.

- (18) Wiberg, K. B.; Breneman, C. M., *J. Am. Chem. Soc.* **1992**, *114*, 831.
- (19) Wiberg, K. B.; Hadad, C. M.; Rablen, P. R.; Cioslowski, J., *J. Am. Chem. Soc.* **1992**, *114*, 8644.
- (20) Wiberg, K. B.; Rablen, P. R.; Rush, D. J.; Keith, T. A., *J. Am. Chem. Soc.* **1995**, *117*, 4261.
- (21) Mo, Y. R.; Schleyer, P. V.; Wu, W.; Lin, M. H.; Zhang, Q.; Gao, J. L., *J. Phys. Chem. A* **2003**, *107*, 10011.
- (22) Laidig, K. E.; Cameron, L. M., *J. Am. Chem. Soc.* **1996**, *118*, 1737.
- (23) Lauvergnat, D.; Hiberty, P. C., *J. Am. Chem. Soc.* **1997**, *119*, 9478.
- (24) Prasad, B. V.; Uppal, P.; Bassi, P. S., *Chem. Phys. Lett.* **1997**, *276*, 31.
- (25) Galabov, B.; Ilieva, S.; Hadjieva, B.; Dinchova, E., *J. Phys. Chem. A* **2003**, *107*, 5854.
- (26) Kaur, D.; Sharma, P.; Bharatam, P. V., *Theochem-J. Mol. Struct.* **2005**, *757*, 149.
- (27) Kaur, D.; Sharma, P.; Bharatam, P. V.; Dogra, N., *Theochem-J. Mol. Struct.* **2006**, *759*, 41.
- (28) Glendening, E. D.; Hrabal, J. A., *J. Am. Chem. Soc.* **1997**, *119*, 12940.
- (29) Bharatam, P. V.; Moudgil, R.; Kaur, D., *J. Phys. Chem. A* **2003**, *107*, 1627.
- (30) Kim, W.; Lee, H. J.; Choi, Y. S.; Choi, J. H.; Yoon, C. J., *J. Chem. Soc.-Faraday Trans.* **1998**, *94*, 2663.
- (31) Lee, H. J.; Lee, M. H.; Choi, Y. S.; Park, H. M.; Lee, K. B., *Theochem-J. Mol. Struct.* **2003**, *631*, 101.
- (32) Wynne, J. H.; Jensen, S. D.; Snow, A. W., *J. Org. Chem.* **2003**, *68*, 3733.
- (33) Goel, A.; Mazur, S. J.; Fattah, R. J.; Hartman, T. L.; Turpin, J. A.; Huang, M. J.; Rice, W. G.; Appella, E.; Inman, J. K., *Bioorg. Med. Chem. Lett.* **2002**, *12*, 767.
- (34) Erian, A. W.; Sherif, S. M., *Tetrahedron* **1999**, *55*, 7957.
- (35) Oh, H. K.; Park, J. E.; Sung, D. D.; Lee, I., *J. Org. Chem.* **2004**, *69*, 3150.
- (36) Hoult, D. I.; Richards, R. E., *Proc. R. Soc. London Ser. A-Math. Phys. Eng. Sci.* **1975**, *344*, 311.

- (37) Wolfram, S. *Mathematica: A System for Doing Mathematics by Computer*, 2nd ed.; Addison-Wesley Publishing Company: Reading, Massachusetts, 1991.
- (38) Pechukas, P., *Annu. Rev. Phys. Chem.* **1981**, *32*, 159.
- (39) Frisch, M. J.; Trucks, G. W.; Schlegel, H. B.; Scuseria, G. E.; Robb, M. A.; Cheeseman, J. R.; Montgomery, J., J. A.; Vreven, T.; Kudin, K. N.; Burant, J. C.; Millam, J. M.; Iyengar, S. S.; Tomasi, J.; Barone, V.; Mennucci, B.; Cossi, M.; Scalmani, G.; Rega, N.; Petersson, G. A.; Nakatsuji, H.; Hada, M.; Ehara, M.; Toyota, K.; Fukuda, R.; Hasegawa, J.; Ishida, M.; Nakajima, T.; Honda, Y.; Kitao, O.; Nakai, H.; Klene, M.; Li, X.; Knox, J. E.; Hratchian, H. P.; Cross, J. B.; Bakken, V.; Adamo, C.; Jaramillo, J.; Gomperts, R.; Stratmann, R. E.; Yazyev, O.; Austin, A. J.; Cammi, R.; Pomelli, C.; Ochterski, J. W.; Ayala, P. Y.; Morokuma, K.; Voth, G. A.; Salvador, P.; Dannenberg, J. J.; Zakrzewski, V. G.; Dapprich, S.; Daniels, A. D.; Strain, M. C.; Farkas, O.; Malick, D. K.; Rabuck, A. D.; Raghavachari, K.; Foresman, J. B.; Ortiz, J. V.; Cui, Q.; Baboul, A. G.; Clifford, S.; Cioslowski, J.; Stefanov, B. B.; Liu, G.; Liashenko, A.; Piskorz, P.; Komaromi, I.; Martin, R. L.; Fox, D. J.; Keith, T.; Al-Laham, M. A.; Peng, C. Y.; Nanayakkara, A.; Challacombe, M.; Gill, P. M. W.; Johnson, B.; Chen, W.; Wong, M. W.; Gonzalez, C.; Pople, J. A. *Gaussian 03*, E.01; Gaussian, Inc., Wallingford CT: 2004.
- (40) Becke, A. D., *Phys. Rev. A* **1988**, *38*, 3098.
- (41) Becke, A. D., *J. Chem. Phys.* **1993**, *98*, 5648.
- (42) Lee, C. T.; Yang, W. T.; Parr, R. G., *Phys. Rev. B* **1988**, *37*, 785.
- (43) Glendening, E. D.; Badenhop, J. K.; Reed, A. E.; Carpenter, J. E.; Bohmann, J. A.; Morales, C. M.; Weinhold, F. *Nbo 5.0*, Theoretical Chemistry Institute, University of Wisconsin: Madison, WI, 2001.
- (44) Headgordon, M.; Pople, J. A.; Frisch, M. J., *Chem. Phys. Lett.* **1988**, *153*, 503.
- (45) Straatsma, T. P.; Aprà, E.; Windus, T. L.; Bylaska, E. J.; de Jong, W.; Hirata, S.; Valiev, M.; Hackler, M.; Pollack, L.; Harrison, R.; Dupuis, M.; Smith, D. M. A.; Nieplocha, J.; V., T.; Krishnan, M.; Auer, A. A.; Brown, E.; Cisneros, G.; Fann, G.; Früchtl, H.; Garza, J.; Hirao, K.; Kendall, R.; Nichols, J.; Tsemekhman, K.; Wolinski, K.; Anchell, J.; Bernholdt, D.; Borowski, P.; Clark, T.; Clerc, D.; Dachsel, H.; Deegan, M.; Dyllal, K.; Elwood, D.; Glendening, E.; Gutowski, M.; Hess, A.; Jaffe, J.; Johnson, B.; Ju, J.; Kobayashi, R.; Kutteh, R.; Lin, Z.; Littlefield, R.; Long, X.; Meng, B.; Nakajima, T.; Niu, S.; Rosing, M.; Sandrone, G.; Stave, M.; Taylor, H.; Thomas, G.; van Lenthe, J.; Wong, A.; Zhang, Z. *Nwchem, a Computational Chemistry Package for Parallel Computers*, Version

4.5; Pacific Northwest National Laboratory: Richland, Washington 99352-0999, USA, 2003.

CHAPTER V

CONCLUSION AND OUTLOOK

Since their inception, both nuclear magnetic resonance (NMR) and *ab initio* calculations have been extensively used to solve important structural and energetic problems in the field of chemistry. The combination of NMR and *ab initio* theory is a powerful tool for chemical research, which allow detailed models of molecular structure and dynamics to be probed and important chemical problems to be tackled. In this work, we show three applications of the combination of the NMR and *ab initio* calculations.

Enzymes are capable of effecting remarkable chemical transformations and the structural and chemical characterization of intermediates in the catalytic process provides insight into the molecular level details involved in enzymatic function. In this study of enzymatic intermediates in tryptophan synthase, X-ray crystallography, nuclear magnetic resonance, and computational chemistry are quite complementary techniques. While X-ray crystallography provides a map of large scale structure and ordering, detailed chemical information of the active site is difficult to discern at this resolution, but can be revealed through the chemical shifts in the solid-state NMR. Bringing them together is computation chemistry, where *ab initio* calculation of the chemical shift, loosely constrained by the X-ray crystal data, allows the interpretation of the chemical shifts in terms of the chemical structure. For quinonoid intermediate, the results support the ketoenamine and dipolar forms that are in fast exchange to each other, which we believe has mechanistic implications.

To further test this model, we are currently acquiring shifts from U-¹³C, ¹⁵N-serine. The Schiff-base linkage, in particular, should be quite sensitive to protonation state. Additional assignments in the pyridine ring of the PLP will require mixed labeling such as ¹⁵N-labeled serine and ¹³C-labeled protein (the PLP is labeled biosynthetically with the protein), and the use of NC and NCC experiments to transfer magnetization to the PLP. Of particular interest is the protonation state of the pyridine ring nitrogen as the β-site reaction occurs (Figure 2.2). While it is expected to be protonated for quinonoid intermediates, its state for the external aldimine and aminoacrylate are less certain. These can be determined by using the PLP phosphate (5.3 Å away and one of only two ³¹P resonance in the enzyme, the other resides on substrate for the α-site), and a ³¹P-¹⁵N TEDOR or double CP¹⁻⁵ experiments in a U-¹³C, ¹⁵N-enzyme. ¹³C and ¹⁵N Shifts in the indoline ring are also accessible by using U-¹³C, ¹⁵N-labeled indoline, which can be readily prepared. The larger the number of shifts that can be obtained throughout the substrate, the more confidence we can place on the chemical models for the substrate structure although clearly full assignments are not necessary, and protonation states can be inferred by their effect on other carbon and nitrogen probes in the molecule. We do expect that interactions with the side-chains in the active site to be important.

How the catalytic residues in the active site effect enzymatic reactions is one of the most important mechanistic questions in biochemistry. In tryptophan synthase, protonation and hydrogen atom abstraction by side chain residues drive the catalysis. Side chains Lys87, which is actively involved in the catalysis in Figure 2.2 as the ENZ-NH₂, Ser277, which H-bonds to the pyridine ring nitrogen, and Glu109 which stabilizes

charge development on the indole ring and acts as acid-base catalyst in the elimination of the L-Ser hydroxyl, are of particular interest. Other important catalytic residues are His86 and Asn236, which are H-bonded to the PLP phosphate, Thr110 and Gln114, which H-bond to the substrate carboxylic acid group, and Asp305 and Arg141, which form a salt bridge that is essential for the switch from the open to the closed, catalytically active conformation⁶. These residues can be interrogated using mixed labeling and ³¹P-edited sequences. Again from the PLP phosphate, ³¹P-¹³C and ³¹P-¹⁵N TEDOR and double CP¹⁻⁵ experiments should prove quite useful in editing out nearby residue and the pyridine ring ¹³C and ¹⁵N shifts in a U-¹³C, ¹⁵N-enzyme, with nearby assignments being made through *J* – MAS transfer. ¹³C-¹⁵N TEDOR⁷ along with ¹³C-¹⁵N double CP⁸ will also give us access to the Lys87 nitrogen for U-¹⁵N-labeled protein and ¹³C, ¹⁵N -labeled serine and indole. Active-site residues near the PLP-ligand complex are highlighted in Figure 5.1(B).

While the initial focus will be on catalysis at the β -site, a parallel effort will be undertaken to characterize catalysis at the α -site (Figure 5.1(A)). At the α -site, 3-indole-D-glycerol-3'-phosphate (IGP) is cleaved to give D-glyceraldehyde-3-phosphate (G3P) and indole, which is channeled to the β -site (Figure 2.1). At the same time, binding at the α -site is critical for switching tryptophan synthase between an open, low-activity, conformation and a closed, high-activity, state. The chemical structures of the ligand and catalytic side chains can again be probed by mixed ¹³C/¹⁵N enzyme-substrate labeling strategies and ³¹P-edited sequences.

As a powerful tool, the combination of NMR and *ab initio* calculation can also be applied to the field of catalysis. Cinchona alkaloids are a group of chiral compounds showing unique chemical behavior in many applications, from medicine to catalysis. Past studies simply attributed the physiological and enantioselective reactivity of these compounds to the chiral pocket formed by the quinoline and quinuclidine rings, the two main constituting moieties of the cinchona. However, this point doesn't give an explanation for the differences observed among similar cinchona alkaloids. Here we make use of NMR and *ab initio* calculation to investigate the variations in basic properties among these different cinchona alkaloids, and successfully show that subtle changes in the position of the substituent groups outside the central chiral pocket elucidate the discrepancies observed in basic physicochemical properties between pairs of near-enantiomers. Both energetic and entropic factors contribute to the overall performance of the cinchona catalytic system.

Furthermore, the use of dynamic NMR allows for the extraction of kinetic and thermodynamic properties without perturbing equilibrium. On the other hand, *ab initio* calculations allow us to propose models with detailed electronic and structural factors that contribute to changes in these energetic processes. An example of this unified approach is our study of the C-N rotational barriers in a series of pyridine thiocarboxamides. The experimentally determined activation enthalpies and entropies are $\Delta H^\ddagger = +16.7 \pm 0.6$ kcal/mol and $\Delta S^\ddagger = -11.6 \pm 1.5$ cal/mol·K for thionicotinamide, and $\Delta H^\ddagger = +17.4 \pm 0.7$ kcal/mol and $\Delta S^\ddagger = -9.9 \pm 1.6$ cal/mol·K for thioisonicotinamide, respectively. *Ab initio* calculations of the rotational barriers are in good agreement with

the experimentally measured values. The 0.7 kcal/mol difference of activation enthalpies between thionicotinamide and thioisonicotinamide highlights the importance of π electron donation from the pyridine ring to thiocarboxamide moieties. Higher rotational barriers (3-4 kcal/mol) have also been observed for thiocarboxamides compared to their corresponding amide analogues. Following NBO analysis indicates that the interaction between amide N lone pairs and C=X π^* antibond ($n_N \rightarrow \pi^*_{C=X}$), evidenced by natural resonance weights, natural bond orders, and electron occupancy, plays a vital role, which is consistent with traditional canonical amide resonance model. Although our attention has been focused on the disparity of the rotational barriers between thiocarboxamides and carboxamide, substitution effects on those pharmaceutical interest compounds are also very important. Work in this field is in progress.

REFERENCE

- (1) McDowell, L. M.; Schmidt, A.; Cohen, E. R.; Studelska, D. R.; Schaefer, J., *J. Mol. Biol.* **1996**, *256*, 160.
- (2) Christensen, A. M.; Schaefer, J.; Kramer, K. J., *Magn. Reson. Chem.* **1991**, *29*, 418.
- (3) Gullion, T.; Schaefer, J., *J. Magn. Reson.* **1989**, *81*, 196.
- (4) Mueller, D. D.; Schmidt, A.; Pappan, K. L.; McKay, R. A.; Schaefer, J., *Biochemistry* **1995**, *34*, 5597.
- (5) Schaefer, J., *J. Magn. Reson.* **1999**, *137*, 272.
- (6) Dunn, M. F.; Niks, D.; Ngo, H.; Barends, T. R. M.; Schlichting, I., *Trends Biochem.Sci.* **2008**, *33*, 254.
- (7) Jaroniec, C. P.; Filip, C.; Griffin, R. G., *J. Am. Chem. Soc.* **2002**, *124*, 10728.
- (8) Petkova, A. T.; Baldus, M.; Belenky, M.; Hong, M.; Griffin, R. G.; Herzfeld, J., *J. Magn. Reson.* **2003**, *160*, 1.

APPENDIX

THE ONIOM OPTIMIZED COORDINATES OF INDOLINE QUINONOID INTERMEDIATE (MODEL 0-1010)

C	-5.70589	-1.7688	-6.72437	L ^a
C	-4.85151	-2.19459	-5.51891	L
C	-4.92422	-0.80686	-7.59741	L
O	-4.47329	-1.16129	-8.68729	L
N	-4.75847	0.407571	-7.08061	L
C	-3.99661	1.470593	-7.73805	L
C	-4.0393	2.715994	-6.84915	L
C	-3.10696	2.637491	-5.68456	L
N	-3.36654	1.861262	-4.57286	L
C	-2.35961	1.964308	-3.72576	L
N	-1.44882	2.760824	-4.25647	L
C	-1.88864	3.189052	-5.48237	L
C	-2.52681	1.075432	-7.98062	L
O	-1.8435	1.674136	-8.78998	L
N	-2.03127	0.072108	-7.26012	L
C	-0.63155	-0.32962	-7.38436	L
C	-0.33554	-1.53957	-6.49438	L
C	-0.53074	-1.27184	-5.01262	L
C	0.452201	-0.24637	-4.4908	L
C	0.466265	-0.23275	-2.9787	L
N	1.401865	0.785035	-2.44122	L
C	-0.22197	-0.63318	-8.81956	L
O	0.933801	-0.43685	-9.20749	L
N	-1.18551	-1.10484	-9.60097	L
H	-5.07118	2.920307	-6.49181	L
H	-3.75133	3.598432	-7.45623	L
H	-1.3009	3.848972	-6.12961	L
H	-0.59763	3.093613	-3.84041	L
H	-2.3298	1.488291	-2.7346	L
H	-4.46705	1.69306	-8.72944	L
H	-5.23238	0.634733	-6.20783	L
H	0.71198	-1.86901	-6.67965	L
H	-0.97359	-2.40415	-6.79118	L
H	-1.57688	-0.94241	-4.8173	L

H	-0.41545	-2.22906	-4.45973	L
H	0.217644	0.758924	-4.90481	L
H	1.471495	-0.48439	-4.88134	L
H	-0.55577	-0.06522	-2.56295	L
H	0.773946	-1.24218	-2.60972	L
H	1.756152	0.434468	-1.56088	L
H	1.001023	1.722551	-2.23824	L
H	2.19925	0.904637	-3.06669	L
H	0.018305	0.526907	-7.03283	L
H	-2.44073	-0.16938	-6.37451	L
H	-6.66895	-1.33625	-6.38126	L
H	-5.97903	-2.66719	-7.31297	L
H	-3.8745	-2.58709	-5.83688	L
H	-4.66634	-1.35765	-4.82978	L
H	-5.35912	-2.97908	-4.94046	L
H	-2.13118	-1.18321	-9.30512	L
H	-1.02522	-1.20544	-10.5757	L
C	8.232661	-6.1755	-1.5717	L
C	8.926192	-5.38054	-0.45654	L
C	8.402256	-3.96244	-0.25898	L
C	8.982622	-2.968	-1.25449	L
O	10.14991	-2.56193	-1.05941	L
O	8.269922	-2.57552	-2.21192	L
C	6.736135	-5.90728	-1.58031	L
O	6.251438	-5.06101	-2.3396	L
N	6.004009	-6.62605	-0.74126	L
C	4.565739	-6.45569	-0.67817	L
C	3.840894	-7.32203	-1.7626	L
O	2.504773	-6.84688	-1.95951	L
C	3.821019	-8.79617	-1.40199	L
C	4.045152	-6.72017	0.729379	L
O	4.610409	-7.53079	1.465895	L
N	2.982433	-6.01418	1.102289	L
C	2.351966	-6.19387	2.408792	L
C	0.941722	-6.72693	2.250612	L
O	0.636137	-7.84489	2.679781	L
N	0.081464	-5.91941	1.633321	L
C	-1.27869	-6.33931	1.302296	L
C	-2.14605	-5.13412	0.96589	L
C	-1.28708	-7.34882	0.149334	L
O	-2.29934	-8.00652	-0.09901	L
N	-0.15428	-7.46842	-0.54529	L
C	-0.01661	-8.41231	-1.64747	L
C	-0.51331	-7.81233	-2.94553	L

O	-0.42035	-8.44254	-3.99853	L
N	-1.04372	-6.59295	-2.87488	L
C	-1.55394	-5.90401	-4.06003	L
C	-2.48351	-4.75275	-3.67844	L
C	-3.89778	-5.17147	-3.27176	L
C	-4.63264	-5.9853	-4.33658	L
O	-5.34328	-6.93961	-4.01643	L
N	-4.463	-5.61607	-5.60103	L
C	-0.42417	-5.40097	-4.95255	L
O	-0.53023	-5.46052	-6.18084	L
N	0.646515	-4.89652	-4.33962	L
C	1.835282	-4.50889	-5.1023	L
C	2.804442	-3.66571	-4.26046	L
C	4.077707	-3.33356	-4.97161	L
N	4.124147	-2.47753	-6.05075	L
C	5.36993	-2.38785	-6.48391	L
N	6.1311	-3.15291	-5.72374	L
C	5.344768	-3.76281	-4.77671	L
C	2.531811	-5.75139	-5.65629	L
O	3.040916	-5.7315	-6.77647	L
N	2.542777	-6.82708	-4.86918	L
C	3.130329	-8.09746	-5.30132	L
C	2.414272	-8.67291	-6.51617	L
O	3.05567	-9.15707	-7.45497	L
N	1.081558	-8.62472	-6.48734	L
H	4.377319	-7.17912	-2.73494	L
H	4.423686	-9.03589	-0.51711	L
H	2.786557	-9.1408	-1.20653	L
H	4.200174	-9.41048	-2.23046	L
H	2.495054	-5.89175	-1.80981	L
H	4.372074	-5.37026	-0.94515	L
H	6.444671	-7.19823	-0.05112	L
H	2.349849	-5.21805	2.951667	L
H	2.943925	-6.88175	3.058229	L
H	2.623755	-5.27505	0.494952	L
H	-2.11864	-4.36766	1.755146	L
H	-3.19713	-5.4396	0.861641	L
H	-1.85885	-4.66057	0.014166	L
H	-1.70301	-6.84541	2.214954	L
H	0.356355	-4.99808	1.349745	L
H	1.055956	-8.72667	-1.72706	L
H	-0.58804	-9.34179	-1.4354	L
H	0.628853	-6.8634	-0.39691	L
H	-2.04846	-4.14285	-2.85408	L

H	-2.55106	-4.05827	-4.54921	L
H	-4.47729	-4.24699	-3.00939	L
H	-3.85285	-5.75795	-2.32986	L
H	-3.7267	-4.97675	-5.82196	L
H	-4.75118	-6.21634	-6.33769	L
H	-2.13416	-6.66388	-4.64959	L
H	-0.78508	-5.94817	-2.12397	L
H	2.302735	-2.71944	-3.95986	L
H	3.075073	-4.18088	-3.31184	L
H	5.752379	-4.39952	-3.95771	L
H	7.10981	-3.26879	-5.79137	L
H	5.671338	-1.76438	-7.33305	L
H	1.506614	-3.88244	-5.97824	L
H	0.63341	-4.69212	-3.33527	L
H	3.078982	-8.81317	-4.45317	L
H	4.210096	-7.96595	-5.53164	L
H	2.414341	-6.73848	-3.8633	L
H	8.651809	-5.87126	-2.55141	L
H	8.456777	-7.25569	-1.46923	L
H	8.815911	-5.94098	0.494518	L
H	10.01359	-5.34782	-0.66218	L
H	8.679758	-3.63705	0.765201	L
H	7.29376	-3.9298	-0.27169	L
H	0.573679	-8.38868	-5.64897	L
H	0.554627	-9.00823	-7.23448	L
C	6.013054	-4.93529	5.574416	L
C	5.041628	-3.78577	5.300161	L
C	5.151832	-2.92613	4.042831	L
C	5.422834	-3.76405	2.787014	L
C	3.861985	-2.1278	3.905369	L
C	7.448352	-4.41751	5.727068	L
O	8.248278	-4.55553	4.798312	L
N	7.772754	-3.82501	6.879853	L
H	5.685647	-5.47277	6.48737	L
H	5.972932	-5.6764	4.747428	L
H	5.049274	-3.10171	6.176162	L
H	4.027891	-4.24622	5.299612	L
H	6.003879	-2.21168	4.160952	L
H	5.422868	-3.14042	1.87472	L
H	6.401254	-4.25996	2.843075	L
H	4.65849	-4.54214	2.660123	L
H	3.751067	-1.42654	4.753535	L
H	3.857359	-1.52495	2.984152	L
H	2.972409	-2.77355	3.880008	L

H	7.040213	-3.60748	7.54586	L
H	8.583095	-3.25332	6.920049	L
C	9.629963	-0.1389	-4.87051	L
C	10.42694	1.0901	-4.42803	L
C	10.65358	1.348614	-2.93173	L
C	11.82478	2.29888	-2.73997	L
C	9.4034	1.899368	-2.23564	L
C	8.143368	0.183856	-5.01518	L
O	7.708496	0.779734	-6.01502	L
N	7.370561	-0.23227	-4.01941	L
C	5.921154	-0.22464	-4.13124	L
C	5.162155	0.9865	-3.63828	L
O	3.93421	0.982729	-3.64716	L
N	5.875068	2.025545	-3.21798	L
C	5.219201	3.21461	-2.67932	L
C	4.895238	3.030695	-1.17556	L
O	4.017716	4.072364	-0.74144	L
C	6.16766	3.055173	-0.33547	L
C	6.032894	4.496469	-2.93263	L
O	7.180411	4.4281	-3.37136	L
N	5.425202	5.651884	-2.66341	L
C	6.080161	6.955926	-2.82649	L
C	5.034096	8.051695	-3.01354	L
C	7.002525	7.289535	-1.65086	L
O	6.893513	8.353063	-1.03821	L
N	7.91021	6.369635	-1.34403	L
H	5.533276	-1.11221	-3.57376	L
H	5.612466	-0.36102	-5.19599	L
H	7.750978	-0.89233	-3.33532	L
H	4.373492	2.051555	-1.02167	L
H	5.902777	3.220375	0.727776	L
H	6.866366	3.852007	-0.61987	L
H	6.707117	2.098911	-0.39707	L
H	3.11658	3.716544	-0.85617	L
H	4.238102	3.364344	-3.23094	L
H	6.871633	1.960691	-3.08262	L
H	5.515336	9.030176	-3.18811	L
H	4.386316	8.168744	-2.13108	L
H	4.385434	7.848912	-3.87787	L
H	6.705488	6.908962	-3.7572	L
H	4.636147	5.623699	-2.03677	L
H	9.805992	-0.98175	-4.16471	L
H	10.00809	-0.4796	-5.85335	L
H	9.972208	1.998006	-4.87677	L

H	11.42868	1.004854	-4.89987	L
H	10.90043	0.368468	-2.44871	L
H	11.98154	2.51827	-1.67584	L
H	11.65992	3.256524	-3.25236	L
H	12.75974	1.874168	-3.12857	L
H	9.513847	1.859773	-1.14421	L
H	9.218669	2.947678	-2.5133	L
H	8.49387	1.336935	-2.49171	L
H	8.493009	6.473995	-0.54843	L
H	7.998569	5.527035	-1.88047	L
C	-5.21433	6.418874	3.157873	L
C	-5.62345	4.956446	3.318325	L
S	-5.19205	3.898	1.930548	L
C	-3.72709	6.536027	2.821277	L
O	-3.34896	6.696566	1.663473	L
N	-2.88677	6.47099	3.847099	L
C	-1.46164	6.684802	3.657558	L
C	-0.9769	8.074134	4.205106	L
C	0.502389	8.316872	3.869637	L
C	-1.78993	9.230724	3.605347	L
C	-0.71457	5.520786	4.306673	L
O	-0.63438	5.431717	5.536001	L
N	-0.21586	4.61489	3.463902	L
C	0.721526	3.569269	3.87114	L
C	2.14518	4.085119	3.739605	L
O	2.770913	4.46635	4.7335	L
N	2.661179	4.099813	2.517023	L
C	3.902366	4.811363	2.220761	L
C	3.610428	6.129876	1.528741	L
O	4.44415	7.035159	1.511551	L
N	2.421592	6.233213	0.938329	L
C	1.973195	7.486988	0.342982	L
C	1.647576	7.514716	-1.1398	L
O	1.352674	8.576882	-1.66788	L
N	1.654617	6.370476	-1.81951	L
C	1.499193	6.398501	-3.28437	L
C	2.017093	5.122224	-3.94509	L
O	1.14262	4.037757	-3.70963	L
C	0.093669	6.728617	-3.78704	L
O	-0.05246	7.581423	-4.66544	L
N	-0.93746	6.065532	-3.26093	L
C	-2.31483	6.366115	-3.7074	L
C	-3.33791	5.294804	-3.22918	L
C	-3.92172	5.573823	-1.84662	L

N	-3.42645	5.077283	-0.82613	L
O	-5.00114	6.323713	-1.81034	L
C	-2.73729	7.790461	-3.34516	L
O	-3.40501	8.46717	-4.12994	L
N	-2.31664	8.240608	-2.16214	L
C	-2.60386	9.589621	-1.67987	L
C	-2.20577	9.746954	-0.21349	L
C	-1.90618	10.6398	-2.52546	L
O	-2.53238	11.60351	-2.94275	L
N	-0.61653	10.46443	-2.78873	L
C	-1.16819	-5.14954	6.00925	L
C	-1.05625	-6.45591	5.250385	L
C	-0.55094	-4.0274	5.191918	L
O	0.640131	-3.76549	5.312942	L
N	-1.37322	-3.3768	4.367936	L
C	-0.91354	-2.33052	3.453785	L
C	-0.53904	-1.00157	4.090859	L
O	0.218624	-0.233	3.514193	L
N	-1.06243	-0.73412	5.280692	L
C	-0.75265	0.483728	6.022302	L
C	-2.05073	1.113961	6.553398	L
C	-3.1662	1.475341	5.556075	L
C	-4.32527	2.188364	6.260733	L
C	-2.63201	2.315555	4.413432	L
C	0.21983	0.204254	7.182456	L
O	0.692107	1.12856	7.852346	L
N	0.520289	-1.07329	7.399026	L
C	1.35303	-1.52491	8.520884	L
C	1.077771	-3.01561	8.79951	L
C	1.510981	-3.45341	10.18802	L
O	1.054782	-4.53073	10.64141	L
O	2.291412	-2.72993	10.84045	L
C	2.846358	-1.28539	8.234679	L
O	3.58804	-2.22529	7.934289	L
N	3.27381	-0.02826	8.361219	L
C	4.624627	0.408026	7.982768	L
C	4.644035	0.723104	6.474774	L
C	5.943541	1.286085	5.951797	L
C	7.08075	0.490366	5.841204	L
C	8.276087	1.015486	5.331361	L
C	8.329127	2.344395	4.89566	L
C	7.190761	3.142271	4.975875	L
C	6.002495	2.603877	5.492413	L
C	5.012877	1.62984	8.841961	L

O	4.268103	2.623293	8.88502	L
N	6.168313	1.563078	9.530677	L
Na	2.216197	4.178002	7.618773	L
O	1.786842	6.538099	7.380682	L
H	-1.0953	8.078731	5.315505	L
H	0.821554	9.31103	4.205148	L
H	1.147686	7.578354	4.363876	L
H	0.689352	8.25191	2.781125	L
H	-1.41557	10.1962	3.969443	L
H	-2.85198	9.173572	3.875103	L
H	-1.72487	9.24258	2.506119	L
H	-1.2344	6.72061	2.552077	L
H	-3.21617	6.355132	4.780896	L
H	0.5221	3.2506	4.920164	L
H	0.537706	2.664882	3.245188	L
H	-0.23174	4.753108	2.444606	L
H	4.495235	4.987002	3.145152	L
H	4.552537	4.161362	1.578103	L
H	2.005474	3.938189	1.739177	L
H	2.732787	8.284962	0.515852	L
H	1.073701	7.824989	0.923018	L
H	1.726997	5.472812	0.901842	L
H	3.044245	4.843945	-3.61686	L
H	2.026722	5.229316	-5.04497	L
H	1.286631	3.741409	-2.79427	L
H	2.174685	7.226956	-3.64064	L
H	1.516016	5.492684	-1.35702	L
H	-4.17406	5.275501	-3.9575	L
H	-3.79903	5.272158	0.083063	L
H	-2.52082	4.588283	-0.85655	L
H	-2.88828	4.286463	-3.24534	L
H	-2.30648	6.30073	-4.82976	L
H	-0.83067	5.314397	-2.55297	L
H	-2.38294	10.77556	0.125619	L
H	-1.14438	9.515124	-0.03206	L
H	-2.79581	9.081167	0.43477	L
H	-3.71181	9.75611	-1.76613	L
H	-1.92864	7.6091	-1.48225	L
H	-1.72458	-2.14797	2.710356	L
H	-0.03559	-2.69915	2.874009	L
H	-2.33602	-3.661	4.205193	L
H	-1.76075	2.040553	7.094582	L
H	-2.49136	0.451581	7.329052	L
H	-3.5791	0.524629	5.104372	L

H	-4.72444	1.58055	7.082217	L
H	-4.00775	3.151149	6.681815	L
H	-5.14846	2.38558	5.558837	L
H	-1.94539	1.754579	3.755211	L
H	-2.08727	3.193315	4.788189	L
H	-3.4515	2.678985	3.770665	L
H	-0.24842	1.231887	5.345994	L
H	-1.90117	-1.20503	5.556017	L
H	-0.0076	-3.22405	8.685589	L
H	1.577618	-3.6545	8.048785	L
H	1.065679	-0.94791	9.4413	L
H	0.287746	-1.78337	6.734518	L
H	3.827192	1.436809	6.229812	L
H	4.411585	-0.20823	5.894125	L
H	7.03355	-0.56457	6.140477	L
H	5.102475	3.236298	5.534764	L
H	9.158019	0.373695	5.246941	L
H	7.20737	4.178285	4.623854	L
H	9.25818	2.747169	4.482527	L
H	5.332685	-0.44335	8.172957	L
H	2.563198	0.697915	8.387112	L
H	-5.4664	6.982467	4.078545	L
H	-5.81146	6.888267	2.348292	L
H	-5.1258	4.502476	4.202785	L
H	-6.7084	4.896567	3.532157	L
H	-6.0987	4.398795	1.000331	L
H	-0.18378	11.0083	-3.49766	L
H	-0.64608	-5.22421	6.988403	L
H	-2.22963	-4.93721	6.256705	L
H	-1.70947	-7.21248	5.719566	L
H	-0.02974	-6.84617	5.248846	L
H	-1.38259	-6.36924	4.200987	L
H	6.546901	2.412582	9.883143	L
H	2.372572	5.879507	7.017815	L
H	-0.12855	9.628322	-2.52045	L
H	6.851376	0.921415	9.198268	L
H	0.9044	6.304907	7.108582	L
C	-9.77113	-2.97397	0.76067	L
C	-8.48267	-2.58108	0.054587	L
C	-9.81149	-2.3795	2.164364	L
O	-10.3787	-1.31371	2.372748	L
N	-9.24424	-3.07485	3.148143	L
C	-9.1849	-2.49007	4.484799	L
C	-8.72557	-3.5254	5.510962	L

C	-9.8608	-4.47011	5.895355	L
C	-9.30929	-5.59497	6.752722	L
C	-10.9665	-3.72286	6.631616	L
C	-8.3479	-1.20472	4.567775	L
O	-8.61437	-0.35307	5.415403	L
N	-7.35732	-1.0654	3.680205	L
C	-6.57203	0.170184	3.551508	L
C	-5.48333	0.015886	2.474821	L
C	-4.35205	-0.99335	2.791726	L
C	-4.74611	-2.46238	2.614355	L
O	-5.73825	-2.76535	1.925256	L
O	-4.05717	-3.33326	3.19417	L
C	-7.48198	1.33228	3.158924	L
O	-7.55257	2.341506	3.861599	L
N	-8.17761	1.172052	2.033009	L
C	-9.11965	2.177675	1.528088	L
C	-9.76019	1.705473	0.214168	L
O	-8.82955	1.007674	-0.59525	L
C	-10.2212	2.489755	2.541262	L
O	-10.6955	3.610931	2.603763	L
N	-10.6401	1.487756	3.310598	L
H	-8.36351	-2.99986	6.41921	L
H	-7.84866	-4.10508	5.143502	L
H	-10.2945	-4.91517	4.966497	L
H	-8.53464	-6.16408	6.220924	L
H	-8.85551	-5.21313	7.677513	L
H	-10.0997	-6.29987	7.041737	L
H	-11.3011	-2.85308	6.041912	L
H	-10.6232	-3.34779	7.604676	L
H	-11.8361	-4.36659	6.811059	L
H	-10.2431	-2.1969	4.758376	L
H	-8.53924	-3.74568	2.913401	L
H	-5.02286	1.020309	2.329207	L
H	-5.93444	-0.26445	1.499395	L
H	-3.97201	-0.78909	3.820952	L
H	-3.50136	-0.78139	2.109607	L
H	-6.08338	0.405682	4.536845	L
H	-6.97421	-1.8477	3.13133	L
H	-10.1966	2.562675	-0.33204	L
H	-10.5527	0.950534	0.368244	L
H	-8.10035	1.599627	-0.8049	L
H	-8.52396	3.113257	1.345503	L
H	-8.2535	0.255317	1.632755	L
H	-10.6431	-2.60719	0.183228	L

H	-9.87137	-4.07706	0.791131	L
H	-7.5972	-3.0221	0.536052	L
H	-8.34797	-1.48997	0.039705	L
H	-8.49175	-2.92124	-0.99063	L
H	-11.2173	1.705147	4.091008	L
H	-10.106	0.654005	3.415131	L
C	-7.44022	2.546514	-3.69285	L
C	-6.26715	2.836466	-2.75652	L
O	-6.50343	2.253676	-1.48472	L
C	-7.46216	1.062269	-4.08687	L
O	-6.68376	0.642368	-4.93453	L
N	-8.33148	0.26474	-3.47296	L
C	-8.42308	-1.14315	-3.84645	L
C	-9.71154	-1.81518	-3.4475	L
O	-10.5227	-1.23952	-2.72391	L
N	-9.88599	-3.05283	-3.9208	L
H	-7.55277	-1.66078	-3.35461	L
H	-8.24605	-1.25155	-4.94472	L
H	-8.97986	0.615969	-2.79688	L
H	-8.39701	2.872077	-3.23687	L
H	-7.31469	3.154266	-4.61078	L
H	-6.08955	3.927296	-2.66363	L
H	-5.3328	2.365682	-3.12071	L
H	-6.76709	2.958261	-0.89991	L
H	-10.5701	-3.62341	-3.47742	L
H	-9.07315	-3.5473	-4.21492	L
O	5.880306	11.68937	-3.59533	L
H	5.708094	10.74915	-3.50554	L
H	5.08425	12.15356	-3.35528	L
O	-1.00751	6.769171	0.27311	L
H	-0.58236	5.897825	0.371655	L
H	-1.75584	6.819991	0.87143	L
O	-2.67817	-4.00743	-7.92975	L
H	-2.02757	-4.69983	-7.84859	L
H	-2.28577	-3.2058	-7.58743	L
O	1.95846	2.728316	-6.19483	L
H	2.141719	1.874545	-6.59549	L
H	2.484356	2.783143	-5.40213	L
O	-7.13873	5.519913	0.05087	L
H	-7.51916	6.296476	0.445831	L
H	-6.47264	5.812829	-0.60211	L
O	2.645844	-0.07459	-7.03756	L
H	3.105965	-0.86768	-6.74303	L
H	2.187839	-0.26278	-7.86427	L

O	-4.40544	-7.12644	6.516873	L
H	-3.47122	-7.11155	6.30579	L
H	-4.83149	-6.45908	5.966189	L
O	5.772153	-3.40527	8.96006	L
H	5.336676	-4.18021	9.300327	L
H	5.079009	-2.79137	8.691992	L
O	2.347639	-5.34706	6.549498	L
H	2.586044	-4.66013	7.167458	L
H	1.663188	-5.01923	5.97122	L
O	-8.44886	-7.80227	-3.13466	L
H	-7.78516	-7.6272	-3.79657	L
H	-7.99368	-7.88436	-2.30263	L
O	-5.64185	-5.20809	4.657506	L
H	-5.97162	-5.76894	3.963429	L
H	-5.07425	-4.53915	4.225064	L
O	6.4603	11.11214	-0.99298	L
H	6.523858	10.16264	-0.84973	L
H	6.533378	11.27088	-1.9366	L
O	4.965873	-7.97831	4.258879	L
H	4.988719	-7.10179	4.637623	L
H	4.792865	-7.88113	3.314272	L
O	-6.99795	-4.22227	-3.15951	L
H	-6.19081	-3.84	-2.8007	L
H	-6.92316	-5.17092	-3.107	L
O	-0.96754	3.938847	-1.33855	H ^b
P	0.142718	3.445414	-0.40292	H
O	0.375493	4.367669	0.80745	H
O	1.43421	3.09942	-1.19584	H
O	-0.28736	1.935241	0.134462	H
C	-1.54858	1.796772	0.799941	H
C	-2.45234	0.822763	0.079669	H
C	-3.71011	1.278749	-0.2585	H
N	-4.62681	0.437008	-0.82073	H
C	-2.08267	-0.51956	-0.21444	H
C	-3.03024	-1.37713	-0.91877	H
O	-2.71799	-2.5488	-1.30512	H
C	-4.32733	-0.8253	-1.17921	H
C	-5.40613	-1.69592	-1.7649	H
C	-0.74568	-0.95264	0.045539	H
N	-0.33471	-2.16263	-0.30475	H
C	0.898813	-2.71639	-0.25371	H
C	1.08417	-3.93683	-1.01382	H
O	2.272655	-4.41949	-0.99462	H
O	0.10143	-4.4131	-1.67011	H

C	2.011746	-2.12062	0.54306	H
N	2.918964	-1.16497	-0.19812	H
C	3.984122	-1.79528	-1.03748	H
C	5.337397	-1.54792	-0.31634	H
C	3.607205	-0.2947	0.683193	H
C	3.003343	0.556963	1.590725	H
C	3.805273	1.235316	2.512407	H
C	5.191543	1.125836	2.495639	H
C	5.799971	0.291034	1.533957	H
C	5.005275	-0.40266	0.623726	H
H	-2.04345	2.774953	0.867022	H
H	-1.35335	1.450212	1.836099	H
H	-4.06543	2.273825	0.000875	H
H	-6.17257	-1.97284	-1.01158	H
H	-4.94073	-2.63257	-2.1216	H
H	-5.9454	-1.23445	-2.62048	H
H	-0.05779	-0.31409	0.579277	H
H	1.608456	-1.55493	1.391771	H
H	2.613426	-2.95067	0.940036	H
H	3.753119	-2.85034	-1.19817	H
H	3.98819	-1.28757	-2.01409	H
H	5.642495	-2.43073	0.284682	H
H	6.156178	-1.35421	-1.02824	H
H	1.927961	0.669783	1.631141	H
H	3.324393	1.831767	3.286132	H
H	5.800208	1.649023	3.238316	H
H	6.884503	0.155411	1.527195	H
H	-5.55535	0.800871	-1.02105	H
H	-1.04779	-2.71663	-0.83847	H

^aL: lower layer, calculated at the PM3 level. ^bH: high layer, calculated at the B3LYP/6-31G(d,p) level.